1225-0767(ISSN Print)
2287-6715(ISSN Online)
한국연구재단 우수등재학술지

Journal of Ocean Engineering and Technology

Vol. 38, No. 2 (Serial Number 177)

April 2024

한국해양공학회지

KSOE

www.joet.org

KSOE The Korean Society of Ocean Engineers

Journal of Ocean Engineering and Technology
한국해양공학회지
Vol. 38 No. 2
(Serial Number 177)
April 30, 2024
www.JOET.org

Published on April 30, 2024
Published by The Korean Society of Ocean Engineers (KSOE)
Room 1302, 13, Jungang-daero 180beon-gil, Dong-gu, Busan, 48821, Korea
TEL: +82-51-759-0656 FAX: +82-51-759-0657 E-mail: ksoehj@ksoe.or.kr URL: http://www.ksoe.or.kr
Printed by Hanrimwon Co., Ltd., Seoul, Korea E-mail: hanrim@hanrimwon.co.kr
ISSN(print) 1225-0767 **ISSN(online)** 2287-6715

This journal was supported by the Korean Federation of Science and Technology Societies (KOFST) grant funded by the Korean government.

Journal of Ocean Engineering and Technology
한국해양공학회지

CONTENTS

Volume 38, Number 2 April, 2024

<Original Research Articles>

<Review Article>

GENERAL INFORMATION

The **"Journal of Ocean Engineering and Technology" (JOET)** was launched in 1987 and is published bimonthly in February, April, June, August, October, and December each year by "The Korean Society of Ocean Engineers (KSOE)." Its ISO abbreviation is "J. Ocean Eng. Technol." JOET publishes original research articles, technical articles, and review articles on all aspects of ocean engineering, including experimental, theoretical, numerical, and field observations. All manuscripts undergo peer-review by two or more reviewers.

The scope of JOET encompasses the following research areas:

- Ships and offshore engineering:

  Design of ships and offshore structures; Resistance and propulsion; Seakeeping and maneuvering; Experimental and computational fluid dynamics; Ocean wave mechanics; Fatigue strength; Plasticity; Optimization and reliability; Arctic technology and extreme mechanics; Noise, vibration, and acoustics; Concrete engineering; Thermodynamics and heat transfer; Hydraulics and pneumatics; Autonomous and unmanned ship; Greenship technology; Digital twin of ships and offshore structures; Marine materials

- Coastal engineering:

  Coastal, port, and harbor structures; Waves transformation; Coastal and estuary hydrodynamics; Sediment transport and morphological change; Subsea geotechnics; Coastal groundwater management; Prevention or mitigation of coastal disaster; Coastal zone development and management; Shore protection technique; Coastal environmental process; Beach safety

- Ocean energy engineering:

  Offshore wind turbines; Wave energy platforms; Tidal current energy platforms; Floating photovoltaic energy platform; Small modular reactor; Combined energy platforms

- Marine robot engineering:

  Robot sensor system; Autonomous navigation; Robot equipment; Marine robot control; Environment mapping and exploration; Underwater communication and networking; Design of marine robots

 It is indexed in databases such as the Korean Citation Index (KCI), Google Scholar, Science Central, Korea Science, and the Directory of Open Access Journals (DOAJ). JOET offers PDF or XML versions for free on its website (https://www.joet.org). For business matters, authors need to contact KSOE Secretariat by email or phone (e-mail: ksoehj@ksoe.or.kr or Tel: +82 51 759 0656). Correspondences for publication matters can be asked via email to the Editor-in-Chief (e-mail: shahn@jwu.ac.kr).

KSOE

Journal of Ocean Engineering and Technology 38(2), 43−52, April, 2024
https://doi.org/10.26748/KSOE.2023.038

pISSN 1225-0767
eISSN 2287-6715

Original Research Article

Investigation of Seakeeping Performance of Trawler by the Influence of the Principal Particulars of Ships in the Bering Sea

Thi Thanh Diep Nguyen[1], Hoang Thien Vu[2], Aeri Cho[3] and Hyeon Kyu Yoon[4]

[1]*Researcher, Department of Naval Architecture and Marine Engineering, Changwon National University, Changwon, Korea*
[2]*Graduate Student, Department of Naval Architecture and Marine Engineering, Changwon National University, Changwon, Korea*
[3]*Graduate Student, Department of Smart Environmental Energy Engineering, Changwon National University, Changwon, Korea*
[4]*Professor, Department of Naval Architecture and Marine Engineering, Changwon National University, Changwon, Korea*

KEYWORDS: Trawler, Ship motion responses, Principal dimensions, Seakeeping performance, Sensitive analysis

ABSTRACT: *Investigating ship motion under real conditions is vital for evaluating the seakeeping performance, particularly in the design process stage. This study examined the influence of the principal particulars of a trawler on its seakeeping performance. The wave conditions in the Bering Sea are investigated using available data. The length-to-beam (L/B) and beam-to-draft (B/T) ratios of the ship are changed by 10% for the numerical simulation. The response amplitude operator (RAO) motion, root mean square (RMS) value and sensitivity analysis are calculated to evaluate the influence of the trawler dimensions on ship motions. The peak RAO motion affected the ship motions noticeably because of the resonance at the natural frequency. The L/B and B/T ratios are important geometric parameters of a ship that significantly influence its RMS motion, particularly in the case of roll and pitch. The change in the B/T ratio has a good seakeeping performance based on a comparison of the roll and pitch with the seakeeping criteria. The present results provide insights into the seakeeping performance of ships due to the influence of the principal dimensions in the design stage.*

1. Introduction

The seakeeping performance of a ship needs to be investigated thoroughly to ensure its safety at sea. The ship motions will affect its performance, the activities of the fisherman and the fishing performance of the fishing vessel. In addition, predicting the seakeeping performance of a ship in the sea is one of the most important concerns for naval architects at the design stage. Therefore, seakeeping performance is an important factor influencing the optimization of the ship hull form and its main dimensions. Moreover, considerable improvements in operability, habitability and survivability can be made by changing the main dimensions of the ship. In particular, identifying the principal particulars of the performance of a ship and those related to safety in the early design stage is important.

Many researchers have studied the influence of the hull form parameters of a fishing vessel on its performance. In particular, the impact of the hull form parameters on a ship performance was analyzed, such as the motion response for destroyer hulls (Bales, 1980), ranking of seakeeping performances (van Wijngaarden, 1984; Trincas et al., 2001; Alkan et al., 2003), the response amplitude operators (RAO) motion and root mean square (RMS) motion. On the other hand, the ship parameters also influence the stability and resistance of a ship (Park et al., 2011; Yu et al., 2011; Jeong et al. 2015; Yaakob et al., 2015; Manullang et al., 2017; Kim et al., 2020; Yu et al., 2021). On the other hand, these studies focus on the influence of the principal dimensions on the seakeeping performance. Therefore, research related to this topic was considered in a literature review. Kukner and Aydin (1997) investigated the influence of the ship parameters on the vertical motion of a fishing trawler in head waves. The length-to-beam (L/B) ratio, Froude number and beam-to-draft (L/T) ratio were examined. Moreover, regression analysis was performed to establish the relationship between heave and the ship length. Sayli et al. (2007) investigated the influence of the ship parameters on the heave and pitch. The functional relationships between hull form parameters and seakeeping characteristics of the fishing vessels were identified. Sayli et al. (2010) developed a

Received 17 November 2023, revised 8 January 2024, accepted 12 March 2024
Corresponding author Hyeon Kyu Yoon: +82-55-213-3683, hkyoon@changwon.ac.kr
This paper was presented at 15th International Symposium on Practical Design of Ships and other Floating Structures (Nguyen et al., 2022)

nonlinear meta-model of heave, pitch and vertical acceleration of a fishing vessel. The seakeeping performance data of the fishing vessel in regular head waves were used. The influence of the hull form parameters on the heave and pitch was obtained. Tello et al. (2011) studied the seakeeping characteristics of a series of fishing vessels to establish the seakeeping criteria for irregular waves. Fishing vessels are considered to operate in sea state 5 and sea state 6 in various Froude numbers and wave directions. The roll and pitch are the most important motion responses of a fishing vessel. Hence, Tello identified the pitch and roll criteria for seakeeping performance in sea state 5 and sea state 6. Cakici and Aydin (2014) identified a relationship between ship parameters and seakeeping characteristics for the YTU Gulet series. The strip method was applied to estimate the ship motion and the statistical short-term was used to analyze the seakeeping performance. The RMS of the heave, pitch and vertical acceleration were investigated in sea state 3 at the head wave.

Sayli et al. (2014) proposed a computer program that analyzed the most influencing parameters on the heave and pitch using a database. Using statistics, the weakest affected parameters were found and removed from the final model. Baree and Afroz (2017) evaluated the seakeeping performance of five series 60 ships regarding the added resistance in various wave directions. The influence of the Froude number, the principal particulars of the ship, wave direction and the seaway were analyzed. Sayli et al. (2016) proposed specifying the relational classification of small vessels based on their form parameters and the seakeeping performance of vertical motion, such as pitch, heave and vertical acceleration. The application was developed in the C# programming language based on the database and the K mean algorithm. Three categories were defined according to the results considering various Froude numbers, loading conditions and the wavelength to the ship length ratio. Manullang et al. (2017) discussed the influence of the ship dimensions and the ship hull shape on the ship motion responses in the following wave, beam wave and head wave. The L/T ratio was changed by 0.2 and 0.4 from the original value. The RMS of the roll and pitch are compared with the criteria reported by Tello et al. (2011).

Against this background, the present study aims to investigate the effect of the ship's principal dimensions of a ship on ship motion response in the Bering Sea. A fishing trawler was chosen to calculate the motion of a ship. First, the sea conditions in the Bering Sea were investigated based on the available data. The wave condition was determined from data obtained from Southeast Bering Sea buoys provided by the National Oceanic and Atmospheric Administration (NOAA). The average significant wave height and average wave period were investigated. Moreover, the average significant wave height and wave period were obtained. The wave conditions were chosen based on the average significant wave height and wave period. The L/B and B/T ratios were changed by 10% to investigate the effects of dimension on the motion responses of a ship. The motion of the fishing trawler was estimated using a numerical method. The RMS of roll and pitch were compared with the fishing vessel criteria suggested by Tello et al. (2011). Finally, the sensitivity of the ship motions due to the influence of the ship dimensions was analyzed. These results can be used to predict the seakeeping performance of fishing vessels and ensure their safety in the design phase.

2. Investigation Wave Condition in the Bering Sea

The trawler fishing vessel in the present study was designed to operate in the Bering Sea. The wave conditions in the Bering Sea were investigated to check the seakeeping performance in real sea conditions. The Bering Sea is one of several biologically productive subarctic seas. Moreover, the Bering Sea biological regime is often described as the richest and most productive. Indeed, the Bering Sea is extremely productive, especially for fish. This study examined the effect of the main ship dimensions on the seakeeping performance in the Bering Sea. The wave conditions in the Bering Sea were investigated to correctly check the seakeeping performance of the fishing vessels that operate in this area. The wave condition was determined using data measured from the Southeast in the Bering Sea buoys provided by NOAA, as shown in Fig. 1 (NOAA, 2022). The statistics for significant wave height and average wave period were investigated. The average significant wave height and wave period were obtained. The wave conditions were collected based on the data in 2022. Fig. 2 presents the significant wave height at the Bering Sea in 2022. A significant wave height is strongly felt in spring and winter due to the effect of storms. On the other hand, the sea is serene in summer and autumn, and the significant wave height changes only slightly. Fig. 3 shows the average wave period in the Bering Sea in 2022. As with the significant wave height, the average wave period is largest in spring and winter. Hence, long and high waves often appear

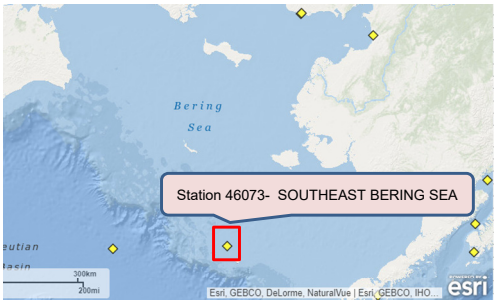

Fig. 1 Buoy position in the Bering Sea

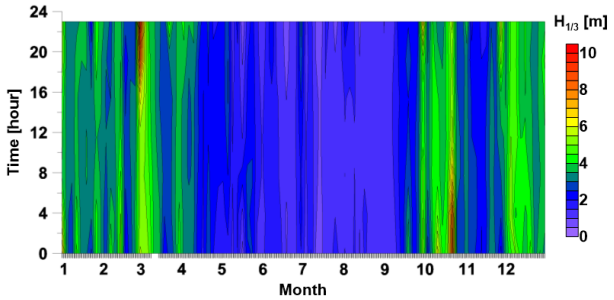

Fig. 2 Significant wave height in 2022

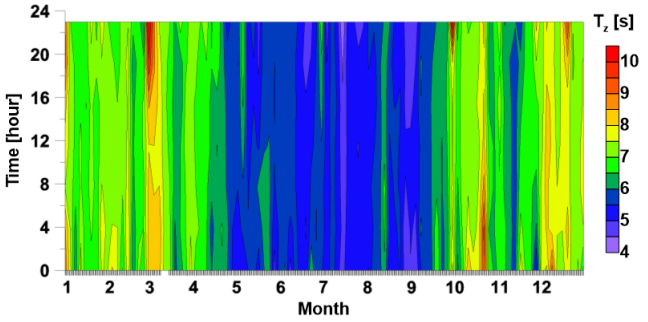

Fig. 3 Wave period in 2022

in the Bering Sea in spring and winter because of the influence of the storms. On the other hand, short and small waves appear in the Bering Sea in summer and autumn. The wave conditions were chosen based on the average significant wave height and wave period. Finally, a sea state with an average significant wave height of 2.44 m and an average wave period of 6.386 s was selected to investigate the seakeeping performance of the trawler fishing vessel.

3. Methodology

3.1 3D Panel Method

In the present study, the six degrees of freedom (6DOF) motion of a ship in regular waves is estimated using the three-dimensional panel method based on the theory of potential. The governing equation becomes the Laplace equation when the fluid is assumed to be inviscid, irrotational and incompressible (Nguyen et al., 2022). The free surface, body boundary and bottom conditions are estimated to calculate the distribution of pressure acting on the ship hull. The three-dimensional Laplace equation of the velocity potential in the fluid domain can be expressed as Eq. (1).

$$\frac{\partial^2\phi}{\partial x^2}+\frac{\partial^2\phi}{\partial y^2}+\frac{\partial^2\phi}{\partial z^2}=0 \tag{1}$$

According to potential theory, the velocity potential need must satisfy Eq. (1) because the velocity potential has the same value at any fluid point. In addition, the boundary condition should be satisfied on the free surface, body and bottom surface. Eq. (2) expresses the classical linear free surface condition of the steady state of the harmonic oscillatory motion of the wave frequency. The bottom boundary condition for the seafloor surface can be represented using Eq. (3). The body boundary condition for the mean wetted hull surface in terms of the diffraction and radiation potential can be expressed as Eqs. (4)–(5). ϕ, ω and d denote the velocity potential, wave frequency and sea depth, respectively.

$$-\omega^2\phi+g\frac{\partial\phi}{\partial z}=0 \quad \text{on} \quad z=0 \tag{2}$$

$$\frac{\partial\phi}{\partial z}=0 \quad \text{on} \quad z=-d \tag{3}$$

$$\frac{\partial\phi}{\partial n}=-\frac{\partial\phi}{\partial n} \quad \text{for diffraction potential} \tag{4}$$

$$\frac{\partial\phi}{\partial n}=-i\omega n_j \quad \text{for radiation potential} \tag{5}$$

The velocity potential is defined by the component of the wave-particle velocity as shown in Eq (6). Eq. (7) expresses the first-order velocity potential. g, ζ, s and θ are the gravity acceleration, wave amplitude, effective water depth and wave phase, respectively.

$$u=\frac{\partial\phi}{\partial x};v=\frac{\partial\phi}{\partial y};w=\frac{\partial\phi}{\partial z} \tag{6}$$

$$\phi^{(1)}=\frac{\zeta g}{\omega}\frac{\cosh ks}{\cosh kd}\sin\theta \tag{7}$$

The total velocity potential is divided into three components: diffraction potential ϕ_D, incident potential ϕ_I and radiation potential ϕ_R. Each component of the velocity potential must satisfy the governing equation in Eq. (1) and the boundary conditions in Eqs. (2)–(5). Eq. (8) expresses the total velocity potential. $\vec{X}=(X,Y,Z)$ is the location point on the body. ϕ_{Rj} and x_j are the potential of radiation waves caused by the ship motion and the ship motion in the j direction, respectively. ω_e is the encounter wave frequency.

$$\phi(\vec{X})e^{-i\omega_e t}=\left[(\phi_I+\phi_D)+\sum_{j=1}^{6}\phi_{Rj}x_j\right]e^{-i\omega_e t} \tag{8}$$

As the velocity potential is obtained, the first-order hydrodynamic distribution of pressure can be estimated using the Bernoulli equation in Eq. (9). ρ is the density of water.

$$p^{(1)}=\rho\left[i\omega_e\phi(\vec{X})+\vec{U}\nabla\phi(\vec{X})\right]e^{-i\omega_e t} \tag{9}$$

The first-order hydrodynamic forces on a ship can be determined by integrating the water pressure on the wetted surface using the pressure distribution. The first-order hydrodynamic forces on the body can be calculated using Eq. (9). Eq. (10) describes the first-order wave force by combining Eqs. (8) and (9). n_j and S are the unit normal vector and mean wetted surface of the ship hull, respectively. The total first-order hydrodynamic force can be written as Eq. (11). F_{Ij}, F_{Dj} and F_{Rjk} are the Froude-Krylov force, diffraction force and radiation force, respectively. These hydrodynamic forces can be calculated using Eqs. (11)–(14).

$$F_j e^{-i\omega_e t}=-\int_{S_0}p^{(1)}n_j dS=-\rho\left[(i\omega_e+\vec{U}.\nabla)\phi(\vec{X})\right]n_j dS \tag{10}$$

$$F_j=\left[(F_{Ij}+F_{Dj})+\sum_{k=1}^{6}F_{Rjk}x_k\right],j=1,\cdots,6 \tag{11}$$

$$F_{Ij}=-\rho\int_{S_0}\left[(i\omega_e+\vec{U}.\nabla)\phi_I(\vec{X})\right]n_j dS \tag{12}$$

$$F_{Dj} = -\rho \int_{S_0} \left[(i\omega_e + \vec{U}.\nabla)\phi_D(\vec{X}) \right] n_j dS \quad (13)$$

$$F_{Rjk} = -\rho \int_{S_0} \left[(i\omega_e + \vec{U}.\nabla)\phi_{Rk}(\vec{X}) \right] n_j dS \quad (14)$$

3.2 RMS Motion

The seakeeping performance of the ship is checked by calculating the RMS motion based on the irregular wave conditions and the RAO motion of the ship. The energy spectrum is estimated using Eqs. (15)–(17). z denotes heave. ϕ and θ denote roll and pitch, respectively. k is the wave number. The RMS motion value is determined as the square root of the variances. The variances and the RMS value of motion can be estimated using Eqs. (18)–(21), respectively. In order to estimate the wave spectrum $S(\omega)$, the ITTC spectrum was calculated using Eq. (22) (ITTC, 2014). $H_{1/3}$ and T_1 are the significant wave height and average wave period, respectively. In the case of the following and quartering waves, the wave frequency is considered to replace the encounter frequency to calculate the RMS motion to avoid the singularity in the encounter wave spectrum (Lewis, 1988).

$$S_z(\omega_e)d\omega_e = \left(\frac{z}{\zeta}\right)^2 S_\zeta(\omega_e)d\omega_e = RAO_z^2 S_\zeta(\omega_e)d\omega_e \quad (15)$$

$$S_\phi(\omega_e)d\omega_e = \left(\frac{\phi}{k\zeta}\right)^2 k^2 S_\zeta(\omega_e)d\omega_e = RAO_\phi^2 S_\alpha(\omega_e)d\omega_e \quad (16)$$

$$S_\theta(\omega_e)d\omega_e = \left(\frac{\theta}{k\zeta}\right)^2 k^2 S_\zeta(\omega_e)d\omega_e = RAO_\theta^2 S_\alpha(\omega_e)d\omega_e \quad (17)$$

where, $S_\alpha(\omega_e) = \frac{\omega^2}{g} S_\zeta(\omega_e) = k^2 S_\zeta(\omega_e)$.

$$m_{0_z} = \int_0^\infty S_z(\omega_e)d\omega_e \quad (18)$$

$$m_{0_\phi} = \int_0^\infty S_\phi(\omega_e)d\omega_e \quad (19)$$

$$m_{0_\theta} = \int_0^\infty S_\theta(\omega_e)d\omega_e \quad (20)$$

$$\sigma_z = \sqrt{m_{0_z}} \;;\; \sigma_\phi = \sqrt{m_{0_\phi}} \;;\; \sigma_\theta = \sqrt{m_{0_\theta}} \quad (21)$$

$$S_\omega = \frac{A}{\omega^5} e^{-\frac{B}{\omega^4}} \quad (22)$$

$$A = 173(H_{1/3})^2/T_1^4 \;;\quad B = 691/T_1^4 \quad (23)$$

3.3 Sensitivity Analysis

In sensitivity analysis, a sensitivity index measures how sensitive the output of a model is to changes in its input parameters or variables. It quantifies the degree to which variations in the inputs affect the output. A higher sensitivity index indicates that a small change in the input parameter has a significant impact on the output, while a lower sensitivity index suggests that the output is less sensitive to changes in that particular input. The sensitivity index for RMS motion S_{ijk} is estimated using Eq. (24). H^* denotes the origin principal dimension of the ship. H represents the deviated value of the principal dimensions of a ship. R^* denotes the value of the corresponding RMS motion value obtained from the original ship using H^*. R represents the corresponding RMS motion values obtained from the modified ship using H. S_{ijk} is the sensitivity index for the i^{th} RMS motion for the $k\%$ change in the j^{th} principal dimension. The influence of principal dimensions on the seakeeping performance, such as the RMS motion, is considered.

$$S_{ijk}^* = \frac{|R - R^*|/R^*}{|H - H^*|/H^*} \quad (24)$$

4. Target Ship and Test Condition

In this study, a fishing trawler is selected to perform assess the seakeeping performance in the Bering Sea. The principal particulars of the fishing trawler in the case of the original are summarized in Table 1. Fig. 4 shows the modeling of the fishing trawler used in the present research. The *L/B* and *B/T* ratios are changed by 10% to investigate the effects of dimensions on the ship's motion response. In the case of a change in the *L/B* ratio, *L* was changed by ± 10% and *B* was kept constant and *B* was changed by ± 10 % and *T* was kept constant in the case of *B/T*. In order to estimate the RMS motion, the numerical simulation of the motion RAO of the fishing trawler is performed at a ship speed of 6 knots. The simulation is conducted to examine the effect of regular waves on the fishing trawler in various wave directions and provide the input data of the RAO motion responses for calculating irregular wave motion responses. The range of wave directions is from 0 degrees to 180 degrees at 30 degrees intervals. The wave frequency ranges from 0.3 rad/s to 3.0 rad/s in 0.1 rad/s intervals. The wave directions are defined, as shown in Fig. 5. In the case of irregular waves, a sea state with an average significant wave height of 2.44 m and an average wave period of 6.386 s were selected to investigate the seakeeping performance of the trawler fishing vessel. Furthermore, according to the ITTC recommendation for numerical estimation of roll damping, roll damping was significantly affected by the viscous effect. In this study, the additional roll damping for the fishing vessel was divided into 5 components: wave making, hull lift, frictional, eddy making and skeg component (ITTC, 2011).

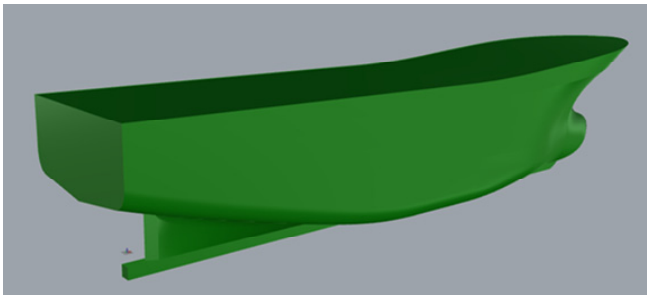

Fig. 4 Trawler fishing vessel

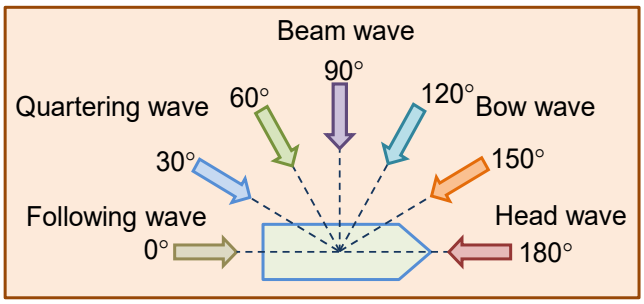

Fig. 5 Definition of the wave direction

Table 1 Principal dimensions

Item	Unit
Length between perpendiculars, L (m)	32.450
Beam, B (m)	9.000
Displacement, △ (t)	587.000
Draft, T (m)	3.000
Speed, U (m/s)	3.086
Roll radius of gyration, k_{xx} (m)	0.400 B
Pitch radius of gyration, k_{yy} (m)	0.250 L
Yaw radius of gyration, k_{zz} (m)	0.250 L
Vertical center of gravity, VCG (m)	3.590

5. Result and Discussion

5.1 RAO Motion

A numerical simulation of the motion RAO of the fishing trawler is carried out to estimate the RMS motion. The effect of the regular waves on the fishing trawler in various wave directions is investigated. The L/B and B/T ratios are changed by 10% to investigate the effect of dimension on the ship's motion response. The natural frequency of heave, roll and pitch are calculated due to the influence of a change in the main dimensions of the ship. The natural frequencies of heave, roll and pitch can be determined using Eqs. (25)–(27). m, m_a and A_W denote the mass of the ship, added mass and water plane area, respectively. GM_T and GM_L are the transverse and longitudinal metacentric heights of the ship, respectively. I_{xx} and I_{yy} are the roll and pitch moment of inertia of the ship, respectively. J_{xx} and J_{yy} are the added inertia moment in roll and pitch, respectively. Table 2 lists the natural frequencies due to the influence of the ship dimensions.

$$\omega_{n_z} = \sqrt{\frac{\rho g A_W}{m+m_a}} \tag{25}$$

$$\omega_{n_\phi} = \sqrt{\frac{mgGM_T}{I_{xx}+J_{xx}}} \tag{26}$$

$$\omega_{n_\theta} = \sqrt{\frac{mgGM_L}{I_{yy}+J_{yy}}} \tag{27}$$

Table 2 Natural frequency

Item	Heave (rad/s)	Roll (rad/s)	Pitch (rad/s)
Original	1.486	0.703	1.547
L/B + 10%	1.488	0.706	1.556
L/B − 10%	1.487	0.704	1.536
B/T + 10%	1.489	0.840	1.571
B/T − 10%	1.489	0.493	1.571

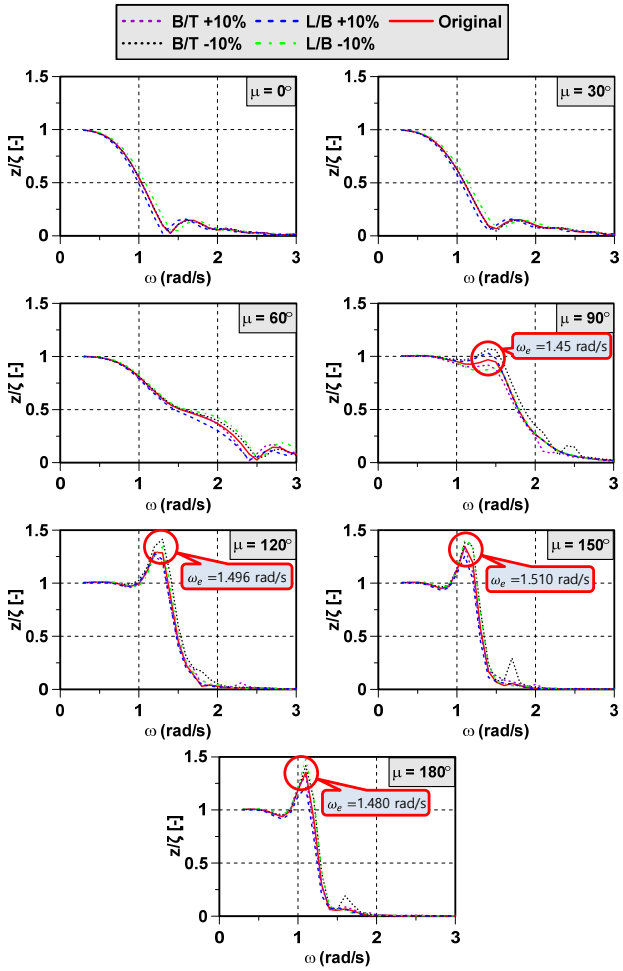

Fig. 6 Heave RAO

Fig. 6 compares the heave RAO according to the change in L/B, B/T ratios and wave directions. The greatest heave RAO of the ship occurs when the wave direction approaches 180 degrees. As the wave frequency increases, the heave RAO tends to decrease. In short waves, however, the heave decreases to zero, especially when the wavelength is short compared to the ship length. The heave RAO tends to be 1 in the long waves because the heave follows the wave elevation. The heave RAO varies slightly depending on the ship dimensions. In general, the heave RAO is the largest when the B/T ratio was reduced by 10% when the wave direction approaches 90 degrees. On the other hand, the heave RAO is the largest when the L/B ratio is reduced by 10% and the wave direction approaches 180 degrees. Hence, the heave RAO does not depend much on the ship dimension. The numerical

results showed that the heave RAO is the largest when the encounter frequency is close to the heave natural frequency. The heave RAO depends on the water plane area and the ship displacement. The ship displacement and water plane area increased when the *L*/*B* and *B*/*T* ratios were increased by 10%. The displacement and waterplane area of a ship are proportional to each other; therefore, the heave natural frequency does not change when the principal dimensions are changed. Table 2 lists the natural frequency of heave according to the *L*/*B* and *B*/*T* ratio.

Fig. 7 shows the roll RAO at various *L*/*B* and *B*/*T* ratios and wave directions. The numerical results showed that the roll RAO becomes dominant when the wave direction is close to 90 degrees and decreases as the wave direction approached 0 degrees and 180 degrees. The roll RAO with different *B*/*T* ratios changes dramatically in various wave directions because of the effect of the breadth of the ship. The roll RAO decreases as the wave frequency increases. The peak roll RAO occurs at an encounter frequency close to the natural frequency of the roll. The numerical results of the roll RAO in the beam wave showed that the peak roll RAO according to the *L*/*B* ratio and the ship origin occurs at encounter frequency of 0.7 rad/s. This value is approximately the roll natural frequency according to the *L*/*B* ratio and the original ship. The peak roll RAO when the *B*/*T* ratio is reduced by 10% occur at the encounter frequency of 0.9 rad/s, which is close to the roll natural frequency of *B*/*T* ratio reduced by 10%. The peak roll RAO when the *B*/*T* ratio is increased by 10% occurs at an encounter frequency of 0.5 rad/s, which is approximately the roll natural frequency of the *B*/*T* ratio increased by 10%.

Fig. 8 presents the numerical results of the pitch RAO of the various *L*/*B* and *B*/*T* ratios and wave directions. The largest pitch RAO of the ship occurs when the wave direction approaches 0 degrees due to the effect of the forward speed. The pitch RAO tended to decrease significantly as the wave frequency increases. Moreover, the pitch response is combined with the heave. Therefore, the motion responses of heave and pitch are the same phenomenon. The pitch RAO is the largest for the *L*/*B* ratio reduced by 10%. From the numerical results, the peak pitch RAO occurs at a wave frequency near the pitch natural frequency. The numerical results of the pitch RAO in the head wave showed that the peak pitch RAO in the original ship occurs at an encounter frequency of 1.5 rad/s. This is approximately the pitch natural pitch frequency of the original ship. The peak pitch RAO when the *L*/*B* ratio was increased by 10% occurs at an encounter frequency of 1.566 rad/s and a wave direction of 120 degrees. The peak pitch RAO when the *L*/*B* ratio is decreased by 10% occurs at an encounter frequency of 1.510 rad/s and a wave direction of 150 degrees. The

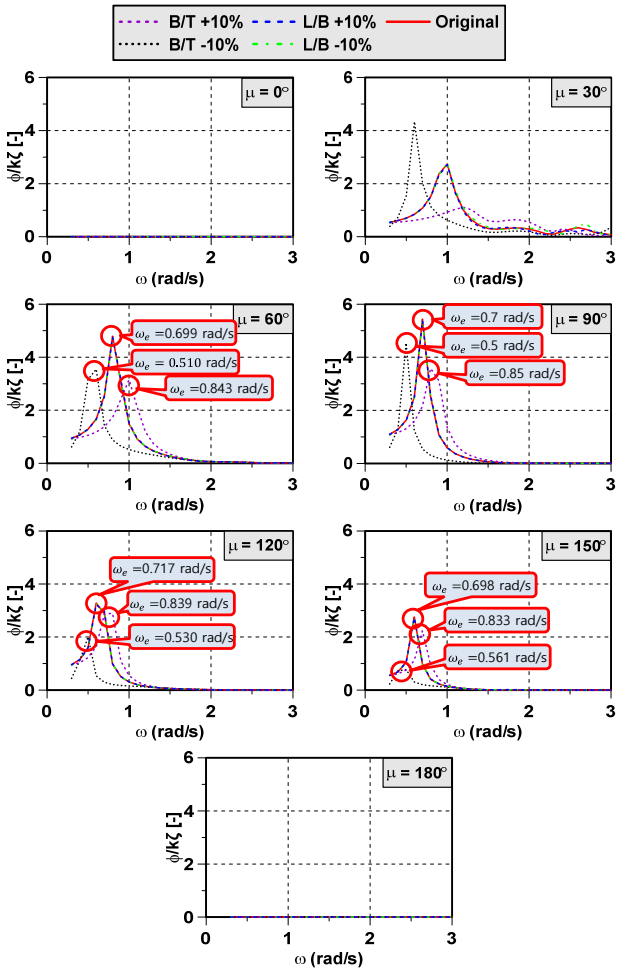

Fig. 7 Roll RAO

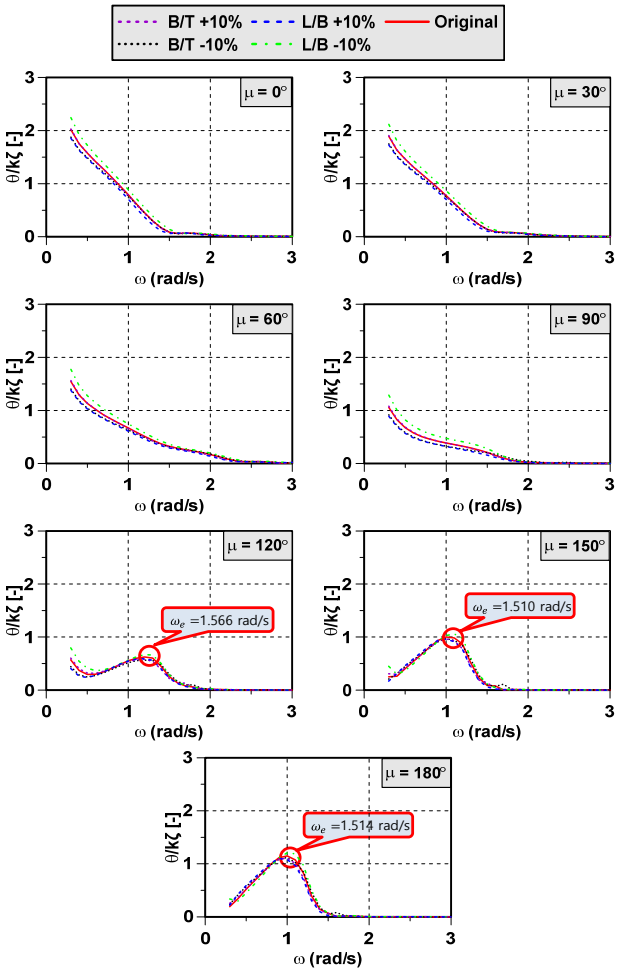

Fig. 8 Pitch RAO

peak pitch RAO when the *B/T* ratio is increased by 10% occurs at an encounter frequency of 1.514 rad/s at a wave direction of 180 degrees. Generally, the peak heave, roll and pitch occur at an encounter frequency close to the natural frequency. Table 2 lists the natural frequency of the heave, roll and pitch due to a change in the ship dimensions.

The ship motion responses are affected noticeably in the peak values due to a change in the *L/B* and *B/T* ratios because of resonance at the natural frequency. The varied ship dimensions affect the inertia moment, displacement and roll damping coefficient directly. The heave tends to increase when the displacement increases. A longer ship may have a longer waterline, which can affect the buoyancy distribution and the response to wave-induced heave. Longer ships tend to experience a reduced pitch. The longer waterline provides more resistance to pitch, and the ship is less sensitive to changes in trim caused by pitching. The increased inertia caused by the longer length contributes to a smoother response to wave-induced pitch motions. Furthermore, the roll is influenced the most by the beam of the ship. Hence, the roll period can determine the comfort of those operating on board.

5.2 RMS Motion

In the case of irregular waves, a sea state is chosen to estimate the wave spectrum in the Bering Sea based on the results of the investigated wave conditions. The average significant wave height and wave period were 2.44 m and 6.386 s, respectively. The ITTC spectrum recommended by the International Towing Tank Conference was used to estimate the wave spectrum.

Fig. 9 compares the RMS heave in the original ship to the RMS heave in the ship with changed ratios of *L/B* and *B/T*. The heave is the strongest in the bow wave, head wave and beam wave. The RMS heave changes slightly as the principal dimensions of the ship changed. In the case of increased and decreased *L/B* ratio, the RMS heave varied by −4.841% and 4.312% in the head wave, respectively, compared to the original case. In the case of increased and decreased *B/T* ratio, the RMS heave varied by −0.270% and 2.561% in the head wave, respectively, compared to the original case.

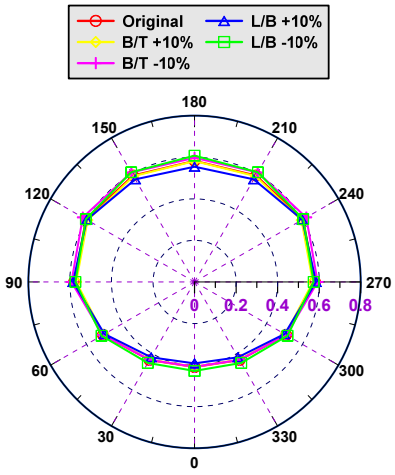

Fig. 9 RMS heave (m)

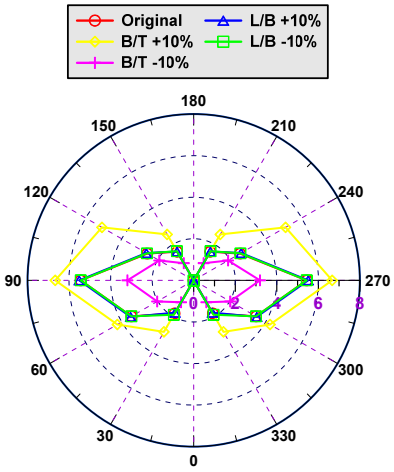

Fig. 10 RMS roll (deg.)

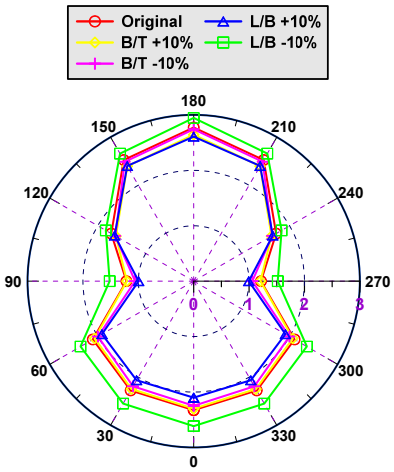

Fig. 11 RMS pitch (deg.)

Fig. 10 compares the RMS roll in the original ship to the RMS roll in the ship according to the *L/B* and *B/T* ratios. The roll changes noticeably in various wave directions. The strongest roll is observed with a wave direction of 90 degrees. The breadth of a ship strongly influences the motion responses, particularly the roll. Based on the RMS roll, the effect of the ship length is not significant. In the case of increased and decreased *L/B* ratio, the RMS roll varied by 1.285% and −0.023% in the beam wave compared to the original case. In the case of increased and decreased *B/T* ratio, the RMS roll varied by 22.514% and −41.347% in the beam wave, respectively, compared to the original case.

The comparison of the RMS pitch in the original ship to the RMS pitch in the ship according to the *L/B* and *B/T* ratios is shown in Fig. 11. The pitch changes strongly in various wave directions. The strongest pitch motion is observed at the head wave. The smallest pitch occurs at the beam wave. On the other hand, the pitch at a wave direction of 90 degrees does not become zero due to the effect of the forward speed. The pitch motion increases dramatically as the wave direction ranges nearly to quartering waves. The principal particulars of the ship strongly affect the pitch motion. Based on the RMS pitch,

Table 3 Verification of the seakeeping criteria in sea state 5 (Satisfied: O; Unsatisfied: X)

Item	Roll RMS (deg.)			Pitch RMS (deg.)		
	Max.	Criteria	Satisfied	Max.	Criteria	Satisfied
Original	6.572	6	X	2.773	3	O
L/*B* + 10%	6.612		X	2.609		O
	6.530		X	2.945		O
	5.938		O	2.642		O
	2.932		O	2.741		O

the effect of the ship's length is larger than the ship's breadth, particularly when the *L*/*B* ratio is decreased by 10%. In the case of increased and decreased *L*/*B* ratio, the RMS pitch varied by −5.910% and 6.201% in the head wave, respectively, compared to the original case. In the case of increased and decreased *B*/*T* ratio, the RMS pitch varied by −4.724% and −1.150% in the head wave, respectively, compared to the original case.

The seakeeping performance is checked by comparing the maximum roll and RMS pitch with the seakeeping criteria suggested by Tello et al. (2011), as listed in Table 3. The pitch motion can meet the seakeeping criteria in the origin ship and the ship with changed *L*/*B* and *B*/*T* ratios. On the other hand, the RMS roll was slightly greater than the seakeeping criteria, except in the case of a change in *B*/*T* ratio.

5.3 Sensitivity Analysis

Sensitivity analysis of the *L*/*B* and *B*/*T* ratios is done by deviating each *L*/*B* and *B*/*T* ratio by 10%. Figs. 12−14 show the effects of the *L*/*B* and *B*/*T* ratios on the RMS heave, roll and pitch, respectively. The sensitivity of the RMS heave is the highest in the head wave and the following wave. Moreover, the *L*/*B* ratio has the greatest influence on the RMS heave. Similar to the same trend of the RMS heave, the *L*/*B* ratio also has the greatest impact on the RMS pitch. The reason for such relationships is the coupling of the heave and pitch motions. The sensitivity of the RMS pitch increases noticeably with the following wave and stern waves. In contrast to the sensitivity of the heave and RMS pitch, the RMS roll sensitivity becomes zero in the following wave and the heave wave because of the direction of the incident wave. The RMS roll sensitivity is strongly affected by the *B*/*T*, ratio, especially at a wave direction of 120 degrees. The *L*/*B* ratio has a negligible influence on the RMS roll sensitivity.

The *L*/*B* and *B*/*T* ratios are important geometric parameters of a ship that significantly influence its RMS motion. The *L*/*B* and *B*/*T* ratios influence the ship motions through their effects on stability, buoyancy distribution, displacement and the response of the ship to wave-induced forces. The sensitivity index of the RMS heave changes slightly in various wave directions. In other words, the sensitivity of RMS heave is negligible under the influence of the *L*/*B* and *B*/*T* ratio. Nevertheless, the sensitivity index of the RMS roll varies significantly in various wave directions because of the influence of the B/T ratio and the roll is influenced the most by the breadth of the ship. In the

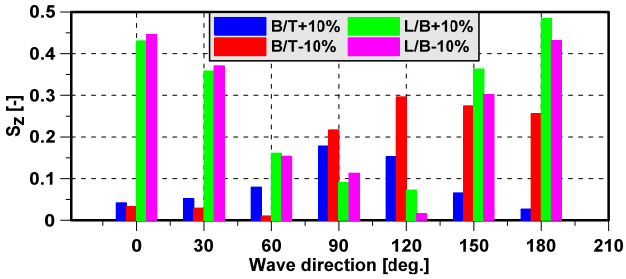

Fig. 12 Sensitivity index of RMS heave

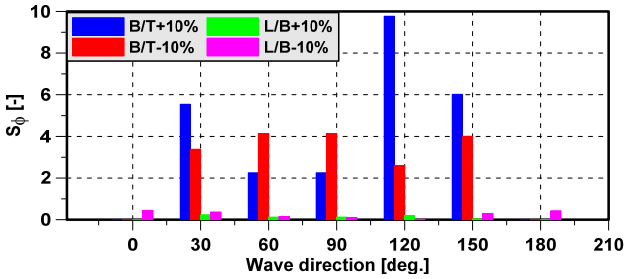

Fig. 13 Sensitivity index of RMS roll

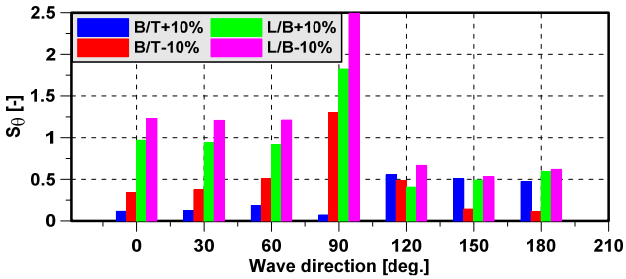

Fig. 14 Sensitivity index of RMS pitch

case of pitch, the sensitivity index of the RMS pitch changes drastically due to the influence of the *L*/*B* ratio.

6. Conclusion

This paper reported the effects of the principal dimensions of a ship on a trawler fishing vessel in the Bering Sea. The final remarks are as follows:

First, the sea condition in the Bering Sea was investigated based on the available data. The statistics of significant wave height and average wave period were analyzed. A sea state was then chosen using the average value of the significant wave height and wave period.

Second, the *L*/*B* and *B*/*T* ratios were changed by 10% to determine the effect of the dimension on the motion responses of a ship. As shown in the RAO and RMS motion results, the *L*/*B* ratio affected the heave and pitch. In contrast, the roll was influenced substantially by the *B*/*T* ratio. Moreover, the influence of the *L*/*B* and *B*/*T* ratios on the RMS motion was also investigated. The maximum RMS roll and pitch were compared with the seakeeping criteria suggested by Tello et al. (2011).

Third, the sensitivity index of the *L*/*B* and *B*/*T* ratios on the RMS

heave, roll and pitch was analyzed. The sensitivity of the RMS heave was highest in the head wave and the following wave. The heave and the pitch were coupled. Therefore, the sensitivity trends of the heave and the pitch are similar and the *L*/*B* ratio has the largest impact on the RMS heave and pitch. In contrast to the sensitivity of the RMS heave and RMS, the sensitivity of the RMS roll becomes zero in the following wave and heave wave because of the direction of the incident wave. The sensitivity of the RMS roll is strongly affected by the *B/T* ratio, especially at a wave direction of 120 degrees. The *L*/*B* ratio has a negligible influence on the sensitivity of the RMS roll.

Finally, the change in *B/T* ratio has a good seakeeping performance based on a comparison of the roll and pitch with the seakeeping criteria. On the other hand, the increased beam can cause ship stability problems due to a change in the righting arm (GZ) curve because the inflection point of the GZ curve occurs at a small inclination angle. The reduced beam shortens the natural period of a ship. Its acceleration and comfort are affected. In addition, the *B/T* ratio influences the wave-making resistance. Generally, lower *B/T* ratios are associated with lower wave resistance, leading to better propulsion efficiency. Nevertheless, extremely low *B/T* ratios may increase the susceptibility to parametric rolling. On the other hand, the change in *L*/*B* has less seakeeping performance, particularly in roll based on a comparison of roll seakeeping criteria. A higher *L*/*B* ratio generally contributes to better stability in waves. Longer ships tend to have smoother motions and are less prone to rolling, which is particularly important for passenger comfort and safety. Longer ships experience less wave resistance, leading to improved fuel efficiency, but extremely long and slender ships may face challenges related to structural strength. Although these ratios provide insights into the seakeeping performance of a ship, they are just one set of parameters that naval architects should consider. The actual impact of these ratios depends on various factors, including the specific design, the purpose of the ship, operational conditions, and intended trade routes.

Conflict of Interest

Hyeon Kyu Yoon serves as a journal publication committee member of the Journal of Ocean Engineering and Technology, but he had no role in the decision to publish this article. The authors have no potential conflict of interest relevant to this article.

Funding

This work was supported by the Korea Institute for Advancement of Technology (KIAT) grant funded by the Korean Government (MOTIE) (P0017006, The Competency Development Program for Industry Specialist).

References

Alkan, A. D., Ozmen, G., & Gammon, M. A. (2003). Parametric relation of seakeeping. In *9th International Symposium on Technics and Technology in Fishing Vessels.*

Bales, N. K. (1980). Optimizing the seakeeping performance of destroyer type hulls. In *13th Symposium on Naval Hydrodynamics.*

Baree, M. S., & Afroz, L. (2017). Seakeeping performance of series 60 ships. *Procedia Engineering, 194*, 189−196. https://doi.org/10.1016/j.proeng.2017.08.134

Cakici, F., & Aydin, M. (2014). Effects of hull form parameters on Seakeeping for YTU gullet series with cruiser stern. *International Journal of Naval Architecture and Ocean Engineering*, *6*(3), 700−714. https://doi.org/10.2478/IJNAOE-2013-0206

ITTC. (2011). *Recommended procedures and guidelines: Numerical estimation of roll damping* (7.5-02-07-04.5). https://www.ittc.info/media/8151/75-02-07-045.pdf

ITTC. (2014). *Recommended procedures and guidelines: Seakeeping experiments* (7.5-02-07-02.1). https://www.ittc.info/media/8101/75-02-07-021.pdf

Jeong, U. C., Kim, H. S., Kwon, S. Y., & Choi, J. H. (2015). Study of hull form development of 5-ton-class catamaran-type coastal fishing boat for welfare accommodation of fishing crew. *Journal of Ocean Engineering and Technology*, *29*(6) 405−410. https://doi.org/10.5574/KSOE.2015.29.6.405

Kim, M. S., Hwang, B. K., & Chang, H.Y. (2020). Analysis of efficiency of fishing operation by the change in the size of coastal composite fishing boat. *Journal of the Korean Society of Fisheries and Ocean Technology*, 56(2), 126−137. https://doi.org/10.3796/ KSFOT.2020.56.2.126

Kukner, A., & Aydin, M. (1997). Influence of design parameters on vertical motion of trawler hull forms in head seas. *Journal of Marine Technology and SNAME News*, 34(3), 181−196. https://doi.org/10.5957/mt1.1997.34.3.181

Lewis, E. V. (Ed.). (1988). *Principal of Naval Architecture: vol. III - Motion in Waves and Controllability*. The Society of Naval Architects and Marine Engineers.

Manullang, S., Fadillah, A., & Irvana, R. (2017). Analysis of stability, resistance and seakeeping accord to dimension and form of fishing vessel 30 GT. *Marine Technology for Sustainable Development*, 68−75.

National Oceanic and Atmospheric Administration (NOAA). (2022). *Station 46073 (LLNR 1199) − Southeast Bering Sea - 205 NM WNW of Dutch Harbor, AK.* Historical data - Standard meteorological data. https://www.ndbc.noaa.gov/station_history.php?station=46073

Nguyen, T. T. D., Nguyen, V. M., & Yoon, H. K. (2022). Experimental and numerical simulation on dynamics of a moored semi-submersible in various wave directions. *Science Progress*, *104*(4). https://doi.org/10.1177/0036850422109600

Park, R. S., Kim, S. G., & Lee, J. B. (2011). Study on motion response characteristics for large inclined state of small fishing vessel in

beam sea condition, *Journal of Ocean Engineering and Technology*, *25*(6). 17−22. https://doi.org/10.5574/KSOE.2011.25.6.017

Sayli, A., Alkan, A. D., & Aydin, M. (2016). Determination of relational classification among hull form parameters and ship motions performance for a set of small vessels. *Brodogradnja*, *67*(4), 1−15. https://doi.org/10.21278 /brod67401

Sayli, A., Alkan, A. D., & Ganiler, O. (2010). Nonlinear meta-models for conceptual seakeeping design of fishing vessels. *Ocean Engineering*, *37*(8−9), 730−741. https://doi.org/10.1016/j.oceaneng.2010.02.005

Sayli, A., Alkan, A. D., Nabergoj, R., & Uysal, A. O. (2007). Seakeeping assessment of fishing vessels in conceptual design stage. *Ocean Engineering*, *34*(5−6), 724−738. https://doi.org/10.1016/j.oceaneng.2006.05.003

Sayli, A., Alkan, A. D., & Uysal, A. O. (2014). Automatic elimination of ship design parameters based on data analysis for seakeeping performance. *Brodogradnja/Shipbilding*, *65*(4), 1−19.

Tello, M., Silva, S. A., & Soares, C. G. (2011). Seakeeping performance of fishing vessels in irregular wave. *Ocean Engineering*, *38*, 763−773, https://doi.org/10.1016/j.oceaneng.2010.12.020

Trincas, G., Nabergoj, R., & Messina, G. (2001). Inverse problem solution to identify optimal hull forms of fishing vessels for efficient operation. In *8th International Symposium on Technics and Technology in Fishing Vessels.*

van Wijngaarden, A. M. (1984). The optimum form of a small hull for the North Sea area. *International Shipbuilding Progress*, *31*(359), 181−187. https://doi.org/10.3233/ISP-1984-3135902

Yaakob, O., Hashim, F. E., Jalal, M. R., & Mustapa, M. A. (2015). Stability, seakeeping and safety assessment of small fishing boats operating in southern coast of Peninsular Malaysia. *Journal of Sustainability Science and Management*, *10*(1), 50−56.

Yu, J. W., Lee, M. K., Kim, Y. I., Suh, S. B., & Lee, I. (2021). An optimization study on the hull form and stern appendage for improving resistance performance of a coastal fishing vessel. *Applied Sciences*, *11*(6124), 6124. https://doi.org/10.3390/app11136124

Yu, J. W., Lee, Y. G., Park, A. S., Ha, Y. J., Park, C. K., & Choi, Y. C. (2011). A study on the resistance performance of Korean high speed small coastal fishing boat. *Journal of the Society of Naval Architects of Korea*, *48*(2), 158−164. https://doi.org/10.3744/SNAK.2011.48.2.158

Author ORCIDs

Author name	ORCID
Nguyen, Thi Thanh Diep	0000-0003-3521-6680
Vu, Hoang Thien	0000-0001-8147-0597
Cho, Aeri	0009-0006-0014-1729
Yoon, Hyeon Kyu	0000-0001-6639-0927

KSOE

Journal of Ocean Engineering and Technology 38(2), 53-63, April, 2024
https://doi.org/10.26748/KSOE.2024.046

pISSN 1225-0767
eISSN 2287-6715

Original Research Article

Optimization Analysis of the Shape and Position of a Submerged Breakwater for Improving Floating Body Stability

Sanghwan Heo[1,3], Weoncheol Koo[2] and MooHyun Kim[4]

[1]*Research Associate, Department of Naval Architecture and Ocean Engineering, Inha University, Incheon, Korea*
[2]*Professor, Department of Naval Architecture and Ocean Engineering, Inha University, Incheon, Korea*
[3]*Visiting Scholar, Department of Ocean Engineering, Texas A&M University, USA*
[4]*Professor, Department of Ocean Engineering, Texas A&M University, USA*

KEYWORDS: Submerged breakwater, Hydrodynamics, Frequency-domain boundary element method, Optimization analysis, Particle swarm optimization

ABSTRACT: *Submerged breakwaters can be installed underneath floating structures to reduce the external wave loads acting on the structure. The objective of this study was to establish an optimization analysis framework to determine the corresponding shape and position of the submerged breakwater that can minimize or maximize the external forces acting on the floating structure. A two-dimensional frequency-domain boundary element method (FD-BEM) based on the linear potential theory was developed to perform the hydrodynamic analysis. A metaheuristic algorithm, the advanced particle swarm optimization, was newly coupled to the FD-BEM to perform the optimization analysis. The optimization analysis process was performed by calling FD-BEM for each generation, performing a numerical analysis of the design variables of each particle, and updating the design variables using the collected results. The results of the optimization analysis showed that the height of the submerged breakwater has a significant effect on the surface piercing body and that there is a specific area and position with an optimal value. In this study, the optimal values of the shape and position of a single submerged breakwater were determined and analyzed so that the external force acting on a surface piercing body was minimum or maximum.*

1. Introduction

With the increasing demand for industrial and residential land, studies have been conducted on the construction of very large floating structures, such as floating airports, floating bridges, and multipurpose marine spaces, by installing floating structures in coastal and offshore areas (Watanabe et al., 2004; Lamas-Pardo et al., 2015). The first step in the design of such floating structures is to conduct a hydrodynamic analysis considering wave loads (Tavana and Khanjani, 2013). To reduce the hydroelastic responses of floating structures, various methods have been presented, including submerged breakwaters, floating breakwaters, and oscillating water column chambers. Among them, submerged breakwaters are the most effective structures (Wang et al., 2010). The main purpose of submerged breakwaters is to increase reflected waves and dissipate the wave energy or reduce the energy of transmitted waves (Huang et al., 2003) for reducing the wave loads acting on floating structures.

Two-dimensional (2D) domain analysis is mainly conducted in studies on submerged breakwaters because breakwaters are installed parallel to the shoreline and have a constant cross-section with a long shape. Studies have been actively conducted to analyze the changes in water surface caused by submerged breakwaters. Koley et al. (2020) conducted an experiment and boundary element method (BEM)-based numerical analysis on permeable rubble mound breakwaters. They conducted a parametric study on the shape of breakwaters and analyzed its effects on reflection, dissipation, and transmission coefficients. Jeong et al. (2021) analyzed the change in the transmission coefficient of submerged breakwaters composed of tetrapods using the environmental conditions of the coast of Korea, empirical formulas, and a wave deformation model (WADEM). Khan et al. (2021) analyzed the reflection and dissipation of incident waves caused by multi-layered trapezoidal porous rubble mound breakwaters using the multi-domain boundary element method (MDBEM). Loukili et al. (2021) analyzed the change in the reflection and transmission

Received 6 February 2024, revised 18 February 2024, accepted 25 February 2024
Corresponding author Weoncheol Koo: +82-32-860-7348, wckoo@inha.ac.kr

coefficients caused by a single rectangular submerged breakwater using the meshless singular boundary method. Ni and Teng (2021a; 2021b) analyzed the reflection coefficient of the porous rectangular and trapezoidal submerged breakwaters installed on a permeable inclined seabed using a modified mild-slope equation. They conducted a parametric analysis of the Bragg resonance caused by the porosity, the number and height of breakwaters, the distance between breakwaters, and the slope of the seabed. Patil and Karmakar (2021) conducted a parametric analysis of the reflection and transmission coefficients of impermeable and permeable submerged breakwaters in various shapes using MDBEM. These numerical analysis studies were conducted in the frequency domain. Time-domain numerical analysis and experimental studies have also been actively conducted. Lee et al. (2019) conducted an experimental study on tide-adapting submerged breakwaters and reported that their wave-breaking performance is superior to that of ordinary submerged breakwaters. Lee et al. (2002) conducted an experimental and numerical study on the distribution of vorticity, turbulence, and wave height according to the density, width, and arrangement of submerged rigid vegetation. Min et al. (2023) analyzed the reflection, transmission, and dissipation coefficients of dual submerged breakwaters using a fully nonlinear numerical wave tank (NWT) based on the boundary element method considering porous domain. They also conducted an analysis of the change in wave height caused by breakwaters and the pressure distribution inside permeable submerged breakwaters.

Studies have been actively conducted considering the interaction between submerged breakwaters and rear structures in the 2D domain. Their main purpose was to reduce the wave load acting on the structures by increasing reflected waves or dissipating the wave energy through the change in flow field caused by submerged breakwaters. Manisha et al. (2019) analyzed the reflected waves and the reduction in the wave load acting on floating bridges caused by various shapes of submerged breakwaters or trenches. Vijay et al. (2021) conducted a parametric analysis of reflection and transmission coefficients and the external forces acting on floating docks considering the interaction between submerged breakwaters in various shapes and fixed floating docks. Jiang et al. (2022) analyzed the reflection, dissipation, and enhancement coefficients by double and triple submerged breakwaters using the volume-averaged Reynolds-averaged Navier–Stokes equation (VARANS). They also analyzed the effect of submerged breakwaters on the external forces acting on a vertical breakwater, and reported that triple submerged breakwaters with high porosity most efficiently reduce the wave external force acting on the rear structure.

The design of submerged breakwaters for the reduction in wave loads acting on floating bodies and their dynamic stability involves numerous design variables, such as the distance between the floating body and breakwaters and the shape of breakwaters. To analyze the optimization problem for these design variables, metaheuristic algorithms that can effectively find the maximum or minimum value based on the objective function are used. Metaheuristic algorithms can be classified into evolutionary algorithms, swarm-based algorithms, physics-based algorithms, and human-based algorithms (Kaveh and Mesgari, 2023). Metaheuristic algorithms are also widely used in the field of ocean engineering. Zhu et al. (2022) conducted an optimization analysis of the layout of wave energy converters using artificial neural networks and adaptive genetic algorithms. Ferri and Marino (2023) conducted an optimization analysis of substructures for 10 MW-class floating offshore wind turbines using genetic algorithms. Gandomi et al. (2023) analyzed the reflection and transmission coefficients of by permeable breakwaters using the conditional value-at-risk method (CvaR) based on the multilayer perceptron neural network and second-generation nondominated sorting genetic algorithm (NSGA-II). Jeong and Koo (2023) conducted an optimization analysis of the power output of wave energy converters using the three-dimensional frequency-domain boundary element method (FD-BEM) based on the potential flow theory. They compared the optimization analysis results for genetic algorithms, simulated annealing, particle swarm optimization (PSO), and advanced PSO (Chen et al., 2018), and described the superiority of advanced PSO. Zhang et al. (2023) conducted an optimization analysis of the structural parameters of articulated offshore wind turbines using the third-generation nondominated sorting genetic algorithm (NSGA-III).

This study aimed to construct an optimization analysis framework to determine the optimal values for the shape and position of submerged breakwaters that can minimize or maximize the external forces acting on the floating structure to improve its stability. To conduct a hydrodynamic analysis considering the interaction between the floating structure and the submerged breakwaters, a 2D FD-BEM program based on the linear potential theory was developed. It was coupled with a metaheuristic algorithm to conduct the optimization analysis. To the best of our knowledge, the development of a linked analysis framework of NWT and an optimization algorithm that can analyze the 2D hydrodynamic problems considering various sea bottoms was attempted for the first time. As a metaheuristic algorithm, the advanced PSO proposed by Chen et al., (2018) and demonstrated superiority by Jeong and Koo (2023) was used in this study. The optimization analysis is performed by calling FD-BEM for each generation, conducting a numerical analysis of the design variables of each particle, and updating the design variables using the collected results. In this study, the optimal values for the shape and position of a single submerged breakwater that minimize or maximize the external forces acting on a fixed surface piercing body were determined and analyzed.

2. Mathematical Formulation

Fig. 1 shows the linked analysis framework of the FD-BEM program and optimization algorithm. The optimization algorithm sets the initial values of the design variable vectors corresponding to the number of particles using the ranges of the design variables entered by the user and the objective function. The opposition-based learning

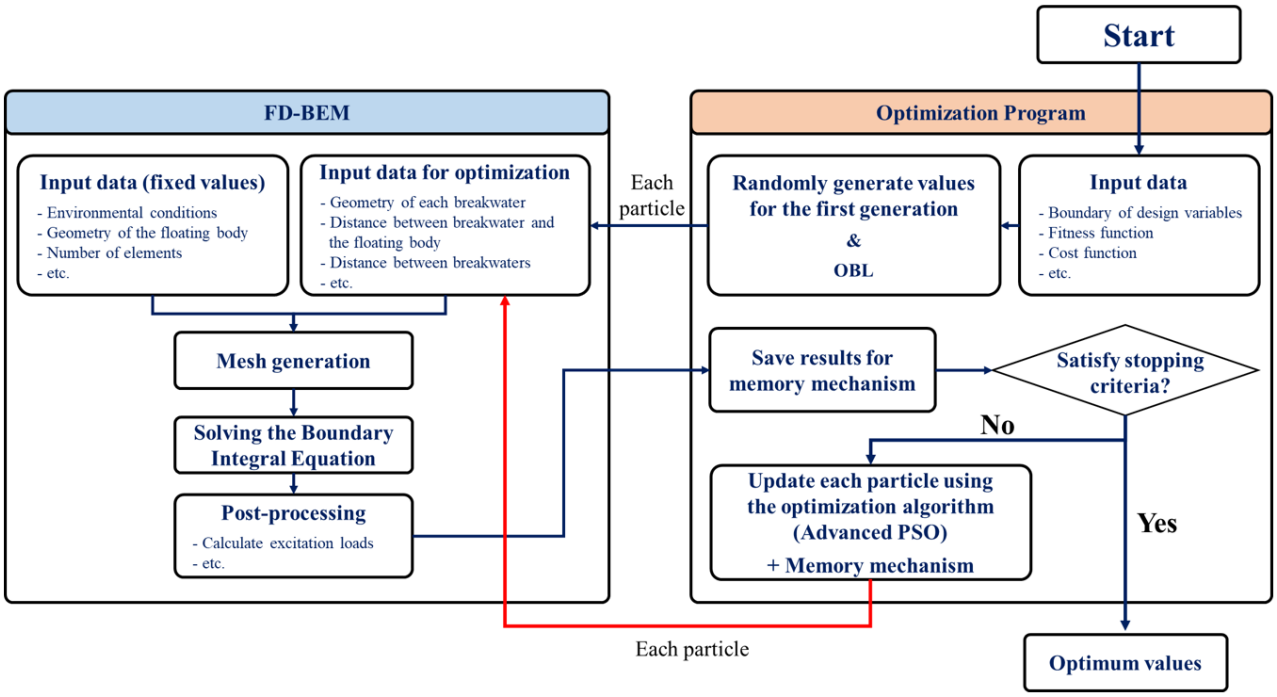

Fig. 1 Description of the linked analysis framework of the FD-BEM program and optimization algorithm

technique is applied to determine the particles of the first generation (Ahandani, 2016). The FD-BEM program is executed using the design variables of each particle, and the objective function is calculated using the output values. The design variables used for computation are stored in memory, and the analysis time can be reduced by preventing the execution of the same calculation. If the objective function satisfies the stopping criteria or the maximum number of iteration, the entire computation is terminated, and the design variable vectors are defined as the optimal values.

2.1 FD-BEM

This study employed a numerical analysis technique (boundary element method) based on the linear potential theory in which the fluid in the computational domain has inviscid, irrotational, and incompressible characteristics to calculate 2D hydrodynamic problems. The governing equation of the computational domain is the Laplace equation, which can be expressed using the velocity potential as follows.

$$\nabla^2\phi = 0 \tag{1}$$

In hydrodynamic problems of general floating bodies, the velocity potential is the sum of the incident, diffraction, and radiation velocity potentials. In this study, it was assumed that the motion of the floating body was fixed, and the effect of the radiated wave was not considered as shown in Eq. (2). The incident wave was assumed to be a linear wave, and the incident velocity potential can be calculated using Eq. (3).

$$\phi = \phi_I + \phi_D \tag{2}$$

$$\phi_I = -i\frac{gH}{2\omega}\frac{\cosh k(z+h)}{\cosh kh}e^{ikx} \tag{3}$$

where ϕ_I and ϕ_D are the velocity potentials of the incident and radiation, respectively. g is the gravitational acceleration, H is the wave height, ω is the frequency of the incident wave, k is the wavenumber, and h is the water depth. x is the horizontal coordinate in the incident wave direction, and z is the vertical displacement from the water surface.

The boundary integral equation can be obtained using Green's function, which is the fundamental solution of the Laplace equation, and Green's second identity as follows.

$$\frac{1}{2}\phi + \int_\Gamma \left(\phi\frac{\partial G}{\partial \boldsymbol{n}}\right)d\Gamma = \int_\Gamma \left(G\frac{\partial \phi}{\partial \boldsymbol{n}}\right)d\Gamma \tag{4}$$

where $G = 1/(2\pi)\cdot ln(1/r)$ is the 2D Green's function, and r is the distance between the source and field points. Γ is the boundary of the computational domain, and $\boldsymbol{n}$ is the normal vector at the boundary. Fig. 2 shows the computational domain for conducting the hydrodynamic numerical analysis considering the interaction between a floating body and a submerged breakwater. To solve Eq. (4), the following boundary conditions were applied to the computational domain.

(1) Free surface boundary conditions

The dynamic and kinematic free surface boundary conditions in the frequency domain may be integrated as follows.

$$\frac{\partial \phi}{\partial \boldsymbol{n}} - \frac{\omega^2}{g}\phi = 0 \quad on\ \Gamma_{Free} \tag{5}$$

(2) Radiation boundary conditions

The Sommerfeld radiation boundary condition was used to implement the open sea condition. The boundary condition (Eq. (6)) that considers the influence of the incident wave was applied to Γ_{Rad1} (Koley et al., 2020).

$$\frac{\partial(\phi-\phi_I)}{\partial \boldsymbol{n}}-ik(\phi-\phi_I)=0 \quad on\ \Gamma_{Rad1} \tag{6}$$

$$\frac{\partial \phi}{\partial \boldsymbol{n}}-ik\phi=0 \quad on\ \Gamma_{Rad2} \tag{7}$$

(3) Sea bottom and submerged breakwater boundary conditions

Non-penetration boundary conditions in which fluid particles cannot pass through the boundary were applied to the sea bottom and the submerged breakwater.

$$\frac{\partial \phi}{\partial \boldsymbol{n}}=0 \quad on\ \Gamma_{Bot} \text{ and } \Gamma_{BW}. \tag{8}$$

(4) Floating body boundary conditions

In this study, it was assumed that the motion of the floating body was fixed, and the external force acting on the floating body was calculated by solving only the diffraction problem without solving the radiation problem. The floating body boundary condition for solving the diffraction problem is as follows.

$$\frac{\partial \phi_D}{\partial \boldsymbol{n}}=-\frac{\partial \phi_I}{\partial \boldsymbol{n}} \quad on\ \Gamma_{FB} \text{ (for the diffractionproblem)} \tag{9}$$

The velocity potentials at all boundaries can be obtained by substituting Eqs. (5)–(9) into Eq. (4) and performing matrix operations through discretization.

The reflection and transmission coefficients at the open sea boundaries can be calculated using the velocity potentials at each radiation boundary (Vijay et al., 2021).

$$K_R=\left|\frac{i\omega}{gAN_0^2}\left[\int_{-h}^{0}\phi|_{Rad1}\,Z_0(z)dz\right]-1\right| \tag{10}$$

$$K_T=\left|\frac{i\omega}{gAN_0^2}\left[\int_{-h}^{0}\phi|_{Rad2}\,Z_0(z)dz\right]\right| \tag{11}$$

where K_R and K_T are the reflection and transmission coefficients, respectively. $Z_0(z)=\cosh k(z+h)/\cosh kh$ is the vertical eigenfunction, i.e., $N_0^2=\int_{-h}^{0}Z_0^2(z)dz$. As there is no wave energy loss, the total energy of the reflected and transmitted waves has a constant value ($K_R^2+K_T^2=1$).

The wave load acting on the floating body can be obtained by integrating the hydrodynamic pressure acting on the submerged surface, and the pressure acting on each element can be calculated using the Bernoulli equation.

$$\boldsymbol{F}=i\rho\omega\int\phi\boldsymbol{n}\,d\Gamma_{FB} \tag{12}$$

$$\boldsymbol{M}=i\rho\omega\int\phi(r_{xg}n_z-r_{zg}n_x)d\Gamma_{FB} \tag{13}$$

where $\boldsymbol{F}$ and $\boldsymbol{M}$ are the external force and moment vectors acting on the floating body, respectively. ρ is the density of the fluid, and r_{xg} and r_{zg} are the horizontal and vertical distances from the center of gravity of the floating body to each element, respectively. The external force components obtained through the frequency-domain analysis can be nondimensionalized as follows.

$$K_F=\frac{|\boldsymbol{F}|}{\rho gHh} \tag{14}$$

$$K_M=\frac{|\boldsymbol{M}|}{\rho gHh^2} \tag{15}$$

2.2 Metaheuristic Algorithm

Metaheuristic algorithms are representative optimization algorithms that are used to find the maximum or minimum values based on the

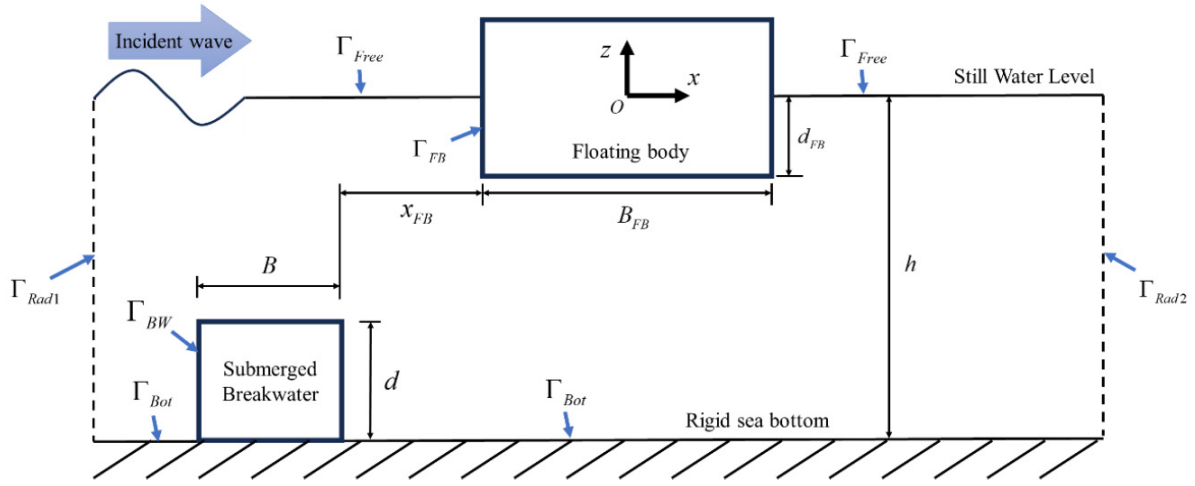

Fig. 2 Illustration of the computational domain and boundaries for a surface piercing body and submerged breakwater

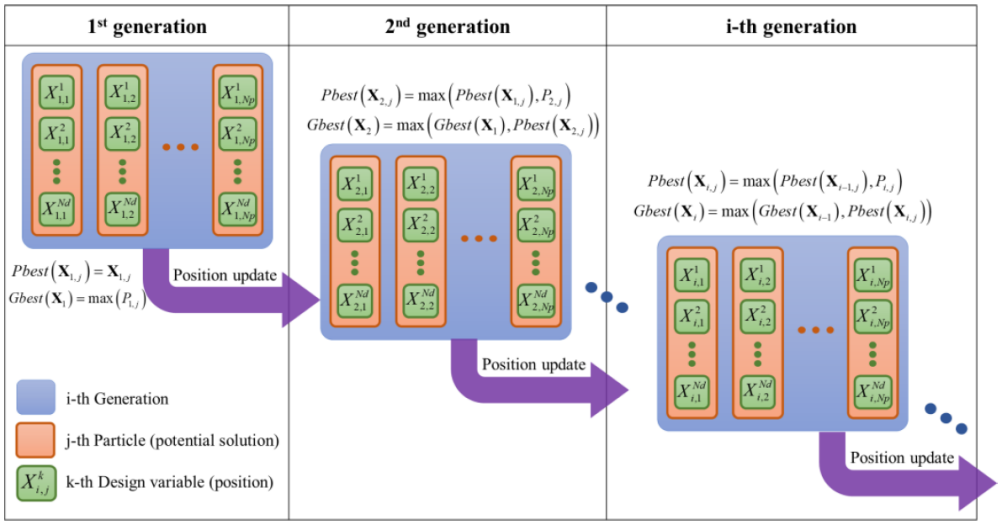

Fig. 3 Illustration of the procedure of the general PSO

objective function in optimization problems with multiple design variables. In this study, advanced PSO, one of a swarm-based algorithms, was applied for the optimization analysis (Eberhart and Kennedy, 1995; Shi and Eberhart, 1998; Chen et al., 2018). Jeong and Koo (2023) verified the superior performance of advanced PSO through the comparison and analysis of various metaheuristic algorithms.

Fig. 3 shows the procedure of the general PSO. Advanced PSO is composed of *Np* particles for each generation (iteration). Each particle is composed of *Nd* design variables, and the solution obtained from these design variables becomes the value of each particle. As the design variables converge from randomly generated initial values to the optimal values, particles can be said to be potential solutions. The value of each design variable in one particle is referred to as a position, which is updated by calculating the relative velocity between the particle and other particles for each generation. The velocity of the *k*-th design variable of the *j*-th particle in the *i*-th generation can be calculated as follows.

$$V_{i,j}^{k} = \alpha V_{i-1,j}^{k} + c_1\, rand_1 \left(Pbest(X_{i-1,j}^{k}) - X_{i-1,j}^{k}\right) + c_2\, rand_2 \left(Gbest(X_{i-1}^{k}) - X_{i-1,j}^{k}\right) \tag{16}$$

where $rand$ is a random variable between 0 and 1. $V_{i,j}^{k}$ and $X_{i,j}^{k}$ are the velocity and position of each design variable, respectively, which can be expressed in the vector form ($\boldsymbol{V}_{i,j} = \left[V_{i,j}^{1} \;\; V_{i,j}^{2} \;\cdots\; V_{i,j}^{Nd}\right]^{T}$, $\boldsymbol{X}_{i,j} = \left[X_{i,j}^{1} \;\; X_{i,j}^{2} \;\cdots\; X_{i,j}^{Nd}\right]^{T}$). $Pbest(\boldsymbol{X}_{i-1,j})$ is the optimal position vector of the *j*-th particle until the previous generation, and $Gbest(\boldsymbol{X}_{i-1})$ is the optimal position vector among all the particles until the previous generation. α is the linearly decreasing inertia weight proposed by Shi and Eberhart (1998). PSO shows an excellent performance when the value of the inertia weight starts with a value close to 1 and linearly decreases to 0.4. Accordingly, the initial value ($\alpha_{\max}$) and final value ($\alpha_{\min}$) of the inertia weight were set to 0.8 and 0.4, respectively, and α can be calculated as follows.

$$\alpha = \alpha_{\max} - \frac{Iter_i}{Iter_{\max}}(\alpha_{\max} - \alpha_{\min}) \tag{17}$$

where $Iter_i$ is the *i*-th generation, and $Iter_{\max}$ is the maximum number of generations. c_1 and c_2 were calculated using sine cosine acceleration coefficients (Chen et al., 2018).

$$c_1 = \partial sin\left(\frac{\pi}{2}\left(1 - \frac{Iter_j}{Iter_{\max}}\right)\right) + \delta, \tag{18}$$

$$c_2 = \partial cos\left(\frac{\pi}{2}\left(1 - \frac{Iter_j}{Iter_{\max}}\right)\right) + \delta, \tag{19}$$

where the values of ∂ and δ were 2 and 0.5, respectively (Chen et al., 2018).

After calculating the velocity using Eq. (16), the position can be updated using the following equation.

$$X_{i,j}^{k} = X_{i-1,j}^{k} + V_{i,j}^{k}. \tag{20}$$

The opposition-based learning technique was applied to improve the performance of the initial random design variables of the first generation (Ahandani, 2016). The computation speed was improved by setting calculations to be omitted when there were previous calculation results for the same design variable vector by applying the memory mechanism (Cao et al., 2022).

3. Numerical Analysis and Results

3.1 Verification of the Computation Results of FD-BEM

Before conducting the optimization analysis, the numerical analysis results were compared with the results of previous studies to verify the

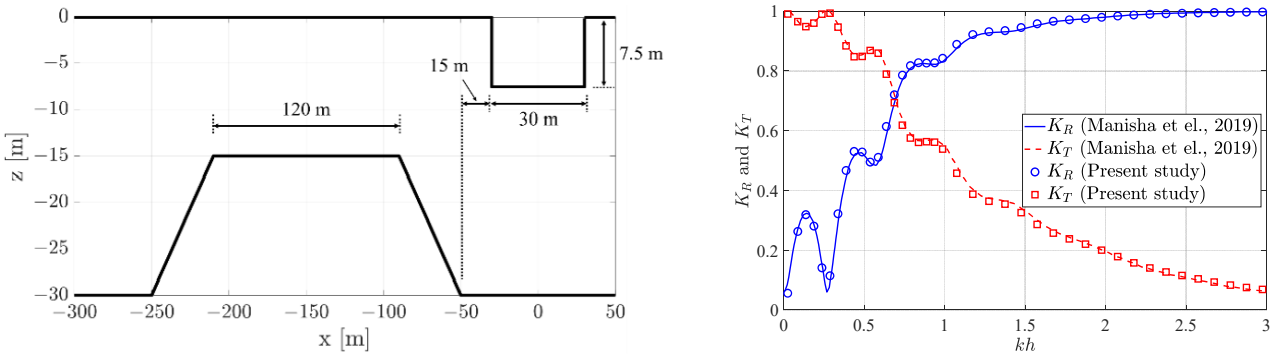

(a) (b)

Fig. 4 Comparison of reflection and transmission coefficients for a surface piercing body and a trapezoidal rigid submerged breakwater: (a) Calculation domain, (b) Reflection and transmission coefficients

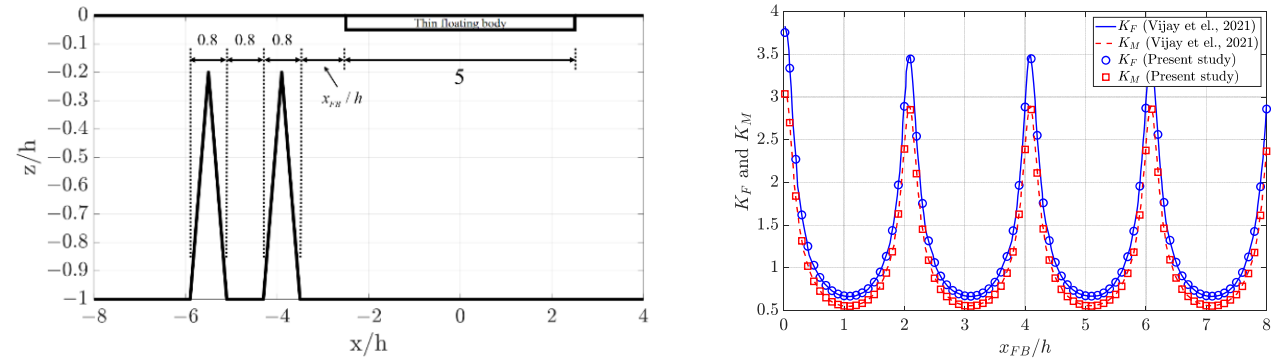

(a) (b)

Fig. 5 Comparison of external forces acting on a thin surface piercing body and two triangular rigid submerged breakwaters: (a) Calculation domain, (b) Vertical force and pitching moment

accuracy of the calculation of the developed 2D FD-BEM. Fig. 4(a) shows a surface piercing body and a trapezoidal rigid submerged breakwater. The width and draft of the structure are 60 and 7.5 m, respectively, and the water depth is 30 m. The lengths of the lower and upper sides of the breakwater are 200 and 120 m, respectively, and its height is 15 m. The distance between the structure and the breakwater is 15 m. Fig. 4(b) compares the reflection and transmission coefficients at the radiation boundary with the results of Manisha et al. (2019). The computation results of the present study were consistent with the results of the previous study, and the error was less than 3%.

Fig. 5(a) shows a thin surface piercing body and two triangular rigid submerged breakwaters. The width of the body is 5*h*, and its draft is very thin. For the two submerged breakwaters, the length of the lower side and the height are 0.8*h*. The distance between the breakwaters is 0.8*h*. Fig. 5(b) compares the vertical external force and pitching moment acting on the body with the results of Vijay et al. (2021) according to the distance between the surface piercing body and the breakwater. The computation results of the present study were consistent with the results of the previous study, and the error was less than 0.5%. Thus, it was determined that the developed FD-BEM program has sufficient accuracy to conduct a hydrodynamic analysis considering the interaction between the surface piercing body and the submerged breakwater.

3.2 Optimization Analysis of the Shape and Position of the Submerged Breakwater

3.2.1 Single submerged breakwater with a constant area

To examine the operational and computational performance of the developed linked analysis framework, the optimization analysis of the single submerged breakwater installed in front of the floating body and incident wave was conducted in the domain shown in Fig. 2. Motion response analysis must be conducted considering the radiated wave and mooring line caused by the floating body motion for evaluating the stability of the actual floating body. However, this study focused on the development of a computational procedure for the optimization analysis of the external forces acting on the floating body according to the shape and position of the submerged breakwater. Therefore, a situation in which the floating body is fixed was assumed. The limitations of this interpretation are that the radiated wave and its interaction with the submerged breakwater cannot be considered, and that the motion response of the floating body cannot be identified. However, the results of Fig. 5(b) show that the external force and pitching moment acting on the floating body have similar tendencies when the floating body is fixed, and accordingly, the total external force ($F_{Total} = \sqrt{F_x^2 + F_z^2}$) acting on the floating body according to the shape and position of the submerged breakwater was set as the objective function. In addition, the overturning moment caused by the

wave force acts on the actual submerged breakwater, and a stability analysis must be conducted considering it. However, as mentioned earlier, the overturning moment was not considered to focus on the development of a computation procedure for the optimization algorithm for the shape and position of the submerged breakwater.

In this study, structures with a width larger than the draft, such as floating docks, bridges, and airports, where stability is important, were assumed. The specifications of the floating body and the water depth (h) remained constant during the entire simulation process, and the width and draft of the floating body were 2h and 0.25h, respectively. The incident wave condition was the nondimensionalized wavenumber kh equal to 1.571 rad/s, and the wavelength of the incident wave was 4h. The distance between the floating body and the submerged breakwater (x_{FB}) and the height of the breakwater (d) were set as the design variables for conducting the optimization analysis. It was assumed that the installation cost of the breakwater (the area of the breakwater) was constant at one-tenth of the submerged area of the floating body ($A_{FB} = B_{FB} d_{FB}$), and the width of the breakwater is determined by its height. In this instance, the width of the breakwater can be calculated as follows.

$$A_{BW} = 0.1 A_{FB} \tag{21}$$

$$B = A_{BW}/d \tag{22}$$

where A_{BW} is the area of the submerged breakwater.

Table 1 presents the range of each design variable. x_{FB} ranged from 0.1h to 2h, and d ranged from 0.1h to various upper limits. The step size of the design variables was h/300, and the total number of possible simulations ranged from 17,701 ($0.1h \leq x_{FB}/h \leq 0.2h$) to 137,611 ($0.1h \leq x_{FB}/h \leq 0.9h$). The objective function was set so that the total external force acting on the floating body could be minimized or maximized, and optimization analysis was conducted for each case. The number of particles for the optimization analysis was set to 100 for all the cases, and the maximum number of generations (maximum iteration) was set to 500. Table 2 presents the configuration of the PC used for the optimization analysis. The analysis was conducted using the same PC for all the cases, and the time required for one simulation was two seconds or less.

Table 1 Boundaries of the design variables

Design variables	Lower limit	Upper limit	Step size
x_{FB}/h	0.1	2.0	1/300
d/h	0.1	0.2, 0.3, 0.4, 0.5, 0.6, 0.7, 0.8, 0.9	1/300

Table 2 PC configuration for simulation

Components	Description
CPU	Intel (R) Xeon (R) Platinum 8260 (2.40 GHz)
RAM	192 GB
OS	Windows 10

Table 3 presents the results of the optimization analysis conducted under the conditions of Table 1. At d/h = 0.9, the total analysis time was approximately 700 s, and approximately 1,200 simulations were performed. The design variables of the particles converged to the same values before 50 generations. The total external force acting on the floating body was nondimensionalized by dividing it by the external force in the absence of the submerged breakwater (F_{No}). In all the cases, the height of the breakwater converged to the largest value within the designated range. This is because the movement of fluid particles rapidly increases toward the water surface, and thus, an increase in the height of the breakwater has a significant influence on the fluid particles. Within the same installation cost (the area of the breakwater), an increase in the height of the breakwater within the permitted range has a significant influence on the floating body. In addition, it was confirmed that the force acting on the floating body can be minimized or maximized depending on the position of the submerged breakwater despite the same breakwater shape. As the force acting on the breakwater and the resulting overturning moment were not considered in this study, the values converged to make the width of the breakwater very thin. Therefore, a detailed analysis is required considering the stability of the breakwater as well as the position and shape of the breakwater based on its installation purpose.

Table 3 Optimal values for minimizing and maximizing the external force according to the upper limit of breakwater height

Upper limit of d/h	Optimal values					
	Minimizing wave force			Maximizing wave force		
	x_{FB}/h	d/h	F_{Total}/F_{No}	x_{FB}/h	d/h	F_{Total}/F_{No}
0.2	1.477	0.2	0.9591	0.447	0.2	1.0526
0.3	1.513	0.3	0.9312	0.480	0.3	1.0909
0.4	1.517	0.4	0.8938	0.487	0.4	1.1452
0.5	1.510	0.5	0.8460	0.483	0.5	1.2202
0.6	1.497	0.6	0.7863	0.470	0.6	1.3234
0.7	1.470	0.7	0.7121	0.447	0.7	1.4692
0.8	1.427	0.8	0.6175	0.407	0.8	1.6903
0.9	1.367	0.9	0.4844	0.347	0.9	2.0910

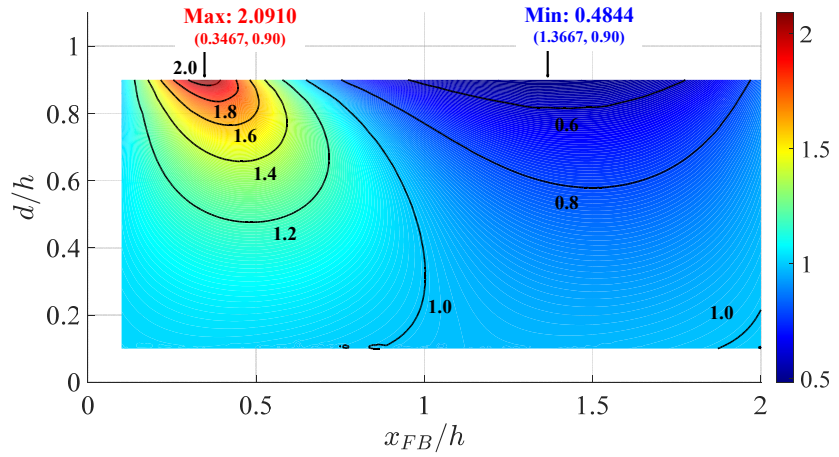

Fig. 6 Contour plot of the ratio of the external force acting on the floating body (values are interpolated)

Fig. 6 shows the contour plot of the ratio of the external force acting on the floating body obtained by conducting the optimization analysis. When x_{FB}/h was lower than approximately 0.6 (when the floating body and submerged breakwater were relatively close), the external force acting on the floating body increased regardless of the height of the breakwater. When it was higher than 1.0 (when the breakwater was relatively far away), the external force acting on the floating body decreased regardless of the height of the breakwater. As for the tendency of the external force, x_{FB}/h showed a tendency to decrease as the height of the breakwater increased when d/h was higher than 0.4 for both the minimum and maximum values. This is because the movement range of fluid particles increases toward the water surface, and thus, the position at which the fluid particles affect the interaction between the floating body and the breakwater also changes.

Fig. 7 compares the magnitude of the wave elevations according to the position of the submerged breakwater when d/h is 0.9. In Fig. 7(a), the black solid line indicates the wave elevation in the absence of the submerged breakwater. Standing waves were generated owing to the

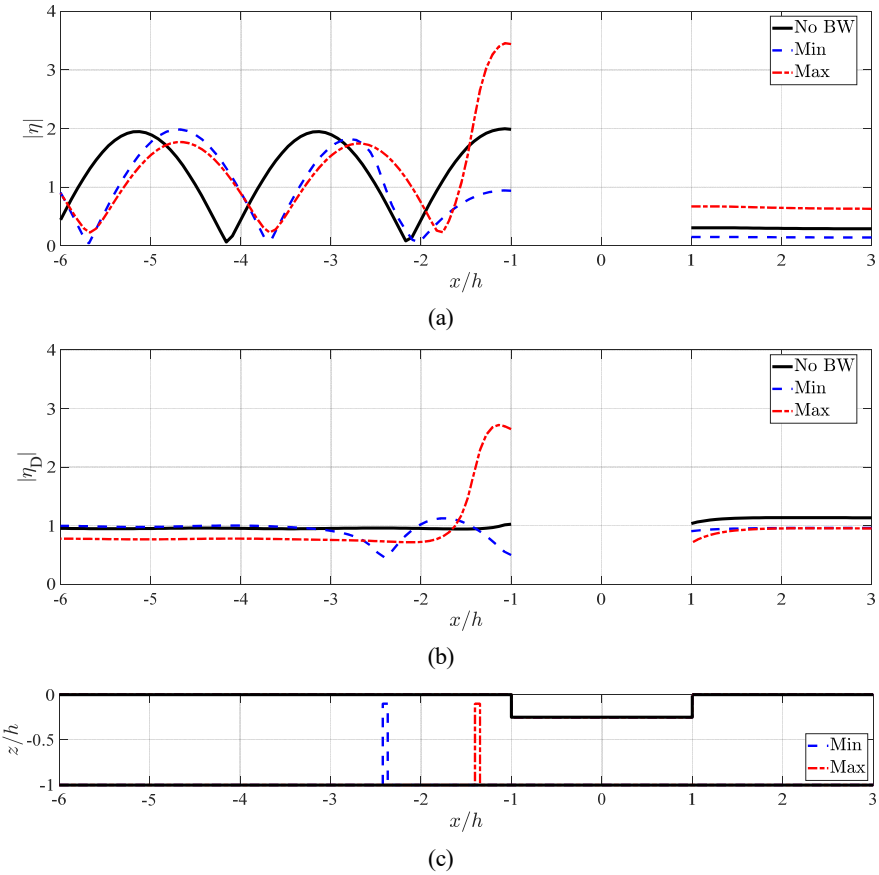

Fig. 7 Comparison of wave elevations according to the position of the submerged breakwater: (a) Total wave elevation, (b) Diffracted wave elevation, (c) Location of the floating body and breakwaters

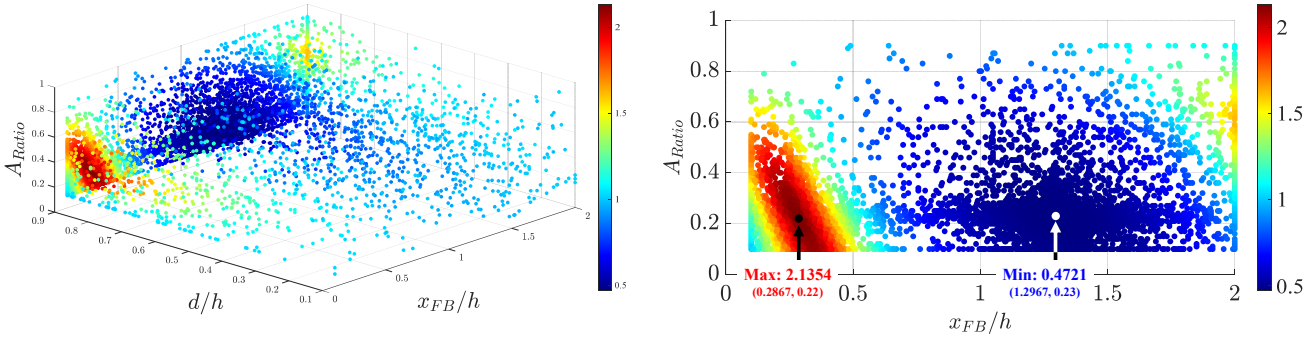

(a) (b)

Fig. 8 Scatter plot of the ratio of the external forces acting on the floating body according to x_{FB}/h, d/h, and A_{Ratio}; (a) Scatter plot for the three design variables, (b) Scatter plot at d/h=0.9

diffracted waves caused by the floating body. In the presence of the submerged breakwater, the wave elevation adjacent to the floating body differed by approximately 3.5 times depending on the position of the breakwater despite the same breakwater size. When the breakwater was close to the floating body, very large diffracted waves were generated and the magnitude of transmitted waves also increased, thereby increasing the external force acting on the floating body. When the breakwater was moved away by a certain distance from the floating body, both the reflected and transmitted waves were reduced by the destructive interference of the incident and diffracted waves, thereby decreasing the external force acting on the floating body.

3.2.2 Single submerged breakwater with various areas

An optimization analysis was conducted considering the area ratio between the submerged breakwater and the floating body as an additional design variable, and the area of the breakwater according to the area ratio was calculated using the following equation.

$$A_{BW} = A_{Ratio} A_{FB}, \tag{23}$$

where A_{Ratio} is the area ratio between the submerged breakwater and the floating body. It was set to range from 0.1 to 0.9 at a step size of 0.01. The total number of possible simulations is approximately 11 million (137,611×81), and the same values as in Section 3.2.1 were used for the objective function, the number of particles, and the maximum number of generations. The total analysis time was approximately 5,200 s, and approximately 7,500 simulations were performed. The design variables of the particles converged to the same values before 150 generations.

Fig. 8(a) shows the optimization analysis results for each design variable in a scatter plot. Dots are concentrated at d/h = 0.9. This is because the particles converged to the value when d/h was 0.9 as optimization calculations were repeated. Fig. 8(b) shows the results at d/h = 0.9. The case in which the ratio of the external forces acting on the floating body was increased by the breakwater (F_{Total}/F_{No}>1.0) mostly occurred when x_{FB}/h was lower than 0.5, and the x_{FB} value that maximized the ratio of the external force decreased as the area ratio increased. The values of x_{FB} that maximized and minimized the ratio of the external force differed by approximately one-fourth of the wavelength ($1h$), which indicates that the wavelength of the incident wave and the ratio of the external force are closely related. Based on the results of the ratio of the external force for the area ratio of the breakwater and x_{FB}/h, a large external force can be expected when d/h is 0.9, the area ratio is 0.22, and x_{FB}/h is 2.3. The ratio of the external force obtained by conducting a numerical analysis using these values was 2.0177, confirming that a large value occurred.

Note that a large area of the submerged breakwater is not necessarily good, and there is a specific position that has the optimal value. This indicates that an optimization analysis that considers various design variables is essential for detailed interpretation. It can also reduce the total analysis time to determine the optimal values because the objective function rapidly converges by preventing unnecessary simulation even if the number of simulation cases increases owing to the increased design variables.

4. Conclusion

In this study, a 2D FD-BEM was developed based on the linear potential theory and boundary element method, and it was coupled with advanced PSO, one of the metaheuristic algorithms, to construct an optimization analysis framework. For the first time, this study attempted to develop a linked analysis framework of a 2D NWT and an optimization algorithm that considers various sea bottoms. The FD-BEM proved the accuracy of the solution through a comparison with the results of previous studies, and advanced PSO is an algorithm with proven superiority. The execution of the FD-BEM program is automatically repeated using the design variable vectors generated in the optimization algorithm process. When the numerical analysis for each particle was finished, a memory mechanism was applied to prevent unnecessary calculations by storing the results in memory. Each design variable vector updates its position value by calculating the relative velocity with the optimal value, and the position value

continues to be updated over generations until the stopping criteria are satisfied.

To examine the operational and computational performance of the developed optimization analysis framework, an optimization analysis was conducted for the height and area of a single rigid submerged breakwater installed in front of a fixed floating body and an incident wave. The optimization analysis confirmed that the height of the submerged breakwater has a significant influence on the floating body, and that there is an optimal position for the breakwater. In addition, even if the number of simulation cases increased, the total analysis time to determine the optimal values could be reduced by preventing unnecessary simulation through the optimization analysis.

The developed 2D FD-BEM has limitations in considering the effects of nonlinearity, viscosity, and turbulence because it is based on the linear potential theory. However, it has sufficient precision to analyze reflected and transmitted waves and the external forces acting on floating bodies when a numerical analysis is conducted on long submerged and floating bodies. It is also suitable for conducting an optimization analysis that requires a large amount of simulation owing to the shorter analysis time compared with that of nonlinear analysis and computational-fluid-dynamics-based (CFD-based) analysis. As this study focused on developing an optimization analysis framework for the specifications of floating bodies and submerged breakwaters, the fixed floating body condition was applied. This has limitations in considering the interaction between the radiated waves caused by the floating body motion and the submerged breakwater. To overcome this, the precision of optimization analysis will be examined in follow-up studies through the motion response analysis of a floating body, including the mooring line, and a comparison with experiment results. In the future, various metaheuristic algorithms will be applied to the developed framework, and it will be expanded to time-domain analysis. Based on this, a hydrodynamic optimization analysis will be conducted on various ocean engineering problems.

Conflict of Interest

MooHyun Kim and Weoncheol Koo serve as editorial board members of the Journal of Ocean Engineering and Technology, but they had no role in the decision to publish this article. No potential conflict of interest relevant to this article was reported.

Funding

This study was supported by the MOTIE (Ministry of Trade, Industry, and Energy) in Korea, under the Human Resource Development Program for Industrial Innovation (Global) (P0017303, Smart Manufacturing Global Talent Training Program) supervised by the Korea Institute for Advancement of Technology (KIAT). This study was also supported by the National Research Foundation of Korea (NRF) grant funded by the Korea government (MSIT) (RS-2023-00278157).

References

Ahandani, M. A. (2016). Opposition-based learning in the shuffled bidirectional differential evolution algorithm. *Swarm and Evolutionary Computation*, *26*, 64−85. https://doi.org/10.1016/j.swevo.2015.08.002

Cao, F., Han, M., Shi, H., Li, M., & Liu, Z. (2022). Comparative study on metaheuristic algorithms for optimising wave energy converters. *Ocean Engineering*, *247*, 110461. https://doi.org/10.1016/j.oceaneng.2021.110461

Chen, K., Zhou, F., Yin, L., Wang, S., Wang, Y., & Wan, F. (2018). A hybrid particle swarm optimizer with sine cosine acceleration coefficients. *Information Sciences*, *422*, 218−241. https://doi.org/10.1016/j.ins.2017.09.015

Eberhart, R., & Kennedy, J. (1995, October). A new optimizer using particle swarm theory. In *MHS'95. Proceedings of the sixth international symposium on micro machine and human science, Nagoya, Japan* (pp. 39−43). IEEE. https://doi.org/10.1109/MHS.1995.494215

Ferri, G., & Marino, E. (2023). Site-specific optimizations of a 10 MW floating offshore wind turbine for the Mediterranean Sea. *Renewable Energy*, *202*, 921−941. https://doi.org/10.1016/j.renene.2022.11.116

Gandomi, M., Pirooz, M. D., Nematollahi, B., Nikoo, M. R., Varjavand, I., Etri, T., & Gandomi, A. H. (2023). Multi-criteria decision-making optimization model for permeable breakwaters characterization. *Ocean Engineering*, *280*, 114447. https://doi.org/10.1016/j.oceaneng.2023.114447

Huang, C. J., Chang, H. H., & Hwung, H. H. (2003). Structural permeability effects on the interaction of a solitary wave and a submerged breakwater. *Coastal engineering*, *49*(1−2), 1−24. https://doi.org/10.1016/S0378-3839(03)00034-6.

Jeong, H. J., & Koo, W. (2023). Analysis of various algorithms for optimizing the wave energy converters associated with a sloped wall-type breakwater. *Ocean Engineering*, *276*, 114199. https://doi.org/10.1016/j.oceaneng.2023.114199

Jeong, J. H., Kim, J. H., & Lee, J. L. (2021). Analysis of wave transmission characteristics on the TTP submerged breakwater using a parabolic-type linear wave deformation model. *Journal of Ocean Engineering and Technology*, *35*(1), 82−90. https://doi.org/10.26748/KSOE.2020.066

Jiang, L., Zhang, J., Tong, L., Guo, Y., He, R., & Sun, K. (2022). Wave motion and seabed response around a vertical structure sheltered by submerged breakwaters with Fabry−Pérot resonance. *Journal of Marine Science and Engineering*, *10*(11), 1797. https://doi.org/10.3390/jmse10111797

Kaveh, M., & Mesgari, M. S. (2023). Application of meta-heuristic algorithms for training neural networks and deep learning architectures: A comprehensive review. *Neural Processing Letters*, *55*(4), 4519−4622. https://doi.org/10.1007/s11063-022-11055-6

Khan, M. B., Behera, H., Sahoo, T., & Neelamani, S. (2021). Boundary element method for wave trapping by a multi-layered trapezoidal breakwater near a sloping rigid wall. *Meccanica*, *56*, 317−334. https://doi.org/10.1007/s11012-020-01286-z

Koley, S., Panduranga, K., Almashan, N., Neelamani, S., & Al-Ragum, A. (2020). Numerical and experimental modeling of water wave interaction with rubble mound offshore porous breakwaters. *Ocean Engineering*, *218*, 108218. https://doi.org/10.1016/j.oceaneng.2020.108218

Lamas-Pardo, M., Iglesias, G., & Carral, L. (2015). A review of very large floating structures (VLFS) for coastal and offshore uses. *Ocean Engineering*, *109*, 677−690. https://doi.org/10.1016/j.oceaneng.2015.09.012

Lee, W. D., Jeong, Y. M., & Hur, D. S. (2019). Wave control by tide-adapting submerged breakwater. *Journal of Ocean Engineering and Technology*, *33*(6), 573−580. https://doi.org/10.26748/KSOE.2019.081

Lee, J., Jeong, Y. M., Kim, J. S., & Hur, D. S. (2022). Analysis of hydraulic characteristics according to the cross-section changes in submerged rigid vegetation. *Journal of Ocean Engineering and Technology*, *36*(5), 326−339. https://doi.org/10.26748/KSOE.2022.028

Loukili, M., Dutykh, D., Nadjib, C., Ning, D., & Kotrasova, K. (2021). Analytical and numerical investigations applied to study the reflections and transmissions of a rectangular breakwater placed at the bottom of a wave tank. *Geosciences*, *11*(10), 430. https://doi.org/10.3390/geosciences11100430

Manisha, Kaligatla, R. B., & Sahoo, T. (2019). Effect of bottom undulation for mitigating wave-induced forces on a floating bridge. *Wave Motion*, *89*, 166−184. https://doi.org/10.1016/j.wavemoti.2019.03.007

Min, E. H., Koo, W., & Kim, M. H. (2023). Wave characteristics over a dual porous submerged breakwater using a fully nonlinear numerical wave tank with a porous domain. *Journal of Marine Science and Engineering*, *11*(9), 1648. https://doi.org/10.3390/jmse11091648

Ni, Y. L., & Teng, B. (2021a). Bragg resonant reflection of water waves by a Bragg breakwater with porous rectangular bars on a sloping permeable seabed. *Ocean Engineering*, *235*, 109333. https://doi.org/10.1016/j.oceaneng.2021.109333

Ni, Y. L., & Teng, B. (2021b). Bragg resonant reflection of water waves by a Bragg breakwater with porous trapezoidal bars on a sloping permeable seabed. *Applied Ocean Research*, *114*, 102770. https://doi.org/10.1016/j.apor.2021.102770

Patil, S. B., & Karmakar, D. (2021). Performance evaluation of submerged breakwater using multi-domain boundary element method. *Applied Ocean Research*, *114*, 102760. https://doi.org/10.1016/j.apor.2021.102760

Shi, Y., & Eberhart, R. C. (1998). Parameter selection in particle swarm optimization. In Porto, V.W., Saravanan, N., Waagen, D., & Eiben, A.E. (Eds.), *Evolutionary Programming VII. EP 1998. Lecture Notes in Computer Science, Vol. 1447*. (pp. 591−600). Springe. https://doi.org/10.1007/BFb00408

Tavana, H., & Khanjani, M. J. (2013). Reducing hydroelastic response of very large floating structure: a literature review. *International Journal of Computer Applications*, *71*(5), 13−17.

Vijay, K. G., Venkateswarlu, V., & Sahoo, T. (2021). Bragg scattering of surface gravity waves by an array of submerged breakwaters and a floating dock. *Wave Motion*, 106, 102807. https://doi.org/10.1016/j.wavemoti.2021.102807

Wang, C. M., Tay, Z. Y., Takagi, K., & Utsunomiya, T. (2010). Literature review of methods for mitigating hydroelastic response of VLFS under wave action. *Applied Mechanics Reviews*, *63*(3), 030802. https://doi.org/10.1115/1.4001690

Watanabe, E., Wang, C. M., Utsunomiya, T., & Moan, T. (2004). Very large floating structures: applications, analysis and design (Report No. 2004-02). *CORE Report*, 2, 104−109.

Zhang, P., Li, Y., Tang, Y., Zhang, R., Li, H., & Gu, J. (2023). Multi-objective optimization and dynamic response predictions of an articulated offshore wind turbine. *Ocean Engineering*, *273*, 114017. https://doi.org/10.1016/j.oceaneng.2023.114017

Zhu, K., Shi, H., Han, M., & Cao, F. (2022). Layout study of wave energy converter arrays by an artificial neural network and adaptive genetic algorithm. *Ocean Engineering*, *260*, 112072. https://doi.org/10.1016/j.oceaneng.2022.112072

Author ORCIDs

Author name	ORCID
Heo, Sanghwan	0000-0003-0033-5022
Koo, Weoncheol	0000-0002-4384-0996
Kim, Moo-Hyun	0000-0001-5793-3707

KSOE

Journal of Ocean Engineering and Technology 38(2), 64−73, April, 2024
https://doi.org/10.26748/KSOE.2024.043

pISSN 1225-0767
eISSN 2287-6715

Original Research Article

Numerical Model Test of Spilled Oil Transport Near the Korean Coasts Using Various Input Parametric Models

Hai Van Dang[1], Suchan Joo[2], Junhyeok Lim[2], Jinhwan Hur[2] and Sungwon Shin[3]

[1]*Ph.D Candidate, Department of Marine Science and Convergent Engineering, Hanyang University ERICA, Ansan, Korea*
[2]*Undergraduate Student, Department of Marine Science and Convergent Engineering, Hanyang University ERICA, Ansan, Korea*
[3]*Professor, Department of Marine Science and Convergent Engineering, Hanyang University ERICA, Ansan, Korea*

KEYWORDS: Oil slick transport simulation, OpenDrift, Hydrodynamic ocean models, Wave models, Atmospheric models, Satellite observations

ABSTRACT: *Oil spills pose significant threats to marine ecosystems, human health, socioeconomic aspects, and coastal communities. Accurate real-time predictions of oil slick transport along coastlines are paramount for quick preparedness and response efforts. This study used an open-source OpenOil numerical model to simulate the fate and trajectories of oil slicks released during the 2007 Hebei Spirit accident along the Korean coasts. Six combinations of input parameters, derived from a five-day met-ocean dataset incorporating various hydrodynamic, meteorological, and wave models, were investigated to determine the input variables that lead to the most reasonable results. The predictive performance of each combination was evaluated quantitatively by comparing the dimensions and matching rates between the simulated and observed oil slicks extracted from synthetic aperture radar (SAR) data on the ocean surface. The results show that the combination incorporating the Hybrid Coordinate Ocean Model (HYCOM) for hydrodynamic parameters exhibited more substantial agreement with the observed spill areas than Copernicus Marine Environment Monitoring Service (CMEMS), yielding up to 88% and 53% similarity, respectively, during a more than four-day oil transportation near Taean coasts. This study underscores the importance of integrating high-resolution met-ocean models into oil spill modeling efforts to enhance the predictive accuracy regarding oil spill dynamics and weathering processes.*

1. Introduction

Maritime shipping of oil and hazardous and noxious substances (HNS) has become a prominent economically advantageous means of long-distance transportation rather than alternative modes. Therefore, the quantity of oil and HNS transported by marine shipping increases substantially, placing a high risk of spill accidents in overcrowded marine traffic zones. Despite the declining trend in the number of tanker spills, the escalating volume of loaded tanker trade suggests a continuous increase in tanker transportation and density, raising the potential for significant spill accidents involving substantial oil and HNS leakage into the marine environment (ITOPF, 2020). South Korea, a major hub for marine transport, has witnessed a series of historic spill accidents. According to the Korean Coast Guard (KCG) White Paper (KCG, 2021), approximately 9,000 accidents and 65,000 kL of spilled oil occurred between 1993 and 2020. Although the number of oil spill accidents has fluctuated over the past 28 years, oil spill accidents significantly impact ecosystems and socioeconomic assets. Therefore, developing a scientific risk assessment framework is necessary to mitigate the effects of oil spills. Hence, the accurate prediction of oil slick transport is paramount to achieve this. When tanker accidents occur, a significant amount of crude oil is released, forming oil slicks as thin layers floating on the sea surface. The fate and movement of these oil slicks are greatly influenced by the baseline environment characteristics and processes. For example, the 2007 Hebei Spirit accident, which was considered one of the worst spill accidents in Korea, occurred near the Taean coasts and resulted in the discharge of approximately 10,900 t of heavy crude oil into the ocean. The adverse weather, characterized by strong winds and currents, was attributed to the quick spread of the oil slick, leading to extensive contamination along the southeast coasts of the Korean Peninsula.

Numerous numerical models designed to predict the movement of

Received 5 January 2024, revised 16 March 2024, accepted 20 March 2024
Corresponding author Sungwon Shin: +82-31-400-5533, sungwshin@hanyang.ac.kr
It is a recommended paper from the proceedings of 2023 Fall Conference of the Korea Society of Ocean Engineering (KSOE) (Dang et al., 2023)

oil spills have proven to be highly effective in rapidly determining the trajectories of spilled oil transport. Accurately forecasting the oil slick transport is a primary finding of numerical models, enabling authorities and relevant agencies with sufficient information to decide a quick response regarding optimizing search, rescue, and cleanup operations. Over the past decades, significant advances in the development of oil spill models have been conducted to simulate the oil slicks, such as DELFT3D (e.g., Abascal et al., 2017), MEDSLIK-II (e.g., De Dominicis et al., 2013), and GNOME (e.g., Jung and Son 2018). On the other hand, most of these numerical models are commercial software that challenges users to modify and configure the source code to suit specific conditions. Thus, a dynamic numerical model has been developed to predict the fate and trajectories of spilled oil over time.

In the current study, OpenOil, an open-source code model, was used to model oil spill transport and fate. The OpenOil model was implemented within the OpenDrift platform and programmed in Python, providing a flexible environment that allows users to adapt and incorporate several modules based on specific purposes. Moreover, the numerical models operate by considering various input met-ocean parameters, including winds, waves, and currents, standing for fundamental components that influence the trajectory of oil slick transport in the marine environment. As a result, the precision and reliability of met-ocean conditions are paramount in evaluating the predictive performance of oil spill numerical models. The parameters characterizing ocean currents are derived from hydrodynamic ocean-circulation models, providing water characteristics that affect the transport of spilled oil on the ocean surface (De Dominicis et al., 2016). The wind velocity and air properties can be assessed using meteorological models that can consider the oil evaporation of floating oil (Keramea et al., 2023). Wave models offer valuable information on wave parameters, including Stoke-drift fields, significant wave heights, and wave periods, which can influence the turbulent and vertical mixing process. Therefore, the forcing data were selected as input parameters based on the objective of each oil spill simulation. The current study focussed on simulating the trajectories of spilled oil on the surface. The primary forcing parameters encompass winds, waves, and currents. Consequently, integrating high-resolution ocean currents, meteorological, and wave models is imperative in oil spill numerical models to ensure the precise estimation of the fate and trajectories of oil slicks.

The principal objective of this study was to use the OpenOil model coupling with the available met-ocean forcing models, specifically currents, winds, and waves, to simulate the 2007 Hebei Spirit oil spill accident. For this purpose, hydrodynamic ocean current data were received from the Hybrid Coordinate Ocean Modeling (HYCOM) and Copernicus Marine Environment Monitoring Services (CMEMS). Various meteorological models, including CMEMS, Climate Forecast System Reanalysis (CFSR), Fifth Generation of the European Reanalysis from the European Centre for Medium-Range Weather Forecasts (ECMWF-ERA5), and Korean Local Analysis Prediction System (KLAPS), were used to extract the wind fields and air temperature. Furthermore, the CMEMS wave models derive wave characteristics for the significant wave height, wave period, and Stoke-drift velocities. The met-ocean forcing models were organized into six combinations to investigate the most influential input variables in predicting oil diffusion in the 2007 accident. The predictive performance of each combination was validated using satellite-observation data of the oil slick at 11 am on December 11, 2007.

The remainder of the paper is organized as follows. Section 2 comprehensively describes the OpenOil simulation model and met-ocean conditions. Section 3 presents a numerical setup and input parameters of the Hebei Spirit oil spill accident. Section 4 reports the numerical results of different combinations validated using the SAR dataset. Finally, Section 5 presents the conclusions and discussions for further work.

2. Met-Ocean Conditions and OpenOil Model

2.1 Meteorological Models

The National Centers for Environmental Prediction (NCEP), administered by the National Oceanic and Atmospheric Administration (NOOA), provides a climate forecast system analysis model (CFSR accessed at https://www.hycom.org/dataserver/ncep-cfsr), which comprehensively represents the dynamic interactions between atmosphere, oceans, and land surfaces from 1992 to now. The CFSR model generates an hourly time-step dataset with a spatial resolution of 1/2°. French-McCay et al. (2021) applied CFSR wind fields to simulate the oil trajectory and fate of the Deepwater Horizon from April to September 2010. Moreover, the wind dataset derived from the CFSR model was used to conduct 896 oil spill simulations to establish a risk assessment framework in the Perdido region near the Gulf of Mexico (Meza-Padilla et al., 2021). In addition, the fifth-generation ECMWF Reanalysis-ERA5 (https://cds.climate.copernicus.eu/cdsapp#!/dataset/reanalysis-era5-single-levels?tab=overview) provides hourly wind-forcing reanalysis data presented in regular longitude and latitude grids at a spatial resolution of 1/4°×1/4 °. The eastward and northward velocity fields measured 10 m above the still water level were collected from 1940 to the present and updated daily. Zhang et al. (2020) tested the ERA5 wind forcing to model the drift trajectories in the South China Sea. The ERA5 meteorological fields were also applied to simulate oil spill movement and behavior in the busiest shipping routes through the Gulf of Suez, Egypt (Abdallah and Chantsev, 2022). Moreover, the CMEMS proposed the global ocean hourly reprocessed sea surface wind fields at 1/8° and 1/4° horizontal spatial resolutions from scatterometer satellite observations and numerical models. The CMEMS dataset was used to correct the persistent biases in the ERA5 dataset. The lower resolution of 1/4° for the air density, eastward and northward wind fields are provided from 08/1999 to 10/2009. On the other hand, a 1/8° spatial resolution of wind fields can be extracted from 01/2009 to 09/2022 (https://data.marine.copernicus.eu/product/WIND_GLO_PHY_L4_MY_012_006/download?dataset=cmems_obs-wind_glo_phy_my_l4_0.25deg_PT1H).

Table 1 Hydrodynamic ocean model

Meteorological models	Organizer	Spatial resolution	Temporal resolution
CFSR	NCEP	1/2°	1-hourly
ERA5	ECMWF	1/4°	1-hourly
CMEMS	CMEMS	1/8°, 1/4°	1-hourly
KLAPS	KMA	1/20°	1-hourly

A very short-term forecast model, a Korean Local Analysis Prediction System (KLAPS) referred to a numerical forecasting system performed to predict the weather on the Korean peninsula provide hourly regional and high-resolution meteorological fields at a spatial resolution of 1/20° (https://data.kma.go.kr/data/rmt/rmtList.do?code=320&pgmNo=66). Kim et al. (2023) deployed the KLAPS wind components in predicting the drift trajectories for maritime search and rescue purposes using the OpenDrift framework. The study indicated that the numerical results in OpenDrift with KLAPS meteorological input parameters show good agreement with satellite observation drifter results. Table 1 provides detailed information on meteorological models.

2.2 Hydrodynamic Ocean Circulation and Wave Models

Numerous ocean circulation models provide hydrodynamic ocean datasets on a global scale, but only datasets that can be applied in an oil slick transport simulation in the Korean peninsula are discussed, as shown in Table 2. Therefore, the CMEMS and HYCOM models are presented. First, the Global Ocean Physics Reanalysis and Global Ocean Physics Analysis and Forecast products (https://data.marine.copernicus.eu/product/GLOBAL_MULTIYEAR_PHY_001_030/description), featuring regular horizontal resolutions of 1/12° obtained from CMEMS for hourly, daily, and monthly for sea surface temperature, sea surface height, currents, and sea ice parameters spanning from the ocean bottom floor to still wave level. Sepp Neves et al. (2020) used CMEMS products for current fields to establish a coastal oil spill hazard map. Similarly, the sea surface temperature and current data derived from CMEMS products were obtained to simulate the potential oil spills from tanker accidents near the Fernando de Noronha Archipelago by the MEDSLIK-II model (Siqueira et al., 2022). The second hydrodynamic ocean current model, Global Ocean Forecasting System (GOFS) in the HYCOM model (https://www.hycom.org/dataserver/gofs-3pt1/reanalysis), provides a global-scale product with a horizontal resolution of 1/12° and current predictions every three hours at 32 vertical depth layers from 0 to 400 m with a distance interval of 50 m. The HYCOM ocean current data were assimilated using a 24-hour numerical model forecast and several observation instruments such as altimeter observation, satellite, and in situ temperature and salinity profiles. Zacharias et al. (2021) conducted a probabilistic approach using the Spill, Transport, and Fate Model (STFM) to identify the multiple potential sources of oil spill sources, in which the input parameters of hydrodynamic currents, including current field, temperature, and depth data were extracted using the HYCOM model. Kim et al. (2023) also applied the sea surface velocities extracted from the HYCOM model to predict the drift trajectories along the Korean coasts.

Table 2 Hydrodynamic ocean models

Hydrodynamic models	Organizer	Spatial Resolution	Temporal resolution
CMEMS	CMEMS	1/12°	Daily
HYCOM	NOAA	1/12°	Three-hourly

Several wave models are available for direct user access. In particular, the CMEMS and ECMWF models provide global geographical coverage, whereas UOM, IFREMER, PdE, CYCOFOS, and HCMR models are used only for the Mediterranean regions. On the Korean peninsula, wave information is sourced from the Korean Operation Oceanographic System (KOOS) database, administered by the Korea Institute of Ocean Science and Technology (KIOST). On the other hand, the KOOS system does not facilitate online access for users to download the dataset. In contrast, the primary objective of this study is to provide a rapid assessment of oil spill transport, enabling expeditious decision-making for authorities responding to oil spill accidents. Consequently, the study emphasizes prioritizing wave models that are easily accessible. Within the context of seven previous case studies involving oil spill transport simulations using the OpenOil model, only ECMWF and CMEMS were examined. Therefore, the reliance is on global wave models, with CMEMS being the sole viable option because the ECMWF database access is currently unavailable because of ongoing system maintenance. The CMEMS model provides a global wave reanalysis product called WAVERYS (https://data.marine.copernicus.eu/product/GLOBAL_MULTIYEAR_WAV_001_032) to describe the wave characteristics covering the period between 1993 and 2019. This product is based on the third-generation wave model of the Meteo-France Wave Model (MFWM) that calculates the wave spectrum on 1/5° of an irregular horizontal grid. The wave parameters obtained from this wave spectrum, including Stoke drift velocities, significant wave height, and average wave period, were proposed on a rectangular 1/5°–grid with a three-hourly integrated time step. This product was assimilated using the altimeter wave data and Sentinel-1-provided directional wave spectra. Law-Chune et al. (2021) comprehensively described the WAVERYS product in the CMEMS models.

2.3 OpenOil Model

OpenOil is a state-of-the-art model for simulating oil-spill transport and fate, which was recently developed by the Norwegian Meteorological Institute. The OpenOil model was based on the Lagrangian trajectory model, which simulates spilled oil movement as many particles moving under the interaction from ocean currents, winds, and waves. Nguyen et al. (2023) reported a detailed description of governing equations on the OpenOil model. The OpenOil model employs hydrodynamic ocean circulation, wave, and meteorological models as input parameters in the oil simulation. The OpenOil model has been applied in several case studies across different regions

Table 3 Tested combination considering input variables applied in the OpenOil model

Combination tests	Hydrodynamic model	Meteorological model	Wave model	Salinity temperature
Combination 1	CMEMS	CMEMS	CMEMS	CMEMS
Combination 2	CMEMS	ERA5	CMEMS	CMEMS
Combination 3	HYCOM	CFSR	CMEMS	CMEMS
Combination 4	HYCOM	ERA5	CMEMS	HYCOM
Combination 5	HYCOM	CMEMS	CMEMS	HYCOM
Combination 6	HYCOM	KLAPS	CMEMS	HYCOM

globally. In detail, Röhrs et al. (2018) examined the vertical and horizontal transport mechanisms of marine oil spills in the Norwegian Sea using the NorShelf model for ocean current fields and ECMWF models for both wind and wave datasets. Moreover, the OpenOil model coupling with GoM- HYCOM and ECMWF models for met-ocean forcing data was used to simulate the impact of river fronts on the oil slick transport in the 2010 DeepWater Horizon accident (Hole et al., 2019). Following this study, the pathways of potential oil spill scenarios were simulated to improve the awareness of planning and preparedness technologies for various offshore sites in Cuba (Androulidakis et al., 2020). Keramea et al. (2022) conducted an operational oil spill model to examine the oil dispersion characteristics using met-ocean datasets from NOAA-GFS and CMEMS for the North Aegean region. On the other hand, studies investigating the predictive performance of the OpenOil model coupling with several met-ocean forecast models for oil slick transport around the Korean peninsula are limited. Therefore, six combinations considering several input met-ocean forecast models used in the OpenOil model were tested to simulate spilled oil in Korea (Table 3).

Fig. 1 presents the flow chart of the proposed methodology. HYCOM and CMEMS were used as hydrodynamic models to provide ocean current parameters. The wind data are received from CMEMS, CFSR, ERA5, and KLAPS models, while CMEMS models are also used to extract the wave parameters. Six combinations were suggested to evaluate the most effective input forcing parameters for simulating spilled oil transport on the ocean surface. The characteristics of oil types were identified using the NOAA oil library. Finally, the met-ocean forcings and oil-type information were used to drive the OpenOil model. The performance of each combination is rigorously assessed by comparing the results with synthetic aperture radar (SAR) observation data at a specific time.

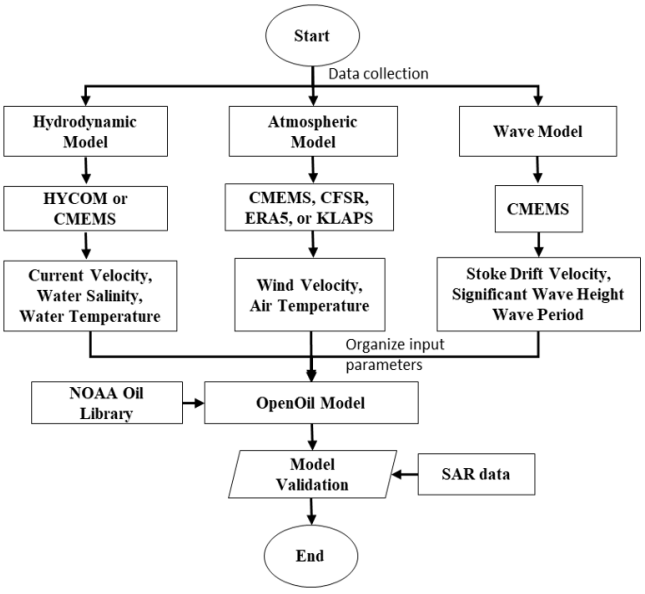

Fig. 1 Flow chart of the proposed methodology

3. Numerical Setup for Hebei Spirit Accident

3.1 Hebei Spirit Accident

On the morning of December 7, 2007, at 7:15 (local time), the very large oil crude oil carrier (VLLC) Hebei Spirit collided with Samsung cranes near the latitude and longitude of 36° 49.93' N, 126° 2.46' E, located approximately 10 km off the Taean coasts, leaking approximately 10,900 t of crude oil. Fig. 2 presents the site location for the spilled oil slick. The Korean Coast Guard (KCG) report indicates that strong northwestern currents and winds blow oil slick transport along approximately 375 km of the west coast of Korean coastlines, heavily contaminating 70 km of the Taean peninsula with crude oil. Remarkably, the oil slick quickly reached the Taean shoreline at 13 h, which was significantly shorter than the predicted time of approximately 24 h, as suggested by the Ministry of Oceans and Fisheries (MOF) (Lee et al., 2020). In particular, oil slicks polluted large areas of the open sea and contaminated Jeju Island, the southern end of the Korean Peninsula (Kim et al., 2014).

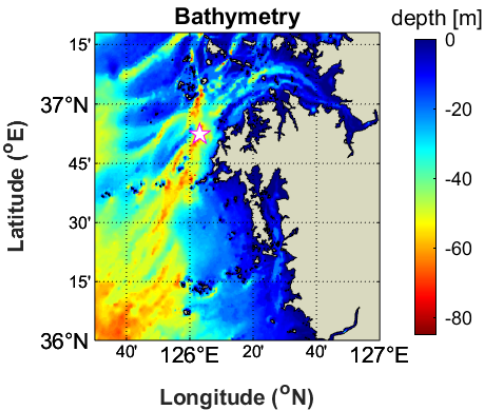

Fig. 2 Bathymetry of Taean coasts for oil spill transport and position of accident (markered star)

Table 4 Initial conditions of the test cases

Initial conditions	Setup
Position	36° 49.93’ N – 126° 2.46’ E
Start time of simulation	2007/12/07
End time of simulation	2007/12/11
Simulation duration	Five days
Oil type	Kuwait export crude
Spill amount (t)	10,900
Model time step (s)	3,600
Output time interval (s)	3,600
Number of particles	10,900
Area coverage	[125.5° 127°] – [36° 37.3°]
Hydrodynamic data	HYCOM, CMEMS
Atmospheric data	CMEMS, CFSR, ERA5, KLAPS
Wave data	CMEMS

The oil slick transport resulting from the Hebei Spirit accident was simulated for five days from 2007/12/07 at 07:15 to 2007/12/07 at 11:00 am. The oil type used in the OpenOil model was Kuwait export crude, with a density of 820.5 kg/m^3 as the representative oil type. Approximately 10,900 oil particles were initially set up. The Openoil model was coupled with the real-time current circulation data from the HYCOM and CMEMS models, winds from CFSR, ERA5, CMEMS, and KLAPS, and waves from CMEMS. Table 4 lists the initial input parameters for the oil slick simulation in the Hebei Spirit accident.

3.2 Simulation of Current, Wind and Wave Fields

The study area on the eastern Yellow Sea is characterized by relatively shallow waters with a water depth of less than 60 m. On the other hand, the topography near the Taean coast is approximately 25 m deep (Fig. 2). Fig. 3 shows the wind velocity fields obtained from CMEMS, CFSR, ERA5, and KLAPS models on December 7, 2007 at 7:15 am. The color map indicates the wind velocity magnitude measured 10 m above the sea water level, and the blue arrows represent the wind direction. The wind fields in the Korean Peninsula follow the characteristics of the seasonal wind areas of Asia. The spring and summer seasons witnessed south/southwestern winds, but the main north/northwestern winds primarily blow in the autumn and winter seasons. Therefore, in the Hebei Spirit accident, the north and northwestern wind fields were recorded with their speed reaching a

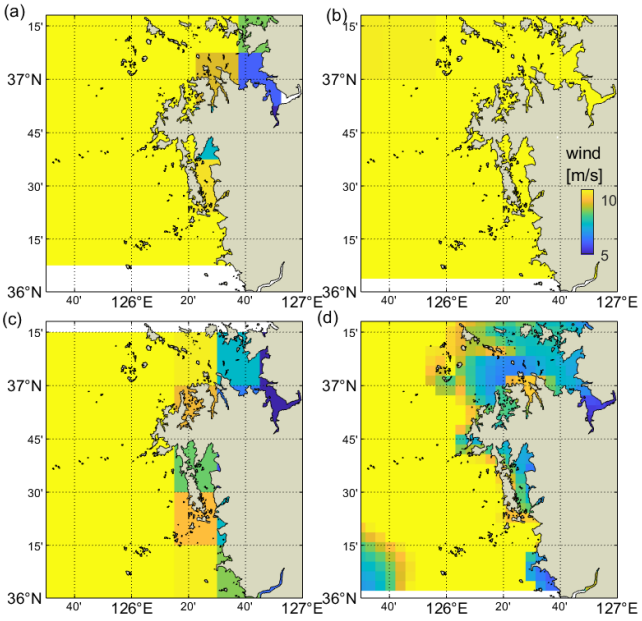

Fig. 3 Computational wind field velocity derived from CMEMS (a), CFSR (b), ERA5 (c), and KLAPS (d) models on December 7, 2007, at 7:00 am.

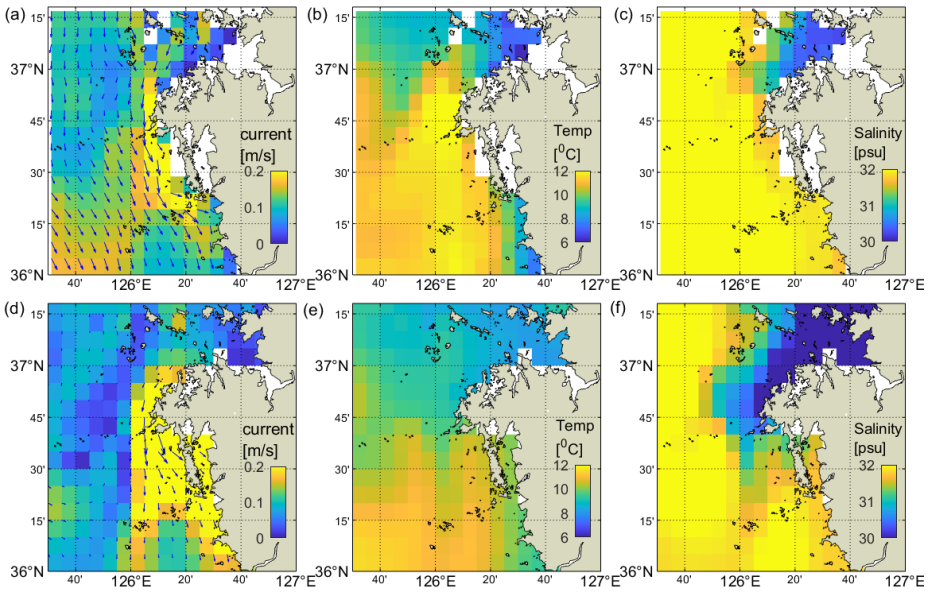

Fig. 4 Computational current field velocity (a, d), sea surface temperature (b, e), and sea surface salinity (c, d) derived from HYCOM (top) and CMEMS (bottom) models on December 7, 2007 at 7:00 am.

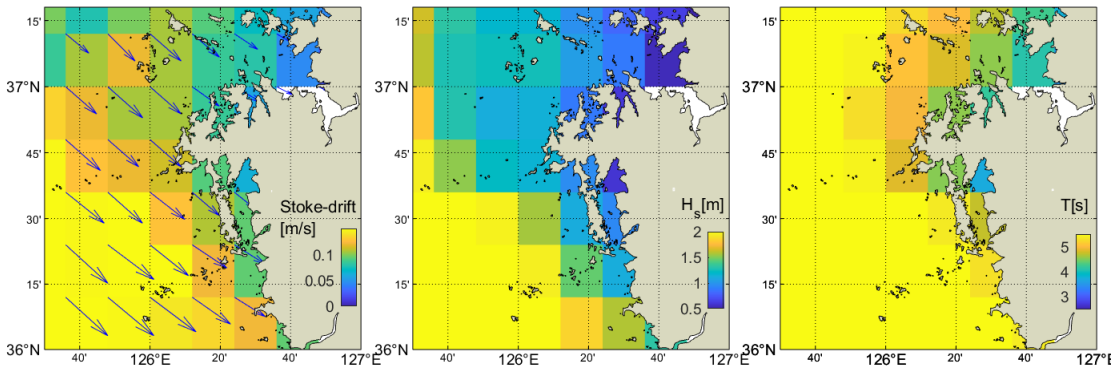

Fig. 5 Computational Stoke Drift field velocity (a), significant wave height (b), and wave period (c) derived from CMEMS model on December 7, 2007 at 7:00 am.

maximum of approximately 14 m/s (Fig. 3). Similarly, for the wind dataset derived from four meteorological models, while approximately less than 6 m/s of wind velocity speed was measured generally close to the Tean coastlines, the wind velocity exceeds 10 m/s in the open sea.

Fig. 4 presents the current circulation parameters, including the current field velocity, sea surface salinity, and sea surface temperature extracted from the HYCOM and CMEMS models. The current velocity ranged from 0.1 m/s to 0.6 m/s in the northwest direction. A slight difference in current velocity was measured near the Taean peninsula. On the other hand, a significant difference is observed in the open sea because HYCOM measured the current parameters every three hours, while the daily dataset was recorded in the CMEMS model. Moreover, the sea surface temperature and salinity magnitude were up to 12°C and 32 psu, respectively.

Keramea et al. (2023) comprehensively reviewed the operation and forcing in oil spill models. The literature review showed that only seven case studies of oil spill simulations were conducted while considering adequate met-ocean data as input parameters. Most studies focused on forecasting hydrodynamic ocean current and meteorological models as met-ocean input parameters while neglecting the wave fields model, represented by the significant wave height, wave period, and Stoke drift velocities, in oil spill models. This limitation may influence the oil slick transport on the ocean surface. Fig. 5 shows the Stoke drift velocities, significant wave height, and period received from the CMEMS model. The maximum significant wave height was approximately 3 m with a wave period of 6.5 s when the accident occurred. Moreover, the Stoke drift velocities ranged from 0.03 m/s to 0.2 m/s in the northwest direction.

4. Numerical Results and Discussion

The oil spill model, OpenOil, was used to simulate oil slick diffusion along the Taean coasts during the Hebei spirit accident. The numerical model was coupled with met-ocean factors of currents, winds, and waves, which were organized into six combinations. The simulation duration was five days, from December 7, 2007, to December 11, 2007. The resulting distribution of spilled oil on the sea surface of each combination was compared with the satellite observation results at 10:40, December 11, 2007. The predictive performance of each combination was evaluated through the matching rate between simulated and observed results, suggesting the most effective combination in simulating oil spill transport in the Korean Peninsula.

4.1 Numerical Model Results

Fig. 6 shows the distribution of oil slick on the sea surface after 99.2 h from the accident. The movement of spilled oil showed good agreement with the current and wind directions presented in Figs. 3 and 4. There are two clear trends for oil diffusion using CMEMS (combinations 1 and 2) and HYCOM models (combinations 3, 4, 5, and 6) as hydrodynamic ocean circulation models in the oil spill model. In combinations 1 and 2, a slight difference is observed in the spilled oil distribution, in which the oil slick moved approximately 92 km from the Taean coast to the Maryang-ri port. By contrast, the combinations from 3 to 6 showed that the distribution of spilled oil slicks ranged from approximately [125.6°–126.1°E] for longitude and [36.4°–36.96°N] for latitude. Table 5 lists the specific dimensions in terms of width and length, as well as the projected area of oil slicks in each combination.

4.2 Numerical Model Validation

The numerical results are validated by comparing the simulated distribution of oil slicks with the observed results obtained from Envisat ASAR at 10:40 on December 11, 2007, for the Hebei Spirit accident. The observation satellite image was processed using the adaptive threshold method (Fig. 7). The significant oil slicks extended longitudinally from 125.6°E to 126.3°E and latitudinally from 36.43°N to 36.99°N, encompassing maximum widths and lengths of 62.27 km and 62.63 km, respectively, and spanning an approximate area of 1600 km^2. Generally, configurations incorporating the HYCOM model as a hydrodynamic input showed reasonable agreement with the observed oil slick distribution in both spatial dimensions and projected area, exhibiting a deviation of less than 20% compared to configurations using CMEMS models, which displayed a

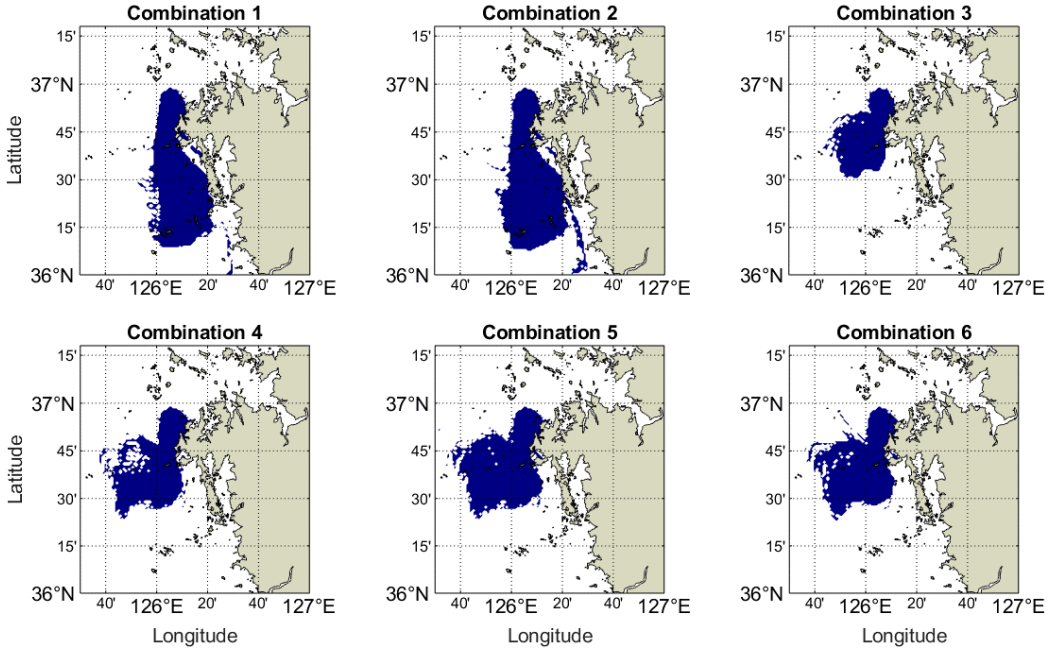

Fig. 6 Oil slick transport distribution acquired over six combinations at 10:40 am, December 11, 2007.

Table 5 Spilled oil distribution over six combinations

Dimensions	Combination 1	Combination 2	Combination 3	Combination 4	Combination 5	Combination 6
Width (km)	44	69	41	48	56	50
Length (km)	92	92	51	66	60	62
Area (km^2)	3155	3183	1131	1965	2056	1991

maximum difference of 50%.

Kim et al. (2014) proposed a thorough validation approach for oil slick movement, enabling users to evaluate the performance of each combination (Fig. 8). First, the study area was divided into grid cells, each measuring 0.5 km × 0.5 km. The second step was to identify each cell containing oil particles in both simulated and observed oil slicks, with blue for the numerical result and pink for the observation result. Subsequently, the overlapped cells between simulated and observed results are extracted. To calculate the percentage of similarity between numerical and SAR results, a matching percent is introduced, which is determined by the fraction between the total number of overlapped cells and the total number of observation cells containing oil particles. Fig. 9 compares the matching percent in each combination with observed results. In the presence of the CMEMS hydrodynamic models, the match percentage was approximately 53%, while the HYCOM hydrodynamic models induced matching rate values from 70% to 88%, indicating a much higher accuracy than the CMEMS combinations. Therefore, the HYCOM model is more effective than the CMEMS model in contributing hydrodynamic ocean circulation parameters for oil spill models. Moreover, significant improvements in matching percentages were observed when a high-resolution meteorological dataset was introduced for HYCOM combinations. For CFSR (spatial resolution ~56 km), the matching percentage was only 70%, which increased to approximately 86% for the ERA5 and CMEMS meteorological models (~27 km) and 88% for the KLAPS model (~5 km). Therefore, increasing the resolution of forecasting met-ocean models is necessary to enhance the performance of numerical models to predict the spilled oil diffusion on the sea surface. Furthermore, the notable precision exhibited by the HYCOM model in simulating the transport of oil slicks underscores the potential for widespread adoption of HYCOM met-ocean datasets coupling with different atmospheric models across the Korean peninsula.

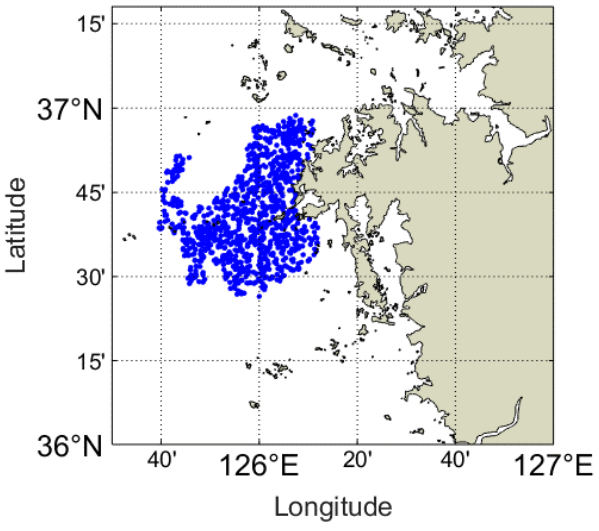

Fig. 7 Oil slick transport distribution measured by SAR observation acquired at 10:40 am, December 11, 2007.

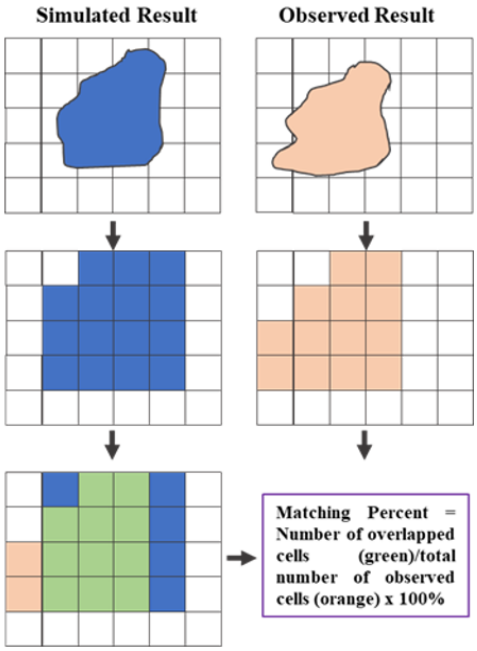

Fig. 8 Flow chart of the model validation process.

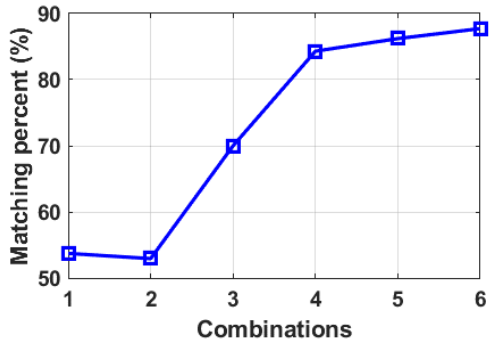

Fig. 9 Matching percentage between six combinations and observation results

4.3 Discussion

The spatial and temporal resolution of met-ocean models significantly influences the accuracy of numerical results in oil spill simulations. Most hydrodynamic, meteorological, and wave models are extracted from open-source global-scale models with coarse resolutions. This highlights the need for further investigation on implementing regional models for oil spill models. The KOOS was established at the KIOST to provide real-time observations and simulated datasets of ocean fields in multiple scales. The KOOS dataset provides waves, currents, sea surface salinity, water temperature, and wind fields, updated twice daily for 72 hours (Park et al., 2015). The system collects observation datasets from real-time marine monitoring platforms. This information was used to calibrate the numerical models. Park et al. (2015) also implemented a 300-m horizontal resolution of atmospheric variables (wind components and atmospheric temperature), current and wave variables (current velocity, water temperature, salinity, and elevation) into the oil spill model, MOHID to simulate the oil spill transport at a quay off Yeosu port. The numerical results effectively replicated the spilled oil transport and satisfied the general acceptable criteria. The KOOS data have been under development since August 2009 by KIOST, and the dataset has not been applied to simulate the Hebei Spirit accident. Nevertheless, the current study suggests that KOOS data can be used to simulate the oil slick transport released from recent accidents and in further research aimed at improving spill modeling.

5. Conclusions

This study conducted a comprehensive examination of the transport of spilled oil slicks resulting from the Hebei Spirit accident, using the OpenOil numerical model operationally coupled with various forecasted met-ocean models. The key findings of this research are summarized as follows:

(1) An extensive literature review was conducted to assess the availability of forecasted met-ocean datasets, which included meteorological models (CMEMS, CFSR, ERA5, and KLAPS), hydrodynamic current circulation models (HYCOM and CMEMS), and a wave model (CMEMS) that can be used as input parameters for simulating the 2007 Hebei Spirit oil spill accident.

(2) Six combinations were tested in OpenOil, incorporating these met-ocean datasets to simulate the transport of the oil slick over five days, spanning from December 7, 2007, to December 11, 2007. The numerical results showed that the selection of hydrodynamic ocean models significantly influenced the distribution of the oil slick. In particular, the hydrodynamic variables derived from the HYCOM model outperformed those from the CMEMS model in replicating the oil slick area compared to the observed dataset, with distribution areas of 1991 km² (combination 6) and 3155 km² (combination 1) compared to the observed oil slick area of 1600 km².

(3) Further validation was carried out by identifying the overlapping cells between the simulated and observed oil slicks on the sea surface. The CMEMS-based combinations exhibited a similarity of 53%, while the HYCOM-based combinations displayed matching percentages ranging from 70% to 88% compared to the SAR-observed oil slicks.

This study provided a comprehensive assessment of the performance of each met-ocean dataset in predicting oil spill transport in the Korean Peninsula. These results highlight the significant impact of the quality of met-ocean datasets on the results of spilled oil distribution. Further research should explore the use of high-resolution KOOS datasets for simulating oil spill transport in the Korean Peninsula. This could contribute to more accurate and reliable oil spill modeling in the region.

Conflict of Interest

Sungwon Shin serves as an editorial board member of the Journal of Ocean Engineering and Technology but played no role in deciding the publication of this article. No potential conflicts of interest relevant to this study are reported.

Funding

This study was based upon work supported by the Korean Evaluation Institute of Industrial Technology (KEIT) grant funded by the Korean government (KCG, MOIS, NFA) [RS-2022-001549812, Development of technology to respond to marine fires and chemical accidents using wearable devices] and Korean Institute of Marine Science & Technology Promotion (KIMST) funded by the Ministry of Oceans and Fisheries, Korea (No. RS-2023-00256687).

References

Abascal, A. J., Castanedo, S., Núñez, P., Mellor, A., Clements, A., Pérez, B., ... & Medina, R. (2017). A high-resolution operational forecast system for oil spill response in Belfast Lough. *Marine Pollution Bulletin*, *114*(1), 302−314. https://doi.org/10.1016/j.marpolbul.2016.09.042

Abdallah, I. M., & Chantsev, V. Y. (2022). Simulating oil spill movement and behavior: a case study from the Gulf of Suez, Egypt. *Modeling Earth Systems and Environment*, *8*(4), 4553−4562. https://doi.org/10.1007/s40808-022-01449-9

Androulidakis, Y., Kourafalou, V., Robert Hole, L., Le Hénaff, M., & Kang, H. (2020). Pathways of oil spills from potential Cuban offshore exploration: Influence of ocean circulation. *Journal of marine science and engineering*, *8*(7), 535. https://doi.org/10.3390/jmse8070535

Dang, H. V., Shin, S., Lim, J., Joo, S., Hur, J. (2023). Numerical model test of spilled oil transport near the Korean coasts using various input parametric modules.*The proceedings of 2023 Fall Conference of the Korea Society of Ocean Engineering (KSOE).*

De Dominicis, M., Bruciaferri, D., Gerin, R., Pinardi, N., Poulain, P. M., Garreau, P., ... & Manganiello, C. (2016). A multi-model assessment of the impact of currents, waves, and wind in modelling surface drifters and oil spill. Deep Sea research part II: topical studies in oceanography, *133*, 21−38. https://doi.org/10.1016/j.dsr2.2016.04.002

De Dominicis, M., Pinardi, N. A. D. I. A., Zodiatis, G., & Archetti, R. J. G. M. D. (2013). MEDSLIK-II, a Lagrangian marine surface oil spill model for short-term forecasting−Part 2: Numerical simulations and validations. *Geoscientific Model Development*, *6*(6), 1871−1888. https://doi.org/10.5194/gmd-6-1871-2013

French-McCay, D. P., Spaulding, M. L., Crowley, D., Mendelsohn, D., Fontenault, J., & Horn, M. (2021). Validation of oil trajectory and fate modeling of the Deepwater Horizon oil spill. *Frontiers in Marine Science*, *8*, 618463. https://doi.org/10.3389/fmars.2021.618463

Hole, L. R., Dagestad, K. F., Röhrs, J., Wettre, C., Kourafalou, V. H., Androulidakis, Y., Kang, H., Le Hénaff, M., & Garcia-Pineda, O. (2019). The Deepwater Horizon oil slick: simulations of river front effects and oil droplet size distribution. *Journal of marine science and engineering*, *7*(10), 329. https://doi.org/10.3390/jmse7100329

ITOPF, (2020). Handbook. https://www.itopf.org/fileadmin/uploads/itopf/data/Documents/Company_Lit/ITOPF_Handbook_2020.pdf.

Jung, T. H., & Son, S. (2018). Oil spill simulation by coupling three-dimensional hydrodynamic model and oil spill model. *Journal of Ocean Engineering and Technology*, *32*(6), 474−484. https://doi.org/10.26748/KSOE.2018.32.6.474

Keramea, P., Kokkos, N., Gikas, G. D., & Sylaios, G. (2022). Operational modeling of North Aegean oil spills forced by real-time met-ocean forecasts. *Journal of Marine Science and Engineering*, *10*(3), 411. https://doi.org/10.3390/jmse10030411

Keramea, P., Kokkos, N., Zodiatis, G., & Sylaios, G. (2023). Modes of operation and forcing in oil spill modeling: state-of-art, deficiencies and callenges. *Journal of Marine Science and Engineering, 11*(6), 1165. https://doi.org/10.3390/jmse11061165

Kim, J. C., Yu, D. H., Sim, J. E., Son, Y. T., Bang, K. Y., & Shin, S. (2023). Validation of opendrift-based drifter trajectory prediction tTechnique for maritime search and rescue. *Journal of Ocean Engineering and Technology*, *37*(4), 145−157. https://doi.org/10.26748/KSOE.2023.018

Kim, T. H., Yang, C. S., Oh, J. H., & Ouchi, K. (2014). Analysis of the contribution of wind drift factor to oil slick movement under strong tidal condition: Hebei Spirit oil spill case. *PloS one*, *9*(1), e87393. https://doi.org/10.1371/journal.pone.0087393

Korean Coast Guard (KCG). (2021). *Korea Coast Guard Annual Report.* https://www.kcg.go.kr/ebook/whitebook/2020/index.html

Law-Chune, S., Aouf, L., Dalphinet, A., Levier, B., Drillet, Y., & Drevillon, M. (2021). WAVERYS: a CMEMS global wave reanalysis during the altimetry period. *Ocean Dynamics, 71*, 357−378. https://doi.org/10.1007/s10236-020-01433-w

Lee, K. H., Kim, T. G., & Cho, Y. H. (2020). Influence of tidal current, wind, and wave in Hebei Spirit oil spill modeling. *Journal of Marine Science and Engineering*, *8*(2), 69. https://doi.org/10.3390/jmse8020069

Meza-Padilla, R., Enriquez, C., & Appendini, C. M. (2021). Rapid assessment tool for oil spill planning and contingencies. *Marine Pollution Bulletin*, *166*, 112196. https://doi.org/10.1016/j.marpolbul.2021.112196

Nguyen, T. H. H., Hou, T. H., Pham, H. A., & Tsai, C. C. (2023). Hindcast of oil spill pollution in the East China Sea in January 2018. *Proceedings of the Institution of Mechanical Engineers, Part M: Journal of Engineering for the Maritime Environment*, 14750902231162171. https://doi.org/10.1177/14750902231162171

Park, K. S., Heo, K. Y., Jun, K., Kwon, J. I., Kim, J., Choi, J. Y., ... & Jeong, S. H. (2015). Development of the operational oceanographic system of Korea. *Ocean Science Journal*, *50*, 353−369. https://doi.org/10.1007/s12601-015-0033-1

Röhrs, J., Dagestad, K. F., Asbjørnsen, H., Nordam, T., Skancke, J., Jones, C. E., & Brekke, C. (2018). The effect of vertical mixing on the horizontal drift of oil spills. *Ocean Science*, *14*(6),

15811601. https://doi.org/10.5194/os-14-1581-2018

Sepp Neves, A. A., Pinardi, N., Navarra, A., & Trotta, F. (2020). A general methodology for beached oil spill hazard mapping. *Frontiers in Marine Science*, *7*, 65. https://doi.org/10.3389/fmars.2020.00065

Siqueira, P. G. S. C., Silva, J. A. M., Gois, M. L. B., Duarte, H. O., Moura, M. C., Silva, M. A., & Araújo, M. C. (2022). Numerical simulations of potential oil spills near Fernando de Noronha archipelago. *Trends in Maritime Technology and Engineering*, 273–282.

Zacharias, D. C., Gama, C. M., Harari, J., da Rocha, R. P., & Fornaro, A. (2021). Mysterious oil spill on the Brazilian coast–part 2: a probabilistic approach to fill gaps of uncertainties. *Marine pollution bulletin*, *173*, 113085. https://doi.org/10.1016/j.marpolbul.2021.113085

Zhang, X., Cheng, L., Zhang, F., Wu, J., Li, S., Liu, J., ... & Li, M. (2020). Evaluation of multi-source forcing datasets for drift trajectory prediction using Lagrangian models in the South China Sea. *Applied Ocean Research*, *104*, 102395. https://doi.org/10.1016/j.apor.2020.102395

Author ORCIDs

Author name	ORCID
Dang, Hai Van	0000-0002-5922-6624
Joo, Suchan	0009-0000-0318-5555
Lim, Junhyeok	0009-0008-7955-5119
Hur, Jinhwan	0009-0001-1444-0299
Shin, Sungwon	0000-0002-4564-2627

KSOE

Review Article

Journal of Ocean Engineering and Technology 38(2), 74−85, April, 2024
https://doi.org/10.26748/KSOE.2024.041

pISSN 1225-0767
eISSN 2287-6715

Foundation Types of Fixed Offshore Wind Turbine

Yun Jae Kim[1], Jin-wook Choe[2], Jinseok Lim[2] and Sung Woong Choi[3]

[1]*Master course student, Department of Mechanical System Engineering, Gyeongsang National University, Tongyeong, Korea*
[2]*Senior researcher, Power Cable Research Center, Korea Electrotechnology Research Institute, Changwon, Korea*
[3]*Professor, Department of Mechanical System Engineering, Gyeongsang National University, Tongyeong, Korea*

KEYWORDS: Fixed offshore wind, Gravity-based foundation, Monopile, Jacket, Tripod, Suction bucket

ABSTRACT: *Offshore wind turbines are supported by various foundations, each with its considerations in design and construction. Gravity, monopile, and suction bucket foundations encounter geotechnical issues, while jacket and tripod foundations face fatigue problems. Considering this, a gravity foundation based on a steel skirt was developed, and a monopile foundation was analyzed for Pile-Soil Interaction using the p–y curve and 3D finite element method (3D FEM). In addition, for suction bucket foundations, the effects of lateral and vertical loads were analyzed using 3D FEM and centrifuge tests. Fatigue analysis for jacket and tripod foundations was conducted using a hotspot stress approach. Some hybrid foundations and shape optimization techniques that change the shape to complement the problems of each foundation described above were assessed. Hybrid foundations could increase lateral resistance compared to existing foundations because of the combined appendages, and optimization techniques could reduce costs by maximizing the efficiency of the structure or by reducing costs and weight. This paper presents the characteristics and research directions of the foundation through various studies on the foundation. In addition, the optimal design method is presented by explaining the problems of the foundation and suggesting ways to supplement them.*

1. Introduction

Countries worldwide adopted the Paris Agreement to cope with climate change. The South Korean government announced its “Renewable Energy 3020 Plan” to reduce greenhouse gas (GHG) emissions, which are the leading cause of climate change. According to the plan, the total renewable energy generation is targeted at 20% with 63.8 GW by 2030 by supplying more than 95% of new facilities with clean energy, such as solar and wind power (Ministry of Trade Industry and Energy, 2017). According to the Global Wind Energy Council (GWEC, 2022), the offshore wind market is expected to grow rapidly. In 2021, 21.2 GW of offshore wind capacity was added, and a total capacity of 316 GW is expected to be supplied with a 16.7% increase in 2030.

In the case of onshore wind power in domestic and overseas wind markets, there are limited sites for constructing large power complexes. The construction causes noise, radio interference, and visual inconvenience, resulting in complaints. The interference of the surrounding geographic features also reduces wind speed, decreasing energy efficiency. In the case of offshore wind power, it is easy to construct large power generation complexes compared to onshore wind power, and the construction causes fewer complaints. It also provides high energy efficiency because the wind speed is 70% higher on average than onshore wind power (Park et al., 2021). Despite this, offshore wind power is difficult to install because of the complex marine environment and requires higher installation costs than onshore wind power. In particular, the foundations of offshore wind turbines (OWTs) increase design costs because of their large and robust design to withstand the loads of the marine environment. The installation and foundation design costs of OWTs are 20% and 12.5% higher, respectively, than those of onshore wind turbines, as shown in Fig. 1 (Guo et al., 2022). In addition, the foundations of OWTs increase in size and weight as the water depth increases, which increases the design cost significantly. Therefore, the selection and optimal design of a foundation type suitable for the water depth are the most important factors in effectively reducing costs (Oh et al., 2018).

OWTs are generally divided into fixed and floating types, which are classified into foundations with various shapes based on the water depth. Therefore, it is important to select a foundation considering the location and purpose. Gravity and monopile foundations with simple

Received 5 December 2023, revised 28 January 2024, accepted 27 February 2024
Corresponding author Sung Woong Choi: +82-55-772-9103, younhulje@gnu.ac.kr

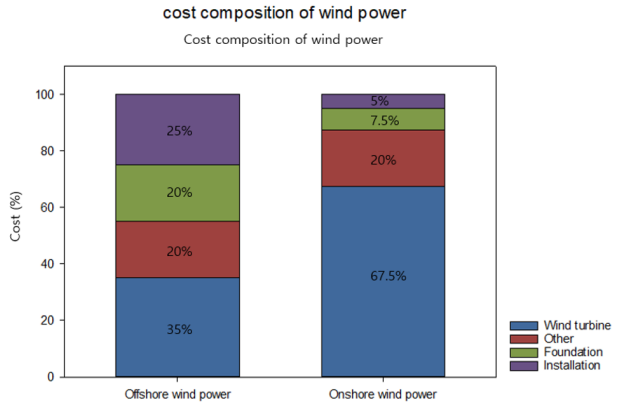

Fig. 1 Cost of onshore wind turbine and offshore wind turbine (Guo et al., 2022)

structures are installed mainly in the shallow sea (0 to 30 m), but gravity foundations are not installed for 3MW or higher OWTs because of the heavy weight and transport costs. Many design cases for monopile foundations have been reported because of the larger power generation capacity and higher installation depth than gravity foundations. In the case of monopile foundations, however, larger diameter piles are applied as the depth and capacity increase, increasing costs due to the increased amount of steel. Therefore, multipod-type (jacket and tripod) foundations are installed mainly in transitional waters (30 to 50 m) and deep waters (50 to 200 m) (Oh et al., 2018).

Li et al. (2020) examined the costs of various foundations for 5MW OWTs. The costs included design, production, and installation, which were expressed in Euro (€) as of 2016. In depths of 30 to 39 m, the costs were found to be 864, 972, 918, and 1024 k€/MW for gravity, steel monopile, steel jacket, and tripod foundations, respectively. Gravity foundations showed the most economical cost, but a maximum cost of 1247 k€/MW may occur considering additional submarine preparation costs. Therefore, jacket-type structures were considered the most economical for 5MW OWTs.

Extending the mechanical life of OWTs, which are significantly affected by the surrounding environment, requires a consideration of the factors involved in the design and construction processes and an understanding of the basic shape of the structure (Jiang, 2021). For OWTs, it is necessary to identify the characteristics of foundations and their technological problems.

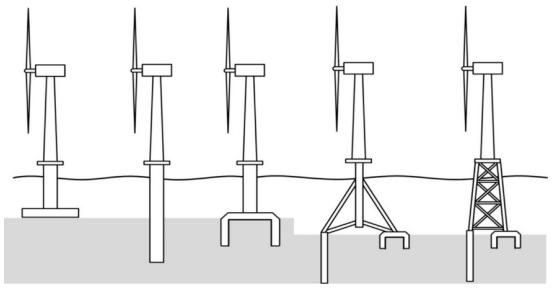

Fig. 2 Foundation types of fixed offshore wind turbines (Oh et al., 2018)

This study examined the foundations of fixed OWTs. The foundations were divided into gravity, monopile, jacket, tripod, and suction bucket types, as shown in Fig. 2. The benefits and limitations of the shape were explained for each foundation, and the results of previous studies and the latest research trends were examined. Technological problems, design, and methodologies were discussed based on the results of previous studies on each foundation, and research directions were presented. In addition, an optimal design method with improved reliability was presented based on research trends.

2. Characteristics of Fixed Offshore Wind Turbine Foundations

2.1 Gravity-Based Foundation

Gravity-based foundations are the foundation type first applied to OWTs. They have benefits, such as inexpensive material cost and easy installation via transport after onshore production, because they consist of materials that can be obtained easily, such as concrete and steel (Saleem, 2011).

Gravity-based foundations can be classified as shown in Fig. 3. These foundations are divided mainly into three types. Vindeby (Barthelmie et al., 1996) and Middelgrunden (Larsen et al., 2005) are first-generation gravity-based foundations. They are solid reinforced concrete structures with large-diameter slabs with no holes and cells. This type can be designed only for very shallow depths of 3 to 7 m (Esteban et al., 2019). For the second-generation gravity-based foundations, Rodsand1(4C Offshore, 2020), which was commissioned in 2003, was applied to a depth of 6 to 10 m. Rodsand2 (4C Offshore, 2020) and Karehamn (4C Offshore, 2020) were also commissioned in 2010 and 2013 and applied to 6 to 12 m and 6 to 20 m depths, respectively. The second-generation gravity-based foundations are similar to the first generation but have holes or cells in the slab (Esteban et al., 2019). A representative third-generation gravity-based foundation is Thornton Bank 1 (Mengé and Gunst, 2008). The foundation was commissioned in 2009 and applied to an 18 to 24 m depth. The third-generation gravity-based foundation has a narrow cylindrical shape for the upper part and a conical shape for the lower part to directly transfer the load of the turbine to the bottom slab. This foundation consists of hollow steel pipes submerged in the seabed after being designed on land, and the empty space is filled with ballast at the installation location (Mengé and Gunst, 2008). Blyth, which was recently commissioned in 2017, is located at a 35 m depth and has a similar shape to that of Thornton Bank. Unlike Thornton Bank, Blyth (ICE, 2017) is towed to the final position by a tugboat using the “float and submerge” technique to save transport costs. Table 1 lists the gravity-based foundations mentioned in this section through references (Esteban et al., 2019; 4C Offshore, 2020).

2.2 Monopile

Monopiles, the most commonly used support structures, are easy to produce and install because a large-diameter pile is connected to piling

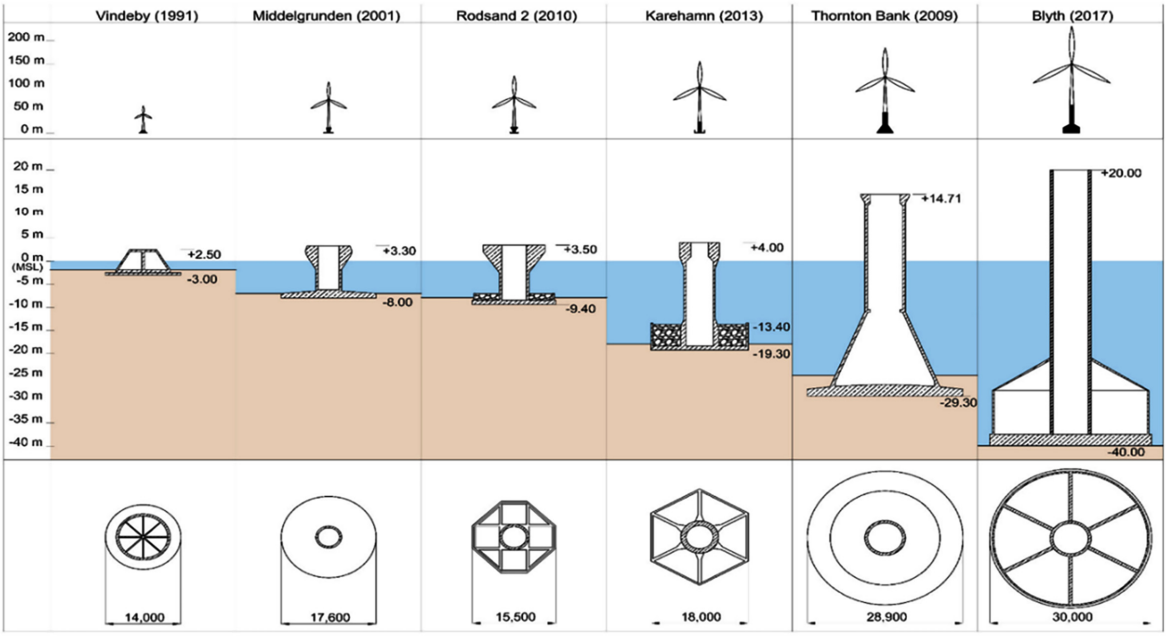

Fig. 3 Fixed offshore wind turbine, gravity-base foundation (Mathern et al., 2021)

Table 1 Development and characteristics of gravity-base foundation

Name	Year	Total power (MW)	Depth (m)	Distance (km)
Vindeby	1991	4.95	2–4	2
Middelgrunden	2001	40	4–8	2–3
Rodsand 1	2003	166	6–12	10
Thornton Bank	2009	30	18–24	30
Rodsand 2	2010	207	7.5–12.5	8
Karenhamn	2013	48	3.8	3.8
Blyth	2017	41.5	35	5.7

with grout. They are economically beneficial at depths of less than 30 m (Saleem, 2011). The structure is completed with grout, which is high-strength concrete for joining the upper tower, after installing a single large-diameter pile, a steel cylinder with a high thickness, using the piling method.

Monopile foundations are affected by lateral loads because of the vertical cylindrical structure. Lateral loads reduce the bearing capacity of the foundation and decrease soil stiffness due to the soil deformation around the foundation. The optimal pile diameter must be determined to secure bearing capacity because lateral loads vary depending on the the water depth (Achmus et al., 2009). The design of the natural frequency that can avoid resonance with the forced frequency generated under environmental loads is also essential to minimize fatigue damage (Andersen et al., 2012; Lombardi et al., 2013). In the design stage, the natural frequency varies according to the stiffness of the foundation and the strength and stiffness of the soil, and it can be transformed by external dynamic loads. The change in stiffness of the foundation and soil must be considered in the design stage because this shortens the life of the structure.

Lombardi et al. (2013) conducted a series of model tests to examine the changes in the natural frequency and attenuation of the monopile OWT foundation under continuous environmental loads. They also expressed the soil strain (ϵ_s) around the foundation as a dimensionless number using three parameters to identify the natural frequency due to soil deformation as expressed in Eq. (1). The early changes in natural frequency were measured using a free vibration test. The changes in natural frequency according to the forced frequency and soil strain under cyclic loads were examined. According to the research results, the natural frequency was reduced most significantly as the ratio (f_f/f_n)) of the forced frequency (f_f) to the natural frequency (f_n) approached one. In addition, when only the soil strain (ϵ_s) was adjusted in a structure where the ratio (f_f/f_n)) approached one under the same cyclic loading condition, the natural frequency of the structure decreased by 37% and 0.02% at soil strain (ϵ_s) values of 34% and 0.02%, respectively. This shows that the deformation of soil has a significant impact on the stiffness of the structure. Monopile foundations are significantly affected by the surrounding soil. Therefore, it is important to identify the life of the structure from the relationship between the foundation and soil.

$$\epsilon_s = f\left(\frac{P}{GD^2}\right) \quad \frac{F}{[FL^{-2}][L]^2} \tag{1}$$

where ϵ_s, P, D, and G are the soil strain, horizontal load acting on the foundation, diameter of the pile, and shear modulus of the soil, respectively.

2.3 Jacket-Based Foundation

Jacket-based foundations have long been used for oil and gas mining facilities. OWTs have been designed based on them at a depth of 30 to

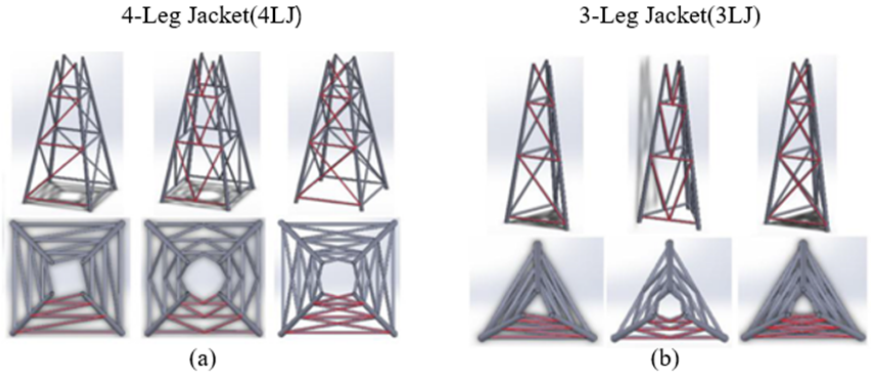

Fig. 4 Various types of jacket foundations (Chen et al., 2016)

80 m owing to their solid and stable characteristics. Jacket-based foundations distribute loads with multiple legs. Hence, they have higher structural stability than other OWT foundations (Wang et al., 2018).

Hao and Liu (2017) compared the impact prevention performance among the monopile, tripod, and jacket foundations for OWTs. They concluded that the jacket type has optimal impact prevention performance because of the highest performance in the collision force and damage area.

Jacket-based foundations improve the axial capacity by connecting the lower structure and the wind turbine using grout. The upper part of the jacket is combined with the tower through the transition piece. The lower part of the jacket is formed by three to four legs under axial and bending loads as well as X, V, and Z-braces that connect the legs, as shown in Fig. 4. The weight and stiffness of jacket-based foundations as well as their dynamic response under external loads vary according to their shape. Therefore, it is vital to find the optimal geometry with stability considering marine characteristics according to the design location for jacket-based foundations (Shi et al., 2013; Chen et al., 2016).

Shi et al. (2013) compared the dynamic responses of jacket-based foundations with X and Z braces according to their weight and marine environment. The marine characteristics were considered based on a depth of 30 m in the southwest sea of Korea, and deterministic and probabilistic simulations were performed for 5MW OWTs. According to the research results, jackets with X-braces showed higher performance in terms of dynamic response, and Z-braces also showed a dynamic response that met design standards. Therefore, designing jackets with relatively lighter Z-braces is more appropriate.

Chen et al. (2016) conducted dynamic analysis and local buckling analysis of various types of jackets that support OWTs, as shown in Fig. 4. The dynamic response was analyzed under normal and extreme conditions because the dynamic analysis of jacket-based foundations is affected by environmental loads, such as wind, tides, and waves. Local buckling analysis of jacket foundations was verified through numerical simulation and scale models. All jacket foundations provided safe values in terms of the critical load and local buckling strength. The results may vary according to the location. Hence, additional dynamic analysis and fatigue analysis are required.

2.4 Tripod

Tripod foundations that can support structures in a wide range are installed at approximately 25 to 50 m depths. Tripod foundations showless resonance by waves because of the high stiffness, and their natural frequency can be adjusted (Lozano-Minguez et al., 2011). Tripod foundations provide triangular support using the cylindrical steel tube column in the center and three legs and braces. They are favorable for securing safety because the central column transfers the load of the structure to pile sleeves through diagonal braces (Saleem, 2011). They are, however, vulnerable to fatigue damage because of the complex structure as with jacket-based foundations. Thus, accurate calculations are required. In addition, the three piles must be designed against extreme load cases to prepare for changes in weather conditions, wind, and waves, which are marine environmental conditions that occur in all directions. In particular, fatigue damage must be examined under FLS conditions (Ma et al., 2018).

2.5 Suction Bucket

The suction bucket is a lid-shaped bucket with a large venthole. When installed in soil, the suction bucket adheres to the soil due to the

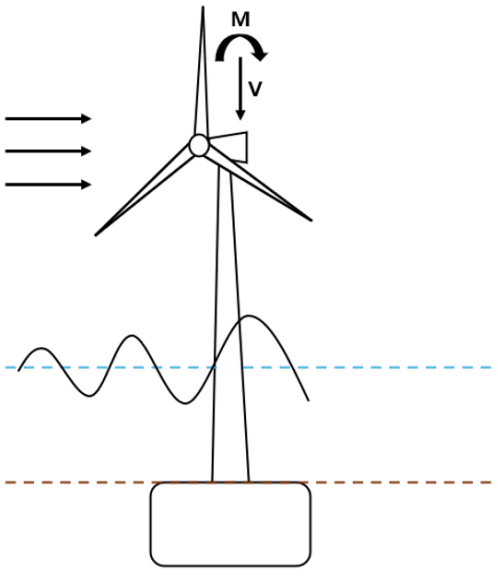

Fig. 5 Fixed offshore wind turbine, suction bucket (Wang et al., 2017a)

pressure difference caused by the vacuum, increasing the bearing capacity of the structure. The suction bucket is designed to have a larger diameter and a shorter length than monopile foundations (Fig. 5), and it applies to a depth of up to 60 m (Wang et al., 2018).

Suction bucket foundations involve less vibration and noise than other foundations installed through piling. They are economically beneficial because of the short construction period. They are also easy to remove when their application is finished because they are installed by introducing seawater (Byrne and Houlsby, 2003). Suction bucket foundations, however, are sensitive to lateral loads, which alter the bearing capacity, deflection, and rotation of the structure. Therefore, research is required to understand and respond appropriately to structural effects. It is also necessary to consider design conditions according to the soil characteristics because they significantly affect the suction bucket.

3. Problems and Analysis of Fixed Offshore Wind Turbine Foundations

3.1 Geotechnical Problems with Fixed Offshore Wind Turbine Foundations

Geotechnical problems with fixed OWT foundations mainly occur from gravity, monopile, and suction bucket foundations that correspond to single foundations. For gravity-based foundations, a gravity-based structure is usually installed after digging the seabed. Therefore, their design can be limited by the soil characteristics. In particular, obtaining sufficient bearing capacity on soft or weak soil is difficult. Lateral loads have a dominant influence on monopile and suction bucket foundations. Lateral loads reduce the bearing capacity of the foundation by decreasing the stiffness of the soil around it, but they also cause local scour. Therefore, it is necessary to identify the characteristics of soil and the displacement of the foundation under external loads, considering the damage caused by the foundation–soil interaction before design. In this regard, geotechnical problems with each foundation were mentioned in this section for gravity, monopile, and suction bucket foundations significantly affected by soil. Solutions and analysis methods to address the problems were presented through papers that dealt with them.

3.1.1 Geotechnical problems with gravity-based foundations and solutions

For gravity-based foundations, a gravity-based structure is usually installed after digging the seabed. This involves detailed work under the sea, and a pipe or other equipment is used to dig the seabed. The gravity-based structure is then placed at the precise location. For gravity-based foundations, soil erosion on the seabed by the tides or waves is prevented by scour protection, a structure to protect the bottom surface of the seabed. Scour protection is placed around the gravity-based structure with stones or rocks to strengthen its stability. Gravity-based structures are difficult to install on poor-quality soil because their bottom structure is located on top of the seabed. Thus,

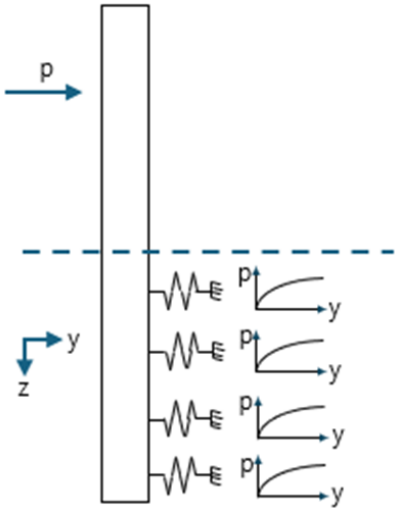

Fig. 6 *p–y* curves method (Sunday and Brennan, 2021)

seabed preparation must be performed for terrain and soil quality to improve the bearing capacity (Esteban et al., 2015). During seabed preparation, it is necessary to examine the soil characteristics and remove soil with low bearing capacity. The soil must also be leveled to install gravity-based foundations, incurring additional costs and economic losses. A gravity-based foundation based on a steel skirt is being developed to address these problems. This can significantly reduce the need for seabed preparation by injecting concrete into the empty space between the foundation and the seabed (Mathern et al., 2021).

3.1.2 Monopile-soil problem and analysis method

Monopile foundations are embedded in the soil. Therefore, it is necessary to reflect their dynamic behavior in the design because of the nature of marine structures. The soil around a monopile foundation has different stiffness and shear strength depending on the drainage condition, which has a significant impact on the displacement of the foundation. For safe design, this needs to be considered through pile-soil interaction (PSI) analysis.

In general, the *p–y* curve that used a beam, which is the nonlinear Winkler (1867) foundation model, is used for PSI according to the guidelines of the American Petroleum Institute (API, 2000). As shown in Fig. 6, The *p-y* curve of API represents the relationship between the subgrade reaction (p) and lateral pile displacement (y) by replacing the stiffness of soil with the stiffness of a spring. Many studies have dealt with PSI for monopile foundations through the *p–y* curve (Bisoi and Haldar, 2014; Sunday and Brennan, 2021).

Bisoi and Haldar (2014) investigated lateral pile displacement in undrained clay under cyclic loads. They also compared and analyzed lateral pile displacement in uniform soil with a constant shear strength along the depth and non-uniform soil with varying shear strength through the *p–y* curve. They reported that the lateral pile displacement in the non-uniform soil was 60% larger than that in the uniform soil when a wind speed of 25 m/s was applied as a lateral load under the resonance condition ($f_f/f_n = 1$).

Fig. 7 Coupled spring model to consider the effect of the foundation (Jung et al., 2015)

The API (2000)-based *p-y* curve is an empirical interpretation of piles with a diameter of up to 2.0 m. This curve may underestimate the soil stiffness and overestimate lateral pile displacement for monopiles with large diameters (Bekken, 2009). Therefore, some researchers presented PSI analysis methods based on the three-dimensional continuum-based finite element method (3D FEM) (Jung et al., 2015; Liu and Kaynia, 2022).

Jung et al. (2015) conducted SSI analysis of monopile foundations using Abaqus software based on 3D FEM. They examined the lateral displacement curve for a later load using a coupled spring model (Zaayer, 2002), as shown in Fig. 7. Monopile foundations were modeled using 3D solid elements. The behavior of sand and clay was simulated using the Mohr–Coulomb model (Hearn and Edgers, 2010) and the Tresca model (Jeanjean, 2009), respectively. When the FEM model and the *p–y* curve were compared, the foundation moment showed a slight difference of less than 4%, but the measured slope of the pile head was more than 14% higher in the FEM model. Therefore, researchers proposed the application of FEM modeling when there are problems with the service life of OWTs because of the high slope.

Liu and Kaynia (2022) conducted a 3D FEM analysis of the PSI of monopile foundations using the SANISAND-MSu model. The SANISAND-MSu model (Liu et al., 2020) analyzes the displacement of the monopile under lateral cyclic loads through 3D FEM analysis by simulating the circulation behavior of sand under drained and undrained conditions. When the pile displacement in sand under drained and undrained conditions was compared, the measured pile displacement in sand was larger under undrained conditions. The severe deformation of soil and reduced soil stiffness caused by the accumulation of pore water pressure significantly affected the pile displacement. Therefore, it is essential to examine the drainage condition of soil for the safe design of monopile foundations.

3.1.3 Local scour at monopile foundations

Local scour occurs around monopile foundations because of severe changes in environmental load. Scouring around monopile foundations is caused by current, waves, and a combination of current and waves. The shear stress near the soil changes when sediment moves from a monopile foundation. Local scour occurs when the critical shear stress of the soil is exceeded. The cyclic loads caused by environmental loads can also cause local scour by reducing the strength and stiffness of soil and promoting the interaction between the pile and soil. Such local scour decreases the bearing capacity of monopile foundations and may destroy the structure (Guan et al., 2022). Therefore, many studies have examined the effects of scour protection to prevent local scour (Askarinejad et al., 2022; Zhang et al., 2023).

Askarinejad et al. (2022) conducted a centrifuge test to examine the scour protection effect for monopiles. This test was conducted on scour prevention layers corresponding to five times (5D) and seven times (7D) the monopile diameter. Under monotonic loading conditions, the lateral resistance of the pile foundation increased by more than 30% for the scour prevention layer of 5D, and the difference in lateral resistance from the scour prevention layer of 7D was less than 5%. Regarding the effects of the scour prevention layer of 5D under cyclic loads, the cumulative deflection decreased by more than 50% compared to the monopile foundation with no scour prevention layer. Hence, the scour protection layer significantly affects the stability of monopiles.

Zhang et al. (2023) explained more than 20 methods to protect monopile foundations from scour based on previous studies. They mentioned the benefits and shortcomings of various scour protection methods, considering the scour protection effect, safety, cost, environmental impact, and additional effects.

3.1.4 Suction bucket-soil problem and analysis method

Suction bucket foundations are mostly sensitive to lateral loads, as with monopile foundations, which significantly reduces the bearing capacity of the structure by deflecting and rotating the structure and causing changes in the soil characteristics. Suction bucket foundations require further analysis because the vertical load and moment affect the final bearing capacity. Therefore, research on effective responses to these effects is required to maintain structural stability.

Wang et al. (2017a) conducted a centrifuge test to examine the lateral support behavior of suction bucket foundations under static and cyclic loading conditions. They analyzed the lateral displacement of the structure under static and cyclic lateral loads considering the soil condition and the aspect ratio of the foundation. Under cyclic lateral loads, the lateral displacement increased rapidly in the early cycles, and it tended to change slowly as the number of cycles increased. In particular, the fifth cycle represented approximately 2/3 of the total displacement.

Liu et al. (2014) analyzed the support behavior of the bucket foundation in drained silty sand through Abaqus version 6.10. They examined the bearing capacity of suction bucket foundations according to the aspect ratio by dividing the vertical load (V), horizontal load (H), and moment (M) into single loads, secondary combined loads (VH, VM, and HM), and a tertiary combined load (VHM). They reported that the vertical load decreased the displacement and rotation of the bucket and increased the horizontal bearing capacity and moment capacity by strengthening the foundation-soil interaction.

Wang et al. (2019) conducted a centrifuge test of the vertical bearing capacity of suction bucket foundations. They also compared the numerical approach with the data of the actual test model to estimate

the bearing capacity of the suction bucket foundation. In the centrifuge test results, the bearing capacity of the presented foundation was higher than that obtained through the numerical approach. The results emphasized the difference between numerical modeling and actual experimental data and evaluated the bearing capacity of the suction bucket foundation in real terrain.

Wang et al. (2017b) conducted a centrifuge test to evaluate seismic response because the soil liquefaction caused by an earthquake can significantly decrease the strength and stiffness of soil. They also conducted research on resistance to liquefaction according to the aspect ratio. They reported that the resistance to soil liquefaction increased as the aspect ratio increased.

3.2 Fatigue Damage Analysis Method for Fixed Offshore Wind Turbine Foundations

Fatigue damage problems with fixed OWT foundations mainly occur from jacket and tripod foundations corresponding to multi-pile foundations. Jacket and tripod foundations have structural stability compared to other OWT foundations because of the complex structure that combines legs and braces, but they are vulnerable to fatigue damage caused by external loads. Fatigue damage occurs mostly at tubular joints, i.e., welded joints. The fatigue life of tubular joints must be estimated because the fatigue life of structural joints determines the design life. Therefore, this section focuses on analysis methods for the fatigue damage of jacket and tripod foundations in this section.

3.2.1 Fatigue damage analysis method for jacket foundations

For jacket foundations, the welded joints, in combination with legs and braces, are referred to as tubular joints. When a stress concentration occurs at the tubular joints under long-term cyclic loads, it can be difficult to secure fatigue resistance and structural safety. Therefore, it is important to evaluate the fatigue damage of tubular joints. Many studies have conducted fatigue analysis to evaluate fatigue damage using the hot spot stress (HSS) approach according to the guidelines of DNVGL-RP-C203 (2016), as shown in Fig. 8 (Ju et al., 2019; Marjan and Hart, 2022).

The HSS approach is used to evaluate fatigue damage at eight points located around a tubular joint, including the axial load for external loads and bending inside and outside the plane, according to the guidelines of DNV (2016). At these points, HSS formulas were expressed as Eq. (2).

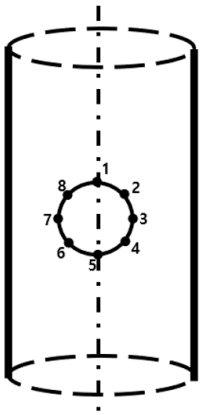

Fig. 8 Positions of hot spots in tubular joints (DNV, 2016)

$$\sigma_1 = SCF_{AC}\,\sigma_x + SCF_{MIP}\sigma_{my} \tag{2}$$

$$\sigma_2 = \frac{1}{2}(SCF_{AC} + SCF_{AS})\,\sigma_x + \frac{1}{2}\sqrt{2}\,SCF_{MIP}\sigma_{my} - \frac{1}{2}\sqrt{2}\,SCF_{Mop}\sigma_{mz}$$

$$\sigma_3 = SCF_{AS}\,\sigma_x - SCF_{MoP}\sigma_{mz}$$

$$\sigma_4 = \frac{1}{2}(SCF_{AC} + SCF_{AS})\,\sigma_x - \frac{1}{2}\sqrt{2}\,SCF_{MIP}\,\sigma_{my} - \frac{1}{2}\sqrt{2}\,SCF_{MoP}\,\sigma_{mz}$$

$$\sigma_5 = SCF_{AC}\,\sigma_x - SCF_{MIP}\,\sigma_{mz}$$

$$\sigma_6 = \frac{1}{2}(SCF_{AC} + SCF_{AS})\sigma_x - \frac{1}{2}\sqrt{2}\,SCF_{MIP}\,\sigma_{my} + \frac{1}{2}\sqrt{2}\,SCF_{MoP}\sigma_{mz}$$

$$\sigma_7 = SCF_{AC}\sigma_x + SCF_{MoP}\,\sigma_{mz}$$

$$\sigma_8 = \frac{1}{2}(SCF_{AC} + SCF_{AS})\,\sigma_x + \frac{1}{2}\sqrt{2}\,SCF_{MIP}\sigma_{my} + \frac{1}{2}\sqrt{2}\,SCF_{MoP}\sigma_{mz}$$

where σ_x is the axial load, and σ_{my} and σ_{mz} are the maximum nominal stresses caused by bending inside and outside the plane, respectively. SCF_{AC} and SCF_{AS} are the stress concentration factors at the crown and saddle for the axial load, respectively. SCF_{MIP} and SCF_{MoP} are the stress concentration factors for the internal and external moments of the plane, respectively. SCFs in Eq. (2) are used for HSS formulae through the Efthymiou equation (Efthymiou, 1988).

Ju et al. (2019) conducted a fatigue analysis of the tubular joints of jacket foundations. They calculated the HSS at eight points around the tubular joints and used the rain-flow counting method (Amzallag et al., 1994) to express the average stress under random loads.

Marjan and Hart (2022) conducted a time-series fatigue analysis of tubular joints through the Sesam software, a marine structure analysis software program, to examine the fatigue life of jacket foundations. They calculated fatigue life through the HSS approach according to the guidelines of DNV (2016). They also used Miner's rule (Miner, 1945) to calculate the total damage of each tubular joint and confirmed the position of the joint with the largest fatigue damage.

3.2.2 Fatigue damage analysis method for tripod foundations

Tripod foundations are vulnerable to fatigue damage because of the complex structure, as with jacket foundations, and stress concentration occurs at tubular joints. Therefore, determining the fatigue life by accurately calculating fatigue damage for tripod foundations is also important.

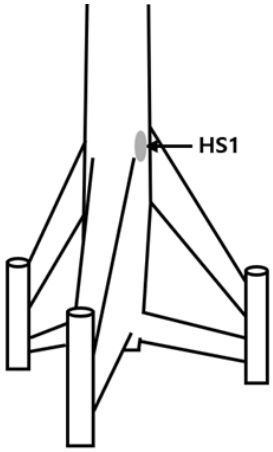

Fig. 9 Location of fatigue damage in tripod foundation (Ma et al., 2018)

Ma et al. (2018) conducted finite element analysis using the ABAQUS software for a 6MW OWT based on a tripod foundation. They examined the loads of the marine environment considering the ultimate limit state (ULS), serviceability limit state (SLS), and fatigue limit state (FLS) at the design location. They presented the maximum cross-sectional area equivalent stress distribution and lateral load for the three piles of the tripod foundation under ULS conditions and examined the deflection distribution of the three piles under SLS conditions. Under FLS conditions, the largest fatigue damage occurred at the tubular joint (HS1) between the central column and the brace, as shown in Fig. 9.

Yeter et al. (2015) performed a time-domain fatigue damage assessment for tripod foundations under various environmental load conditions. They derived the dynamic response spectrum under environmental loads using a high-speed Fourier transform and obtained the average stress through the rain-flow counting method (Amzallag et al., 1994), considering cyclic loads. Yeter et al. (2015) also calculated fatigue damage using the S–N approach. The largest fatigue damage was observed from the tubular joint between the central column and the brace. The accurate fatigue life was obtained by comparing the fatigue lives obtained using the rain-flow counting method, the Dirlik method (Dirlik, 1985), and the Narrow-band solution (Bendat, 1964).

Lu et al. (2023) introduced the Stress Influence Matrix (SIM) to simplify the fatigue analysis of tripod foundations. The SIM approach considers the cyclic loads from external loads and expresses the unit force and moment in each component direction using a matrix. Approximately 25 minutes were required to obtain the fatigue analysis results using this proposed method, which could efficiently reduce the calculation time.

4. Shape Changing Techniques for Fixed Offshore Wind Turbine Foundations

In fixed OWTs, studies have been conducted to address problems with each foundation, as described in section 3. Despite the considerable research efforts, there are still limitations to fully overcoming chronic problems with OWT foundations. Single foundations (gravity, monopile, and suction buckets) are easy to manufacture and install and have economic benefits at shallow depths. Owing to the structural characteristics, however, they are sensitive to lateral loads and soil characteristics, which limits the design depth. Multi-pile foundations (jacket and tripod) have structural stability because of the complex structure, but they involve considerable fatigue damage and design cost. Therefore, some researchers have attempted to address chronic problems with wind turbine foundations by changing their geometry. Among them, hybrid foundations and optimization techniques have attracted attention. Hybrid foundations solve existing geotechnical problems, such as interactions with soil and local scour, by combining them with foundations or attaching appendages. In addition, optimization techniques allow optimal geometry by reducing the weight along with the safety and performance of the structure. Therefore, this section presents research on hybrid foundations and optimization techniques, which address chronic problems with previous foundations through changes in geometry.

4.1 Hybrid Foundations

In recent years, various studies have been conducted on hybrid foundations, which changed the geometry by attaching appendages around the foundations or in combination with foundations to address geotechnical problems, such as lateral loads and local scour. Hybrid foundations can provide larger lateral capacity than conventional ones and increase lateral resistance with combined appendages.

Kim and Kim (2018) proposed a hybrid pile-type concrete foundation composed of steel shafts and a concrete base to overcome the geotechnical limits of conventional monopile and gravity-based foundations. This foundation overcame the heavy weight of concrete and the shortcomings of installation cost by introducing steel shafts while maintaining the low cost and safety of concrete. They also conducted quasi-static analysis and natural frequency analysis to verify the validity of the hybrid foundation and found that the allowable displacement and stress met the conditions.

Chen et al. (2020) proposed a hybrid foundation by attaching a broad and shallow bucket skirt to a monopile foundation. For this foundation, the bucket is placed on soil, and the water inside is then discharged to make the bucket adhere to the seabed. The monopile is stably fixed to the seabed after passing through the center of the bucket. The two components are then combined using a grout material. They compared the behavior of the hybrid foundation under static and dynamic loads with that of conventional monopiles to examine its performance. The hybrid foundation exhibited excellent lateral displacement, rotation, and bending moment performance compared to conventional monopiles.

Li et al. (2020) examined a foundation that combined pile-wheel-bucket. A vertical load was applied to the bucket by loading gravel or stone on the wheel to increase frictional force. In the monotonic loading test, the final bearing capacity of the hybrid foundation was

100 to 300% higher than that of conventional monopile foundations. Li et al. (2022) introduced the discrete continuum numerical approach to identify the behavior of a hybrid pile-bucket foundation under circulatory lateral loads. Numerical modeling was based on a 3D discrete-continuum coupling approach that combined the discrete element method (DEM) and the finite difference method (FDM). They compared the hybrid foundation with conventional monopiles under 20,000 loading cycles to identify its displacement under cyclic lateral loads. The cumulative displacement of conventional monopiles was smaller in the first 30 cycles, but it exceeded the cumulative displacement of the hybrid foundation after 250 cycles. They suggested that the hybrid foundation can provide higher performance over the long term.

4.2 Optimization Technique to Reduce the Weight of Structures

As the power generation capacity of fixed OWTs increases, their design depth also increases. Therefore, foundations have evolved into more complex forms to meet the load conditions in the marine environment, which causes economic losses. Therefore, many studies have attempted to give foundations the optimal geometry by meeting the design conditions and reducing weight through optimization design.

Kaveh and Sabeti (2018) performed an optimization design for jacket foundations using Colliding Bodies Optimization (CBO), a heuristic algorithm. They dealt with 20 design variables, including the diameter and thickness of the foundation. When the proposed algorithm was applied, the weight of the substructure decreased to 2,742.9 kN, which is approximately half of the initial structure.

Motlagh et al. (2021) optimized a jacket foundation by performing WCF and CF optimization using genetic algorithms. WCF optimization involves optimizing stress and buckling within a structure, and CF optimization minimizes the fatigue damage considering all design conditions. Consequently, WCF optimization reduced the initial weight of the jacket foundation by 15%, and CF optimization that considered fatigue damage decreased the weight by 13%.

Tian et al. (2022) designed an optimal jacket foundation by applying a three-step topology optimization technique using the Optistruct optimization module of the HyperWorks software. In the first step, the stiffness of the structure was maximized, and its weight was reduced through mathematical calculations. In the second step, the stress state of the jacket was optimized, and shape optimization was performed by determining the optimal jacket node positions. In the final step, the overall volume was reduced through size optimization. The structure was simplified through this optimization process, and the weight of the optimized structure was 38.24% lower than that of the initial model.

Lu et al. (2023) designed a tripod foundation using the topology optimization technique. They also analyzed the static and dynamic behavior of the structure, considering external loads, including wind and waves. They compared the optimized structure with the existing structure, considering natural frequency, ultimate strength, and fatigue strength. The optimized structure exhibited a weight reduction effect of 16.29%.

Tian et al. (2024) proposed a topology optimization technique considering fatigue damage for a jacket structure. The proposed optimization technique reconstructed the optimization computational formula through the P-norm formula used in stress-based topology optimization methods. This could reduce the volume of the structure by approximately 14.58% while meeting the fatigue life.

5. Conclusions

This study examined the gravity, monopile, jacket, tripod, and suction bucket foundations for fixed offshore wind turbines (OWTs). The benefits and shortcomings of each foundation type were analyzed comprehensively using the results of previous studies and the latest research. Technological problems were presented based on the results of studies on each foundation type, and studies on optimization design methods that improved reliability were presented. The comprehensive analysis of each foundation type can be summarized as follows.

(1) For gravity-based foundations, the substructure is located on top of the seabed. Therefore, it is necessary to investigate the soil characteristics before installation and remove soil with low bearing capacity to secure sufficient bearing capacity. The soil also needs to be leveled for the installation of gravity-based foundations. A gravity foundation based on a steel skirt is being developed to address these problems. The need for seabed preparation can be reduced significantly by injecting concrete into the empty space between the foundation and the seabed.

(2) Monopile foundations are significantly affected by the surrounding soil, and it is important to assess the life of the structure from the relationship between the foundation and soil. In general, the pile–soil interaction (PSI) was examined through the p–y curve that used a beam, which is the nonlinear Winkler (1867) foundation model. Nevertheless, the curve may underestimate soil stiffness and overestimate lateral pile displacement for monopiles with large diameters. Therefore, research has been conducted on PSI analysis methods based on the three-dimensional continuum-based finite element method (3D FEM).

(3) Jacket-based foundations involve significant fatigue damage because stress concentration easily occurs at tubular joints under long-term cyclic loads. Therefore, it is necessary to assess the fatigue life of the structure by evaluating the fatigue damage of tubular joints. Many studies conducted fatigue analysis using the hot spot stress (HSS) approach for fatigue damage assessment. In addition, the rain-flow counting method was used to express the average stress under random loads, and total damage was calculated using Miner's rule. Time-series fatigue analysis was conducted using Sesam software, a marine structure analysis software program, to examine fatigue life through the latest research.

(4) Tripod foundations also showed the most severe fatigue damage at tubular joints, and the largest fatigue damage occurred at the tubular joint between the central column and the brace. Therefore, the Dirlik method (Dirlik, 1985) and narrow-band solution (Bendat, 1964) can

obtain the fatigue life by accurately calculating the fatigue damage at the position. In addition, the SIM was presented to simplify fatigue analysis through the latest research.

(5) Suction bucket foundations are most sensitive to lateral loads, which alter the bearing capacity, deflection, and rotation of the structure. Suction bucket foundations require further analysis because the vertical load and moment affect the final bearing capacity. Many studies revealed the effects of lateral and vertical loads through 3D FEM and centrifuge tests. Under cyclic lateral loads, the lateral displacement increased rapidly in the early cycles, and it tended to change slowly as the number of cycles increased. The vertical load decreased the displacement and rotation of the bucket and increased the horizontal bearing capacity and moment capacity by strengthening the foundation-soil interaction.

For OWTs, foundations that directly affect the system performance and stability must be designed to meet conditions that can respond to various environmental loads and external factors. Some researchers examined hybrid foundations with geometry change and shape optimization techniques to address the problems with each foundation type described above. Hybrid foundations can provide larger lateral capacity than conventional ones and increase lateral resistance with combined appendages. Optimization techniques can maximize the efficiency of structures or reduce costs through weight reduction under given conditions using mathematical modeling and algorithms.

This study identified the characteristics and research directions of fixed structures and presented the optimal substructure design methods for each purpose. These results are expected to be used as basic data for the design of OWT structures.

Conflict of Interest

Sung Woong Choi serves as a journal publication committee member of the Journal of Ocean Engineering and Technology, but he had no role in the decision to publish this article. No potential conflict of interest relevant to this article was reported.

Acknowledgments

This work was supported by the Korea Institute of Energy Technology Evaluation and Planning (KETEP) grant funded by the Korean government (MOTIE) (20213000000020, Development of core equipment and evaluation technology for construction of subsea power grid for offshore wind farm)

References

4C Offshore. (2020*). Global offshore wind farms database and intelligence*. https://www.4coffshore.com/windfarms/

Achmus, M., Kuo, Y. S., & Abdel-Rahman, K. (2009). Behavior of monopile foundations under cyclic lateral load. *Computers and Geotechnics, 36*(5), 725−735. https://doi.org/10.1016/j.compgeo.2008.12.003

American Petroleum Institute (API). (2000). *API 2A-WSD: Recommended practice for planning, designing and constructing fixed offshore platforms-working stress design*. American Petroleum Institute.

Amzallag, C., Gerey, J. P., Robert, J. L., & Bahuaud, J. (1994). Standardization of the rainflow counting method for fatigue analysis. *International journal of fatigue, 16*(4), 287−293. https://doi.org/10.1016/0142-1123(94)90343-3

Andersen, L. V., Vahdatirad, M. J., Sichani, M. T., & Sørensen, J. D. (2012). Natural frequencies of wind turbines on monopile foundations in clayey soils—A probabilistic approach. *Computers and Geotechnics, 43,* 1−11. https://doi.org/10.1016/j.compgeo.2012.01.010

Arshad, M., & O'Kelly, B. C. (2015). Analysis and design of monopile foundations for offshore wind-turbine structures. *Marine Georesources & Geotechnology, 34*(6), 503−525. https://doi.org/10.1080/1064119X.2015.1033070

Askarinejad, A., Wang, H., Chortis, G., & Gavin, K. (2022). Influence of scour protection layers on the lateral response of monopile in dense sand. *Ocean Engineering, 244*, 110377. ps://doi.org/10.1016/j.oceaneng.2021.110377

Barthelmie, R. J., Courtney, M. S., Højstrup, J., & Larsen, S. E. (1996). Meteorological aspects of offshore wind energy: Observations from the Vindeby wind farm. *Journal of Wind Engineering and Industrial Aerodynamics, 62*(2−3), 191−211. https://doi.org/10.1016/S0167-6105(96)00077-3

Bekken, L. (2009). *Lateral behavior of large diameter offshore monopile foundations for wind turbines.*

Bendat, J. S. (1964). *Probability functions for random responses: prediction of peaks, fatigue damage, and catastrophic.*

Bisoi, S., & Haldar, S. (2014). Dynamic analysis of offshore wind turbine in clay considering soil−monopile−tower interaction. *Soil Dynamics and Earthquake Engineering, 63*, 19−35. https://doi.org/10.1016/j.soildyn.2014.03.006

Byrne, B. W., & Houlsby, G. T. (2003). Foundations for offshore wind turbines. *Philosophical Transactions of the Royal Society of London. Series A: Mathematical, Physical and Engineering Sciences, 361*(1813), 2909-2930. https://doi.org/10.1098/rsta.2003.1286

Chen, D., Gao, P., Huang, S., Li, C., & Yu, X. (2020). Static and dynamic loading behavior of a hybrid foundation for offshore wind turbines. *Marine Structures, 71*, 102727. https://doi.org/10.1016/j.marstruc.2020.102727

Chen, I. W., Wong, B. L., Lin, Y. H., Chau, S. W., & Huang, H. H. (2016). Design and analysis of jacket substructures for offshore wind turbines. *Energies, 9*(4), 264. https://doi.org/10.3390/en9040264

Dirlik, T. (1985). *Application of computers in fatigue analysis* (Doctoral dissertation, University of Warwick).

DNV. (2016). *Fatigue design of offshore steel structures* (DNVGL-RP-C203). Norwegian University of Science and Technology. Veritas As, Offshore Standard DNV-OS-j101.

Efthymiou, M. (1988). *Development of SCF formulae and generalised influence functions for use in fatigue analysis.*

Guan, D. W., Xie, Y. X., Yao, Z. S., Chiew, Y. M., Zhang, J. S., & Zheng, J. H. (2022). Local scour at offshore windfarm monopile foundations: A review. *Water Science and Engineering, 15*(1), 29−39. https://doi.org/10.1016/j.wse.2021.12.006

Guo, Y., Wang, H., & Lian, J. (2022). Review of integrated installation technologies for offshore wind turbines: Current progress and future development trends. *Energy Conversion and Management, 255*, 115319. https://doi.org/10.1016/j.enconman.2022.115319

GWEC. (2022). *Global offshore wind report 2022. https://gwec.net/gwecs- global-offshore-wind-report/*

Esteban, M. D., López-Gutiérrez, J. S., & Negro, V. (2019). Gravity-based foundations in the offshore wind sector. *Journal of Marine Science and Engineering, 7*(3), 64. https://doi.org/10.3390/jmse7030064

Esteban, M. D., Couñago, B., López-Gutiérrez, J. S., Negro, V., & Vellisco, F. (2015). Gravity based support structures for offshore wind turbine generators: Review of the installation process. *Ocean Engineering, 110*(Part A), 281−291. https://doi.org/10.1016/j.oceaneng.2015.10.033

Hao, E., & Liu, C. (2017). Evaluation and comparison of anti-impact performance to offshore wind turbine foundations: Monopile, tripod, and jacket. Ocean engineering, 130, 218-227. https://doi.org/10.1016/j.oceaneng.2016.12.008

Hearn, E. N., & Edgers, L. (2010). Finite element analysis of an offshore wind turbine monopile. In *GeoFlorida 2010: Advances in Analysis, Modeling & Design* (pp. 1857−1865). https://doi.org/10.1061/41095(365)188

ICE. (2017). *The EDF renewables Blyth offshore demonstrator windfarm project*. Institution of Civil Engineers. https://www.ice.org.uk/what-is-civil-engineering/what-do-civil-engineers-do/the-edf-renewables-blyth-offshore-demonstrator-windfarm-project

Jiang, Z. (2021). Installation of offshore wind turbines: A technical review. *Renewable and Sustainable Energy Reviews, 139*, 110576. https://doi.org/10.1016/j.rser.2020.110576

Jung, S., Kim, S. R., & Patil, A. (2015). Effect of monopile foundation modeling on the structural response of a 5-MW offshore wind turbine tower. *Ocean Engineering, 109*, 479−488. https://doi.org/10.1016/j.oceaneng.2015.09.033

Jeanjean, P. (2009, May). Re-assessment of P-Y curves for soft clays from centrifuge testing and finite element modeling. *In Offshore technology conference* (pp. OTC-20158), OTC. https://doi.org/10.4043/20158-MS

Ju, S. H., Su, F. C., Ke, Y. P., & Xie, M. H. (2019). Fatigue design of offshore wind turbine jacket-type structures using a parallel scheme. *Renewable Energy, 136,* 69−78. https://doi.org/10.1016/j.renene.2018.12.071

Kaveh, A., & Sabeti, S. (2018). Optimal design of jacket supporting structures for offshore wind turbines using CBO and ECBO algorithms. *Periodica Polytechnica Civil Engineering, 62*(3), 545−554. https://doi.org/10.3311/PPci.11651

Kim, H. G., & Kim, B. J. (2018). Feasibility study of new hybrid piled concrete foundation for offshore wind turbine. *Applied Ocean Research, 76*, 11−21. https://doi.org/10.1016/j.apor.2018.04.005

Larsen, J. H., Soerensen, H. C., Christiansen, E., Naef, S., & Vølund, P. (2005, October). Experiences from Middelgrunden 40 MW offshore wind farm. In *Copenhagen offshore wind conference* (pp. 1−8). Denmark: Copenhagen.

Liu, H., Diambra, A., Abell, J. A., & Pisanò, F. (2020). Memory-enhanced plasticity modeling of sand behavior under undrained cyclic loading. *Journal of Geotechnical and Geoenvironmental Engineering*, *146*(11), 04020122. https://doi.org/10.1061/(ASCE)GT.1943-5606.000236

Liu, M., Yang, M., & Wang, H. (2014). Bearing behavior of wide-shallow bucket foundation for offshore wind turbines in drained silty sand. *Ocean Engineering, 82*, 169−179. https://doi.org/10.1016/j.oceaneng.2014.02.034

Lu, F., Long, K., Zhang, C., Zhang, J., & Tao, T. (2023). A novel design of the offshore wind turbine tripod structure using topology optimization methodology. *Ocean Engineering, 280*, 114607. https://doi.org/10.1016/j.oceaneng.2023.114607

Li, L., Zheng, M., Liu, X., Wu, W., Liu, H., El Naggar, M. H., & Jiang, G. (2022). Numerical analysis of the cyclic loading behavior of monopile and hybrid pile foundation. *Computers and Geotechnics, 144*, 104635. https://doi.org/10.1016/j.compgeo.2022.104635

Li, X., Zeng, X., & Wang, X. (2020). Feasibility study of monopile-friction wheel-bucket hybrid foundation for offshore wind turbine. *Ocean Engineering, 204*, 107276. https://doi.org/10.1016/j.oceaneng.2020.107276

Li, X., Zeng, X., & Wang, X. (2020). Feasibility study of monopile-friction wheel-bucket hybrid foundation for offshore wind turbine. *Ocean Engineering, 204*, 107276. https://doi.org/10.1016/j.oceaneng.2020.107276

Liu, H. Y., & Kaynia, A. M. (2022). Monopile responses to monotonic and cyclic loading in undrained sand using 3D FE with SANISAND-MSu. *Water Science and Engineering, 15*(1), 69−77. https://doi.org/10.1016/j.wse.2021.12.001

Lombardi, D., Bhattacharya, S., & Wood, D. M. (2013). Dynamic soil−structure interaction of monopile supported wind turbines in cohesive soil. *Soil Dynamics and Earthquake Engineering, 49*, 165−180. https://doi.org/10.1016/j.soildyn.2013.01.015

Lozano-Minguez, E., Kolios, A. J., & Brennan, F. P. (2011). Multi-criteria assessment of offshore wind turbine support structures. *Renewable Energy, 36*(11), 2831−2837. https://doi.org/10.1016/j.renene.2011.04.020

Lu, F., Long, K., Diaeldin, Y., Saeed, A., Zhang, J., & Tao, T. (2023). A time-domain fatigue damage assessment approach for the tripod structure of offshore wind turbines. *Sustainable Energy Technologies and Assessments, 60*, 103450. https://doi.org/10.1016/j.seta.2023.103450

Ma, H., Yang, J., & Chen, L. (2018). Effect of scour on the structural response of an offshore wind turbine supported on tripod foundation. *Applied Ocean Research, 73*, 179−189. https://doi.org/10.1016/j.apor.2018.02.007

Marjan, A., & Hart, P. (2022). Impact of Design Parameters on the Dynamic Response and Fatigue of Offshore Jacket Foundations. *Journal of Marine Science and Engineering, 10*(9), 1320. https://doi.org/10.3390/jmse10091320

Mathern, A., von der Haar, C., & Marx, S. (2021). Concrete support structures for offshore wind turbines: Current status, challenges, and future trends. *Energies, 14*(7), 1995. https://doi.org/10.3390/en14071995

Mengé, P., & Gunst, N. (2008). Gravity based foundations for the wind turbines on Thorntonback−Belgium. 15de Innovatieforum Geotechniek. Antwerpen, Belgium.

Miner, M. A. (1945). Cumulative fatigue damage. *Journal of applied mechanics, 12*(3), A159-A164. https://doi.org/10.1115/1.4009458

Ministry of Trade Industry and Energy. (2017). *Korea's renewable energy 3020 implementation plan. https://gggi.org/wp-content/uploads/2018/10/Presentation-by-Mr.-Kyung-ho-Lee-Director-of-the-New-and-Renewable-Energy-Policy-Division-MOTIE.pdf*

Oh, K. Y., Nam, W., Ryu, M. S., Kim, J. Y., & Epureanu, B. I. (2018). A review of foundations of offshore wind energy convertors: Current status and future perspectives. *Renewable and Sustainable Energy Reviews, 88*, 16−36. https://doi.org/10.1016/j.rser.2018.02.005

Park, M., Park, S. G., Seong, B. C., Choi, Y. J., & Jung, S. H. (2021). Current status and prospective of offshore wind power to achieve Korean renewable energy 3020 plan. *Journal of Korean Society of Environmental Engineers, 43*(3), 196−205.

Saleem, Z. (2011). Alternatives and modifications of monopile foundation or its installation technique for noise mitigation. *TUDelft Report,* TUDelft University.

Shi, W., Park, H., Chung, C., Baek, J., Kim, Y., & Kim, C. (2013). Load analysis and comparison of different jacket foundations. *Renewable Energy, 54*, 201−210. https://doi.org/10.1016/j.renene.2012.08.008

Sunday, K., & Brennan, F. (2021). A review of offshore wind monopiles structural design achievements and challenges. *Ocean Engineering, 235*, 109409. https://doi.org/10.1016/j.oceaneng.2021.109409

Tian, X., Sun, X., Liu, G., Deng, W., Wang, H., Li, Z., & Li, D. (2022). Optimization design of the jacket support structure for offshore wind turbine using topology optimization method. *Ocean Engineering, 243*, 110084. https://doi.org/10.1016/j.oceaneng.2021.110084

Tian, X., Liu, G., Deng, W., Xie, Y., & Wang, H. (2024). Fatigue constrained topology optimization for the jacket support structure of offshore wind turbine under the dynamic load. *Applied Ocean Research, 142*, 103812. https://doi.org/10.1016/j.apor.2023.103812

Winkler, E. (1867). *Die Lehre von Elastizitat und Festigkeit* [The theory of elasticity and stiffness]. H. Domenicus, Prague.

Wang, X., Zeng, X., Li, J., Yang, X., & Wang, H. (2018). A review on recent advancements of substructures for offshore wind turbines. *Energy conversion and management, 158*, 103−119. https://doi.org/10.1016/j.enconman.2017.12.061

Wang, X., Yang, X., & Zeng, X. (2017a). Centrifuge modeling of lateral bearing behavior of offshore wind turbine with suction bucket foundation in sand. *Ocean Engineering, 139*, 140−151. https://doi.org/10.1016/j.oceaneng.2017.04.046

Wang, X., Yang, X., & Zeng, X. (2017b). Seismic centrifuge modelling of suction bucket foundation for offshore wind turbine. *Renewable energy, 114*, 1013−1022. https://doi.org/10.1016/j.renene.2017.07.103

Wang, X., Zeng, X., & Li, J. (2019). Vertical performance of suction bucket foundation for offshore wind turbines in sand. *Ocean Engineering, 180*, 40−48. https://doi.org/10.1016/j.oceaneng.2019.03.049

Liu, H., & Kaynia, A. M. (2022). Monopile responses to monotonic and cyclic loading in undrained sand using 3D FE with SANISAND-MSu. *Water Science and Engineering, 15*(1), 69−77. https://doi.org/10.1016/j.wse.2021.12.001

Yeter, B., Garbatov, Y., & Soares, C. G. (2015). Fatigue damage assessment of fixed offshore wind turbine tripod support structures. *Engineering Structures, 101*, 518−528. https://doi.org/10.1016/j.engstruct.2015.07.038

Zaayer, M. B. (2002). Foundation models for the dynamic response of offshore wind turbines. *Proceedings of the international conference on marine renewable energy, Newcastle, UK* (pp. 111−117). Institute of Marine Engineering, Science and Technology.

Zhang, F., Chen, X., Yan, J., & Gao, X. (2023). Countermeasures for local scour around offshore wind turbine monopile foundations: A review. *Applied Ocean Research, 141*, 103764. https://doi.org/10.1016/j.apor.2023.103764

Author ORCIDs

Author name	ORCID
Kim, Yun Jae	0009-0006-7814-8410
Choe, Jin-wook	0000-0002-4629-6789
Lim, Jinseok	0009-0009-8098-0312
Choi, Sung Woong	0000-0001-7285-4257

Instructions for Authors

General information

To submit a manuscript to the Journal of Ocean Engineering and Technology (JOET), it is advised to first carefully read the aims and the scope section of this journal, as it provides information on the editorial policy and the category of papers it accepts. Unlike many regular journals, JOET usually has no lag in acceptance of a manuscript and its publication. Authors that find a match with the aims and the scope of JOET are encouraged to submit as we publish works from all over the world. JOET adheres completely to guidelines and best practices published by professional organizations, including Principles of Transparency and Best Practice in Scholarly Publishing (joint statement by COPE, DOAJ, WAME, and OASPA (http://doaj.org/bestpractice) if otherwise not described below. As such, JOET would like to keep the principles and policies of those professional organizations during editing and the publication process.

Research and publication ethics

Details on publication ethics are found in http://joet.org/authors/ethics.php. For the policies on research and publication ethics not stated in the Instructions, Guidelines on Good Publication (http://publicationethics.org/) can be applied.

Publication type

Article types include scholarly monographs (original research articles), technical articles (technical reports and data), and review articles. The paper should have not been submitted to other academic journal. When part or whole of a manuscript was already published to conference papers, research reports, and dissertations, then the corresponding author should note it clearly in the manuscript.

Copyright

After published to JOET, the copyright of manuscripts should belong to KSOE. A transfer of copyright (publishing agreement) form can be found in submission website (http://www.joet.org).

Manuscript submission

Manuscript should be submitted through the on-line submission website (http://www.joet.org). The date that manuscript was received through on-line website is the official date of receipt. Other correspondences can be sent by an email to the Editor in Chief or secretariat. The manuscript must be accompanied by a signed statement that it has been neither published nor currently submitted for publication elsewhere. The manuscript should be written in English or Korean. Ensure that online submission are in a standard word processing format. Corresponding author must write the manuscript using the JOET template provided in Hangul or MS Word format. Ensure that graphics are high-resolution. Be sure all necessary files have been uploaded/ attached.

Authors' checklist

Please refer to “Authors' Checklist” for details.

Article structure

Manuscript must be edited in the following order: (1) Title, (2) Authors' names and affiliations, (3) Keywords, (4) Abstract, (5) Nomenclature (optional), (6) Introduction, (7) Main body (analyses, tests, results, and discussions), (8) Conclusions, (9) Conflict of interest, (10) Funding (optional), (11) Acknowledgements (optional), (12) References, (13) Appendices (optional), (14) Author’s ORCIDs.

Abstract

A concise and factual abstract is required. The abstract should state briefly the background, purpose and methods of the research, the principal results and conclusions. An abstract should be written in 150-200 words. References are not cited in abstract whenever possible. Also, non-standard or uncommon abbreviations should be avoided, but if essential they must be defined at their first mention in the abstract itself.

Keywords

Immediately after the abstract, provide a maximum of 5 or 6 keywords.

Unit

Use the international system units(SI). If other units are mentioned, please give their equivalent in SI.

Equations

All mathematical equations should be clearly printed/typed using well accepted explanation. Superscripts and subscripts should be typed clearly above or below the base line. Equation numbers should be given in Arabic numerals enclosed in parentheses on the right-hand margin.

Tables

Tables should be numbered consecutively with Arabic numerals. Each table should be fully titled. All tables should be referred to in the texts.

Figures

Figures should be numbered consecutively with Arabic numerals. Each figure should be fully titled. All figures should be referred to in the texts. All the illustrations should be of high quality meeting with the publishing requirement with legible symbols and legends.

Conflict of interest

It should be disclosed here according to the statement in the Research and publication ethics regardless of existence of conflict of interest. If the authors have nothing to disclose, please state: “No potential conflict of interest relevant to this article was reported.”

Funding

Funding to the research should be provided here. Providing a FundRef ID is recommended including the name of the funding agency, country

and if available, the number of the grant provided by the funding agency. If the funding agency does not have a FundRef ID, please ask that agency to contact the FundRef registry (e-mail: fundref.registry@crossref.org). Additional detailed policy of FundRef description is available from http://www.crossref.org/fundref/. Example of a funding description is as follows:

The study is supported by the Inha University research fund (FundRef ID: 10.13039/501100002632), and the Korea Health Personnel Licensing Examination Institute research fund (FundRef ID: 10.13039/501100003647).

Acknowledgments

Any persons that contributed to the study or the manuscript, but not meeting the requirements of an authorship could be placed here. For mentioning any persons or any organizations in this section, there should be a written permission from them.

References in text

References in texts follow the APA style. Authors can also see how references appear in manuscript text through the 'Template'.

Reference list

Reference list follows the APA style. Authors can see how references should be given in reference section through the 'Template'.

Appendices

The appendix is an optional section that can contain details and data supplemental to the main text. If there is more than an appendix, they should be identified as A, B, C, etc. Formulae and equations in appendices should be given separate numbering: Eq. (A1), Eq. (A2), etc.; in a subsequent appendix, Eq. (B1) and so on. Similarly for tables and figures: Table A1; Fig. A1, etc.

ORCID (Open Researcher and Contributor ID)

All authors are recommended to provide an ORCID. To obtain an ORCID, authors should register in the ORCID web site: http://orcid.org. Registration is free to every researcher in the world. Example of ORCID description is as follows:

Joonmo Choung: https://orcid.org/0000-0003-1407-9031

Peer review and publication process

The peer review process can be broadly summarized into three groups: author process, review process, and publishing process for accepted submissions. General scheme is presented in Figure 1.

Check-in process for review

If the manuscript does not fit the aims and scope of the Journal or does not adhere to the Instructions to Authors, it may be rejected immediately after receipt and without a review. Before reviewing, all submitted manuscripts are inspected by Similarity Check powered by iThenticate (https://www.crossref.org/services/similarity-check/), a plagiarism-screening tool. If a too high degree of similarity score is found, the Editorial Board will do a more profound content screening. The criterion for similarity rate for further screening is usually 15%; however, rather than the similarity rate, the Editorial Board focuses on cases where specific sentences or phrases are similar. The settings for Similarity Check screening are as follows: It excludes quotes, bibliography, small matches of 6 words, small sources of 1%, and the Methods section.

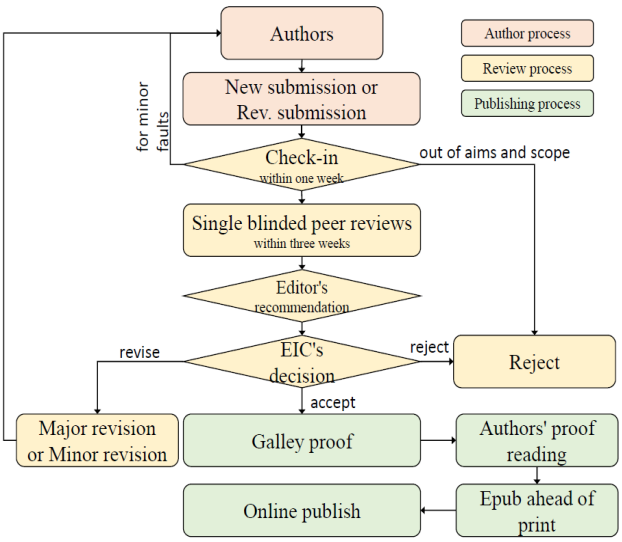

Figure 1 Flow chart of the peer review and publication process of JOET

Number of reviewers

Reviewers will be selected from the list of reviewers. Manuscripts are then peer reviewed by at least 2 experts in the corresponding field, usually by 2.

Peer review process and the author response to the reviewer comments

JOET adopts single blind review, which means that the authors do not know the identity of the reviews. All papers, including those invited by the Editor, are subject to peer review.

The review period is 4 weeks. Usually the first decision is made within a week after completion of the review. The Editorial Board's decision after the review will be one of followings: Accept, Minor revision, Major revision, or Rejection. The Editorial Board may request the authors to revise the manuscript according to the reviewers' comments. If there are any requests for revision of the manuscript by the reviewers, the authors should do their best to revise the manuscript. If the reviewer's opinion is not acceptable or is believed to misinterpret the data, the author should reasonably indicate that. After revising the manuscript, the author should upload the revised files with a separate response sheet to each item of the reviewer's commentary. The author's revisions should be completed within 3 months after the request. If it is not received by the due date, the Editorial Board will notify the author. To extend the revision period beyond 3 months, the author should negotiate that with the Editorial Board. The manuscript review process can be provided for up two rounds. If the authors wish further review, the Editorial Board may consider it. The Editorial Board will make a final decision on the approval of the submitted manuscript for publication and can request any further corrections, revisions, and deletions of the article text if necessary. Statistical editing is also performed if the data requires professional statistical review by a statistician.

Processing after acceptance

If the manuscript is finally accepted, the galley proof will be sent to the corresponding author after professional manuscript editing and English proofreading. Proofreading should be performed for any misspellings or errors by the authors. Proofreading manuscript for publication is provided to the corresponding author, and the corresponding author must review the proofreading manuscript.

Corresponding authors are responsible for the content of the proofreading manuscript and any errors. After final proofreading, the manuscript may appear at the journal homepage as an article in press with a unique DOI number for rapid communication. All published articles will be replaced by the replacement XML file and a final PDF.

Feedback after publication

If the authors or readers find any errors, or contents that should be revised, it can be requested from the Editorial Board. The Editorial Board may consider erratum, corrigendum or a retraction. If there are any revisions to the article, there will be a CrossMark description to announce the final draft. If there is a reader's opinion on the published article with the form of Letter to the editor, it will be forwarded to the authors. The authors can reply to the reader's letter. Letter to the editor and the author's reply may be also published.

How the journal handle complaints and appeals

The policy of JOET is primarily aimed at protecting the authors, reviewers, editors, and the publisher of the journal. If not described below, the process of handling complaints and appeals follows the guidelines of the Committee of Publication Ethics available from: https://publicationethics.org/appeals

- *Who complains or makes an appeal?*

Submitters, authors, reviewers, and readers may register complaints and appeals in a variety of cases as follows: falsification, fabrication, plagiarism, duplicate publication, authorship dispute, conflict of interest, ethical treatment of animals, informed consent, bias or unfair/inappropriate competitive acts, copyright, stolen data, defamation, and legal problem. If any individuals or institutions want to inform the cases, they can send a letter via the contact page on our website: https://www.joet.org/about/contact.php. For the complaints or appeals, concrete data with answers to all factual questions (who, when, where, what, how, why) should be provided.

- *Who is responsible to resolve and handle complaints and appeals?*

The Editorial Board or Editorial Office is responsible for them. A legal consultant or ethics editor may be able to help with the decision making.

- *What may be the consequence of remedy?*

It depends on the type or degree of misconduct. The consequence of resolution will follow the guidelines of the Committee of Publication Ethics (COPE).

Article processing charge

Payment due

Article processing charge (APC) covers the range of publishing services JOET provides. This includes provision of online tools for editors and authors, article production and hosting, and customer services. Upon editorial acceptance of an article for the regular review service and upon submission of an article for the fast review service, the corresponding author will be notified that payment is due.

APC

The APC for up to 6 pages amounts to 400,000 KRW (or 400 USD) for the regular review service and 750,000 KRW (or 750 USD) for the fast review service, respectively. An extra APC of 100,000 KRW (or 100 USD) per page is charged for papers longer than 6 pages. If the first author or corresponding author who submits a paper or papers is a member of the Korean Society of Ocean Engineers (KSOE), the APC could be reduced by 100,000 KRW (or 100 USD). No taxes are included in this charge. For the fast review service, an advance fee of 250,000 KRW (or 250 USD) should be paid upon submission.

Payment methods

Credit card payment can be made online using a secure payment form as soon as the manuscript has been editorially accepted.

Invoice payment is due within 7 days of the manuscript receiving editorial acceptance. Receipts are available on request.

JOET Template 2022.08.27

Journal of Ocean Engineering and Technology 00(0), 000-000, December, 2100
https://doi.org/10.26748/KSOE.2100.000
pISSN 1225-0767
eISSN 2287-6715

Original Research Article, Technical Article, Review Article, etc

Title of Article

Firstname Lastname[1], Firstname Lastname[2] and Firstname Lastname[3]

[1]*Professor, Department of OO, OO School, OO University, Busan, Korea*
[2]*Graduate Student, Department of OO, OO University, Seoul, Korea*
[3]*Senior Researcher, Department of OO, OO Engineering. Corp., Seoul, Korea*

KEYWORDS: Lumped mass line model, Explicit method, Steel lazy wave riser (Provide a maximum of 5 or 6 keywords.)

ABSTRACT:

Abstract Construction Guidelines
1) Describe the research background and aims in 1-2 sentences
2) Describe the research/analysis method (method section) in 2-3 sentences.
3) Describe the research/analysis results (results) in 2-3 sentences.
4) Describe the research conclusion in 1-2 sentences.
Abstract Editing Guidelines
1) Review English grammar.
2) Describe in 150-200 words.
3) When using an abbreviation or acronym, write the acronym after full words.
4) Abbreviations (acronyms) used only once should be written in full words only, and no acronyms.
5) References are not included in the abstract.

Nomenclature (Optional)

ITOC	Increment of total operating cost ($/yr)
LHV	Lower heating value (kJ/kg)
Pw	Power (kW)
T	Temperature (K)
V	Volume (m^3)
ρ	Density (kg/m^3)

1. Introduction

The introduction should briefly place the study in a broad context and highlight why it is important. It should define the purpose of the work and its significance. The current state of the research field should be reviewed carefully and key publications cited. Please highlight controversial and diverging hypotheses when necessary. Finally, briefly mention the main aim of the work and highlight the principal conclusions. As far as possible, please keep the introduction comprehensible to scientists outside your particular field of research.

Received 00 February 2100, revised 00 October 2100, accepted 00 October 2100
Corresponding author Firstname Lastname: +82-51-759-0656, e-mail@e-mail.com
It is a recommended paper from the proceedings of 2019 spring symposium of the Korea Marine Robot Technology (KMRTS).

2. General Information for Authors

2.1 Research and Publication Ethics

Authorship should be limited to those who have made a significant contribution to the conception, design, execution, or interpretation of the reported study. All those who have made significant contributions should be listed as co-authors. Where there are others who have participated in certain substantive aspects of the research project, they should be acknowledged or listed as contributors.

The corresponding author should ensure that all appropriate co-authors and no inappropriate co-authors are included on the paper, and that all co-authors have seen and approved the final version of the paper and have agreed to its submission for publication.

Details on publication ethics are found in the journal's website (http://joet.org/authors/ethics.php). For the policies on research and publication ethics not stated in the Instructions, Guidelines on Good Publication (http://publicationethics.org/) can be applied.

2.2 Requirement for Membership

One of the authors who submits a paper or papers should be member of The Korea Society of Ocean Engineers (KSOE), except a case that editorial board provides special admission of submission.

2.3 Publication Type

Article types include scholarly monographs (original research articles), technical articles (technical reports and data), and review articles. The paper should have not been submitted to another academic journal. When part or whole of a manuscript was already published to conference papers, research reports, and dissertations, then the corresponding author should note it clearly in the manuscript.

Example: It is noted that this paper is revised edition based on proceedings of KAOST 2100 in Jeju.

2.4 Copyright

After published to JOET, the copyright of manuscripts should belong to KSOE. A transfer of copyright (publishing agreement) form can be found in submission website (http://www.joet.org).

2.5 Manuscript Submission

Manuscript should be submitted through the on-line submission website (http://www.joet.org). The date that manuscript was received through on-line website is the official date of receipt. Other correspondences can be sent by an email to the Editor in Chief or secretariat. The manuscript must be accompanied by a signed statement that it has been neither published nor currently submitted for publication elsewhere. The manuscript should be written in English or Korean. Ensure that online submission is in a standard word processing format. Corresponding author must write the manuscript using the JOET template provided in Hangul or MS Word format. Ensure that graphics are high-resolution. Be sure all necessary files have been uploaded/ attached.

2.5.1 Authoer’s checklist

Authoer’s checklist and Transfer of copyright can be found in submission homepage (http:/www.joet.org).

3. Manuscript

Manuscript must be edited in the following order: (1) Title, (2) Authors' names and affiliations, (3) Keywords, (4) Abstract, (5) Nomenclature (optional), (6) Introduction, (7) Main body (analyses, tests, results, and discussions), (8) Conclusions, (9) Conflict of interest, (10) Funding (optional), (11) Acknowledgements (optional), (12) References, (13) Appendices (optional), (14) Author’s ORCIDs.

3.1 Unit

Use the international system units (SI). If other units are mentioned, please give their equivalent in SI.

3.2 Equations

All mathematical equations should be clearly printed/typed using well accepted explanation. Superscripts and subscripts should be typed clearly above or below the base line. Equation numbers should be given in Arabic numerals enclosed in parentheses on the right-hand margin. The parameters used in equation must be defined. They should be cited in the text as, for example, Eq. (1), or Eqs. (1)–(3).

$$G_{GEV}(x;\mu,\sigma,\xi)=\begin{cases}\exp[-(1+\xi(x-\mu)/\sigma)^{-1/\xi}] & \xi\neq 0\\ \exp[-\exp(-(x-\mu)/\sigma)] & \xi=0\end{cases} \quad (1)$$

in which μ, σ, and ξ represent the location ("Shift" in figures), scale, and shape parameters, respectively.

3.3 Tables

Tables should be numbered consecutively with Arabic numerals. Each table should be typed on a separate sheet of paper and be fully titled. All tables should be referred to in the texts.

Table 1 Tables should be placed in the main text near to the first time they are cited

Item	Buoyancy riser
Segment length[1)] (m)	370
Outer diameter (m)	1.137
Inner diameter (m)	0.406
Dry weight (kg/m)	697
Bending rigidity ($N\cdot m^2$)	1.66E8
Axial stiffness (N)	7.098E9
Inner flow density ($kg\cdot m^3$)	881
Seabed stiffness ($N/m/m^2$)	6,000

[1)]Tables may have a footer.

3.4 Figures

Figures should be numbered consecutively with Arabic numerals. Each figure should be fully titled. All the illustrations should be of high quality meeting with the publishing requirement with legible symbols and legends. All figures should be referred to in the texts. They should be referred to in the text as, for example, Fig. 1, or Figs. 1−3.

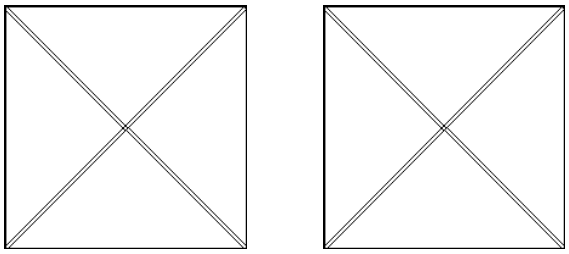

(a) (b)

Fig. 1 Schemes follow the same formatting. If there are multiple panels, they should be listed as: (a) Description of what is contained in the first panel; (b) Description of what is contained in the second panel. Figures should be placed in the main text near to the first time they are cited

3.5 How to Describe the References in Main Texts

- JOET recommends to edit authors' references using MS-Word reference or ZOTERO plug-in
- How to add a new citation and source to a document using MS-Word is found in MS Office web page: https://support.microsoft.com/en-us/office/add-citations-in-a-word-document-ab9322bb-a8d3-47f4-80c8-63c06779f127
- How to add a new citation and source to a document using ZOTERO is found in zotero web page: https://www.zotero.org/

4. Results

This section may be divided by subheadings. It should provide a concise and precise description of the experimental results, their interpretation as well as the experimental conclusions that can be drawn. Tables and figures are recommended to present the results more rapidly and easily. Do not duplicate the content of a table or a figure with in the Results section. Briefly describe the core results related to the conclusion in the text when data are provided in tables or in figures. Supplementary results can be placed in the Appendix.

5. Discussion

Authors should discuss the results and how they can be interpreted in perspective of previous studies and of the working hypotheses. The findings and their implications should be discussed in the broadest context possible. Future research directions may also be highlighted

6. Conclusions

This section can be added to the manuscript.

Conflict of Interest

It should be disclosed here according to the statement in the Research and publication ethics regardless of existence of conflict of interest. If the authors have nothing to disclose, please state: “No potential conflict of interest relevant to this article was reported.”, “The authors declare no potential conflict of interest.”, “The authors declare that they have no conflict of interests.”

Funding (Optional)

Please add: “This research was funded by Name of Funder, grant number XXX” and “The OOO was funded by XXX”. Check carefully that the details given are accurate and use the standard spelling of funding agency names at https://search.crossref.org/funding

Acknowledgments (Optional)

In this section you can acknowledge any support given which is not covered by the author contribution or funding sections. This may include administrative and technical support, or donations in kind (e.g., materials used for experiments). For mentioning any persons or any organizations in this section, there should be a written permission from them.

References

JOET follows the American Psychological Association (APA) style.

- Some samples are found in following web pages: https://apastyle.apa.org/style-grammar-guidelines/references/examples or https://www.ntnu.edu/viko/apa-examples
- JOET recommends editing authors’ references using MS-Word reference or ZOTERO plug-in
- How to add a new citation and source to a document using MS-Word is found in MS Office web page: https://support.microsoft.com/en-us/office/add-citations-in-a-word-document-ab9322bb-a8d3-47f4-80c8-63c06779f127
- How to add a new citation and source to a document using ZOTERO is found in ZOTERO web page: https://www.zotero.org/

Appendix (Optional)

The appendix is an optional section that can contain details and data supplemental to the main text. For example, explanations of experimental details that would disrupt the flow of the main text, but nonetheless remain crucial to understanding and reproducing the research shown; figures of replicates for experiments of which representative data is shown in the main text can be added here if brief, or as Supplementary data. Mathematical proofs of results not central to the paper can be added as an appendix.

All appendix sections must be cited in the main text. In the appendixes, Figures, Tables, etc. should be labeled starting with ‘A’, e.g., Fig. A1, Fig. A2, etc.

Examples:

https://doi.org/10.26748/KSOE.2019.022

https://doi.org/10.26748/KSOE.2018.4.32.2.095

Author ORCIDs

All authors are recommended to provide an ORCID. To obtain an ORCID, authors should register in the ORCID web site: http://orcid.org. Registration is free to every researcher in the world. Example of ORCID description is as follows:

Author name	**ORCID**
So, Hee	0000-0000-000-00X
Park, Hye-Il	0000-0000-000-00X
Yoo, All	0000-0000-000-00X
Jung, Jewerly	0000-0000-000-00X

Authors' Checklist

The following list will be useful during the final checking of a manuscript prior to sending it to the journal for review. Please submit this checklist to the KSOE when you submit your article.

< Checklist for manuscript preparation >

☐ I checked my manuscript has been 'spell-checked' and 'grammar-checked'.

☐ One author has been designated as the corresponding author with contact details such as
- E-mail address
- Phone numbers

☐ I checked abstract 1) stated briefly the purpose of the research, the principal results and major conclusions, 2) was written in 150−200 words, and 3) did not contain references (but if essential, then cite the author(s) and year(s)).

☐ I provided 5 or 6 keywords.

☐ I checked color figures were clearly marked as being intended for color reproduction on the Web and in print, or to be reproduced in color on the Web and in black-and-white in print.

☐ I checked all table and figure numbered consecutively in accordance with their appearance in the text.

☐ I checked abbreviations were defined at their first mention there and used with consistency throughout the article.

☐ I checked all references mentioned in the Reference list were cited in the text, and vice versa according to the APA style.

☐ I checked I used the international system units (SI) or SI-equivalent engineering units.

< Authorship checklist >

JOET considers individuals who meet all of the following criteria to be authors:

☐ Made a significant intellectual contribution to the theoretical development, system or experimental design, prototype development, and/or the analysis and interpretation of data associated with the work contained in the article.

☐ Contributed to drafting the article or reviewing and/or revising it for intellectual content.

☐ Approved the final version of the article as accepted for publication, including references.

< Checklist for publication ethics >

☐ I checked the work described has not been published previously (except in the form of an abstract or as a part of a published lecture or academic thesis).

☐ I checked when the work described has been published previously in other proceedings without copyright, it has clearly noted in the text.

☐ I checked permission has been obtained for use of copyrighted material from other sources including the Web.

☐ I have processed Plasgiarism Prevention Check through reliable web sites such as www.kci.go.kr, http://www.ithenticate.com/, or https://www.copykiller.org/ for my submission.

☐ I agree that final decision for my final manuscript can be changed according to results of Plasgiarism Prevention Check by JOET administrator.

☐ I checked one author at least is member of the Korean Society of Ocean Engineers.

☐ I agreed all policies related to 'Research and Publication Ethics'

☐ I agreed to transfer copyright to the publisher as part of a journal publishing agreement and this article will not be published elsewhere including electronically in the same form, in English or in any other language, without the written consent of the copyright-holder.

☐ I made a payment for reviewing of the manuscript, and I will make a payment for publication on acceptance of the article.

☐ I have read and agree to the terms of Authors' Checklist.

Title of article	:	
Date of submission	: DD/MM/YYYY	
Corresponding author	:	signature
Email address	:	

※ E-mail this with your signature to ksoehj@ksoe.or.kr

Publishing Agreement

ARTICLE DETAILS

Title of article :

Corresponding author :

E-mail address :

DOI : https://doi.org/10.26748/KSOE.2XXX.XXX

YOUR STATUS

I am one author signing on behalf of all co-authors of the manuscript.

ASSIGNMENT OF COPYRIGHT

I hereby assign to the Korean Society of Ocean Engineers, the copyright in the manuscript identified above and any tables, illustrations or other material submitted for publication as part of the manuscript (the "Article"). This assignment of rights means that I have granted to Korean Society of Ocean Engineers the exclusive right to publish and reproduce the Article, or any part of the Article, in print, electronic and all other media (whether now known or later developed), in any form, in all languages, throughout the world, for the full term of copyright, and the right to license others to do the same, effective when the Article is accepted for publication. This includes the right to enforce the rights granted hereunder against third parties.

SCHOLARLY COMMUNICATION RIGHTS

I understand that no rights in patents, trademarks or other intellectual property rights are transferred to the Journal owner. As the author of the Article, I understand that I shall have: (i) the same rights to reuse the Article as those allowed to third party users of the Article under the CC-BY-NC License, as well as (ii) the right to use the Article in a subsequent compilation of my works or to extend the Article to book length form, to include the Article in a thesis or dissertation, or otherwise to use or re-use portions or excerpts in other works, for both commercial and non-commercial purposes. Except for such uses, I understand that the assignment of copyright to the Journal owner gives the Journal owner the exclusive right to make or sub-license commercial use.

USER RIGHTS

The publisher will apply the Creative Commons Attribution-Noncommercial Works 4.0 International License (CC-BY-NC) to the Article where it publishes the Article in the journal on its online platforms on an Open Access basis.
The CC-BY-NC license allows users to copy and distribute the Article, provided this is not done for commercial purposes and further does not permit distribution of the Article if it is changed or edited in any way, and provided the user gives appropriate credit (with a link to the formal publication through the relevant DOI), provides a link to the license, and that the licensor is not represented as endorsing the use made of the work. The full details of the license are available at http://creativecommons.org/licenses/by-nc/4.0/legalcode.

REVERSION OF RIGHTS

Articles may sometimes be accepted for publication but later rejected in the publication process, even in some cases after public posting in "Articles in Press" form, in which case all rights will revert to the author.

☑ I have read and agree to the terms of the Journal Publishing Agreement.

Corresponding author:

name signature

※ E-mail this with your signature to ksoehj@ksoe.or.kr (Papers will not be published unless this form is signed and returned)

Research and Publication Ethics

Journal of Ocean Engineering and Technology (JOET) adheres to the guidelines published by professional organizations, including Committee on Publication Ethics (COPE; https://publicationethics.org/)

1. Authorship

JOET considers individuals who meet all of the following criteria to be authors:

1) Made a significant intellectual contribution to the theoretical development, system or experimental design, prototype development, and/or the analysis and interpretation of data associated with the work contained in the article.
2) Contributed to drafting the article or reviewing and/or revising it for intellectual content.
3) Approved the final version of the article as accepted for publication, including references.

Contributors who do not meet all of the above criteria may be included in the Acknowledgment section of the article. Omitting an author who contributed to your article or including a person who did not fulfill all of the above requirements is considered a breach of publishing ethics.

Correction of authorship after publication: JOET does not correct authorship after publication unless a mistake has been made by the editorial staff.

2. Originality and Duplicate Publication

All submitted manuscripts should be original and should not be in consideration by other scientific journals for publication. Any part of the accepted manuscript should not be duplicated in any other scientific journal without permission of the Editorial Board, although the figures and tables can be used freely if the original source is verified according to the Creative Commons Attribution License (CC BY-NC). It is mandatory for all authors to resolve any copyright issues when citing a figure or table from other journal that is not open access.

3. Conflict-of-Interest Statement

Conflict of interest exists when an author or the author's institution, reviewer, or editor has financial or personal relationships that inappropriately influence or bias his or her actions. Such relationships are also known as dual commitments, competing interests, or competing loyalties. These relationships vary from being negligible to having a great potential for influencing judgment. Not all relationships represent true conflict of interest. On the other hand, the potential for conflict of interest can exist regardless of whether an individual believes that the relationship affects his or her scientific judgment. Financial relationships such as employment, consultancies, stock ownership, honoraria, and paid expert testimony are the most easily identifiable conflicts of interest and the most likely to undermine the credibility of the journal, the authors, or of the science itself. Conflicts can occur for other reasons as well, such as personal relationships, academic competition, and intellectual passion. If there are any conflicts of interest, authors should disclose them in the manuscript. The conflicts of interest may occur during the research process as well; however, it is important to provide disclosure. If there is a disclosure, editors, reviewers, and reader can approach the manuscript after understanding the situation and the background of the completed research.

4. Management Procedures for the Research and Publication Misconduct

When JOET faces suspected cases of research and publication misconduct such as a redundant (duplicate) publication, plagiarism, fabricated data, changes in authorship, undisclosed conflicts of interest, an ethical problem discovered with the submitted manuscript, a reviewer who has appropriated an author's idea or data, complaints against editors, and other issues, the resolving process will follow the flowchart provided by the Committee on Publication Ethics (http://publicationethics.org/resources/flowcharts). The Editorial Board of JOET will discuss the suspected cases and reach a decision. JOET will not hesitate to publish errata, corrigenda, clarifications, retractions, and apologies when needed.

5. Editorial Responsibilities

The Editorial Board will continuously work to monitor and safeguard publication ethics: guidelines for retracting articles; maintenance of the integrity of the academic record; preclusion of business needs from compromising intellectual and ethical standards; publishing corrections, clarifications, retractions, and apologies when needed; and excluding plagiarism and fraudulent data. The editors maintain the following responsibilities: responsibility and authority to reject and accept articles; avoiding any conflict of interest with respect to articles they reject or accept; promoting publication of corrections or retractions when errors are found; and preservation of the anonymity of reviewers.

6. Hazards and human or animal subjects

If the work involves chemicals, procedures or equipment that have any unusual hazards inherent in their use, the author must clearly identify these in the manuscript. If the work involves the use of animal or human subjects, the author should ensure that the manuscript contains a statement that all procedures were performed in compliance with relevant laws and institutional guidelines and that the appropriate institutional committee(s) has approved them. Authors should include a statement in the manuscript that informed consent was obtained for experimentation with human subjects. The privacy rights of human subjects must always be observed.

Ensure correct use of the terms sex (when reporting biological factors) and gender (identity, psychosocial or cultural factors), and, unless inappropriate, report the sex and/or gender of study participants, the sex of animals or cells, and describe the methods used to determine sex and gender. If the study was done involving an exclusive population, for example in only one sex, authors should justify why, except in obvious cases. Authors should define how they determined race or ethnicity and justify their relevance.

7. Secondary publication

It is possible to republish manuscripts if the manuscripts satisfy the conditions of secondary publication. These are:

- The authors have received approval from the Editorial Board of both journals (the editor concerned with the secondary publication must have access to the primary version).
- The priority for the primary publication is respected by a publication interval negotiated by editors of both journals and the authors.
- The paper for secondary publication is intended for a different group of readers
- The secondary version faithfully reflects the data and interpretations of the primary version.
- The secondary version informs readers, peers, and documenting agencies that the paper has been published in whole or in part elsewhere, for example, with a note that might read, "This article is based on a study first reported in the [journal title, with full reference]"
- The title of the secondary publication should indicate that it is a secondary publication (complete or abridged republication or translation) of a primary publication.

8. Complaints and Appeals

The process of handling complaints and appeals follows the guidelines of the COPE available from: https://publicationethics. org/appeals

9. Post-publication discussions and corrections

The post-publication discussion is available through letter to editor. If any readers have a concern on any articles published, they can submit letter to editor on the articles. If there found any errors or mistakes in the article, it can be corrected through errata, corrigenda, or retraction.

The Korean Society of Ocean Engineers